NASA CR-134768
NRTC 75-23R

DAMAGE COEFFICIENTS IN LOW RESISTIVITY SILICON

by J. R. Srour, S. Othmer, K. Y. Chiu, and O. L. Curtis, Jr.

NORTHROP RESEARCH AND TECHNOLOGY CENTER

prepared for

NATIONAL AERONAUTICS AND SPACE ADMINISTRATION

NASA Lewis Research Center

Contract NAS 3-17849

1. Report No.	2. Government Accession No.	3. Recipient's Catalog No.
NASA CR-134768		

4. Title and Subtitle	5. Report Date
DAMAGE COEFFICIENTS IN LOW RESISTIVITY SILICON	May 1975
	6. Performing Organization Code

7. Author(s)	8. Performing Organization Report No.
J. R. Srour, S. Othmer, K. Y. Chiu, and O. L. Curtis, Jr.	NRTC 75-23R
	10. Work Unit No.

9. Performing Organization Name and Address	11. Contract or Grant No.
Northrop Research and Technology Center 3401 W. Broadway Hawthorne, California 90250	NAS 3-17849
	13. Type of Report and Period Covered Final Report July 1973 to November 1974

12. Sponsoring Agency Name and Address	14. Sponsoring Agency Code
National Aeronautics and Space Administration Washington, D. C. 20546	

15. Supplementary Notes

Project Monitor: C. R. Baraona, NASA Lewis Research Center, Cleveland, Ohio 44135

16. Abstract

Electron and proton damage coefficients have been determined for low resistivity silicon based on minority-carrier lifetime measurements on bulk material and diffusion length measurements on solar cells. Irradiations were performed on bulk samples and cells fabricated from four types of boron-doped 0.1 ohm-cm silicon ingots, including the four possible combinations of high and low oxygen content and high and low dislocation density. Measurements were also made on higher resistivity boron-doped bulk samples and solar cells. Major observations made and conclusions reached in the investigation are the following. 1) Diffusion-length damage coefficients (K_L) increase with decreasing resistivity (ρ) for boron-doped silicon. For low-resistivity solar cells, this decrease in radiation tolerance must be weighed against potential advantages when considering such devices for utilization in a space radiation environment. 2) For 0.5-, 1.0-, and 2.5-MeV electron bombardment, empirical fits to experimental data can be approximately expressed as $K_L \propto \rho^{-2/3}$ for $0.1 \leq \rho \leq 20$ ohm-cm. For 10-MeV proton bombardment, an empirical fit of the form $K_L \propto \rho^{-0.44}$ was found to describe the data reasonably well. 3) The dependence of damage coefficient on resistivity can be qualitatively accounted for quite well using a two-level Hall-Shockley-Read model. 4) Damage coefficients for solar cells were observed to be larger than their bulk-material counterparts. 5) Bulk samples and solar cells prepared from float-zone material were generally observed to be more radiation tolerant than their Czochralski counterparts at all resistivities examined. 6) No dependence of damage coefficient on dislocation density was apparent for 0.1 ohm-cm bulk samples and solar cells.

17. Key Words (Suggested by Author(s))	18. Distribution Statement
silicon, solar cells, electron damage, proton damage, minority-carrier lifetime, damage coefficient	Unclassified-unlimited

19. Security Classif. (of this report)	20. Security Classif. (of this page)	21. No. of Pages	22. Price*
Unclassified		95	

* For sale by the National Technical Information Service, Springfield, Virginia 22151

FOREWORD

A number of individuals contributed to this program in various ways and the authors wish to express their gratitude by mentioning the major contributors. The cooperation of Bruce Anspaugh during electron irradiations at the JPL Dynamitron was appreciated. Peter Iles provided timely delivery of solar cells and bulk silicon specimens and also made the Centralab solar simulator available to us. Proton irradiations at the Cal Tech Tandem Van de Graaff facility were performed with the cooperation of Frederick Mann and Prof. Tombrello. Low resistivity silicon ingots of high quality were supplied by Dow Corning. Surface photovoltage measurements were made at JPL through the cooperation of Richard Stirn. Expert technical assistance during the entire investigation was provided by Joe Woods and Gerald Hurwitz. Helpful discussions were held with Cosmo Baraona and Henry Brandhorst of NASA-Lewis Research Center and their continued encouragement and interest in this program has been appreciated.

TABLE OF CONTENTS

SECTION 1.0

INTRODUCTION

The output power from silicon solar cells employed in space applications degrades with time due to electron and proton bombardment. These charged particles displace silicon atoms from their normal lattice sites, resulting in the creation of recombination centers which reduce the minority-carrier lifetime, and hence the diffusion length. This diffusion-length degradation process is commonly characterized by a damage coefficient K_L, defined through the relationship

$$L^{-2} - L_0^{-2} = K_L \phi . \qquad (1)$$

In this expression L_0 and L are pre- and post-irradiation diffusion length, respectively, and ϕ is the fluence of the irradiating particles (either electrons or protons) of energy E. Thus, a relatively large K_L-value is indicative of vulnerability to radiation damage.

Recent analyses performed by Brandhorst[1] indicate that the use of low-resistivity ($<<$ 1 ohm-cm) bulk silicon for fabricating solar cells should result in devices with a considerably larger conversion efficiency than that typical of conventional units. Increased open-circuit voltage is the primary reason for such expectations. In predicting the radiation response of a solar cell fabricated from low-resistivity silicon, the problem arises that electron and proton damage coefficients are not known for such material and thus experimental determinations of these quantities are required.

In this report, we present the results of an experimental program aimed at determining electron and proton damage coefficients in low-resistivity boron-doped silicon. Minority-carrier lifetimes were measured before and after irradiation for bulk silicon samples using a steady-state photoconductivity technique. In addition to measurements on 0.1 ohm-cm material, comparison data were obtained for higher resistivity samples, thus permitting determination of the dependence of damage coefficient on resistivity. Pre- and post-irradiation measurements of two types were also made for n-on-p solar cells of various base resistivities, including 0.1 ohm-cm: 1) diffusion length measurements using penetrating radiation (Co-60 source); 2) determination of current-voltage characteristics during illumination of cells with a solar simulator. For low-resistivity bulk silicon, the possible dependence of K_L on growth technique (oxygen concentration) and dislocation density was examined. Electron irradiations were performed at three energies (0.5, 1.0, and 2.5 MeV) to permit examination of the energy dependence of K_L. Following irradiation, isothermal annealing studies were conducted at room temperature and 60°C for selected bulk samples. In addition to experimental findings, analytical results pertaining to certain aspects of the investigation are also presented.

SECTION 2.0

EXPERIMENTAL TECHNIQUES

In this section, experimental techniques employed and additional related information are presented. Included are descriptions of: a) measurement techniques; b) sample preparation procedures; c) radiation facilities and irradiation procedures.

2.1 Measurement Techniques

The ASTM standard method for measuring minority-carrier lifetime in bulk silicon is the photoconductivity decay technique.[2] However, implementation of this technique becomes increasingly difficult as resistivity is decreased. Furthermore, data interpretation can be a problem when trapping effects are significant. In an attempt to overcome such problems, we have devised a steady-state method of lifetime measurement for low-resistivity material. As shown in Figure 1, a bulk silicon specimen with ohmic contacts attached is situated in an enclosed chamber and is illuminated by penetrating light from a steady-state source (projection lamp--GE DCA). Non-penetrating wavelengths are eliminated by a silicon filter considerably thicker than the test sample, and therefore a condition of uniform carrier excitation is obtained. A Corning 7-57 filter was employed to reduce heating of the Si filter. A variable-frequency light chopper (0-300 Hz) is employed between the specimen and the projection lamp. A chopping frequency of 277 Hz was utilized for all lifetime measurements in this program. The purpose of chopping the light is to permit the use of phase-sensitive detection - a convenient approach to enhancing the signal-to-noise ratio. The light chopper also provides the reference signal in such a detection scheme. Also shown in Figure 1 is a silicon photodiode which provides a signal proportional to light intensity. Background lamps (unchopped) were employed to fill traps, and this aspect of the experiment is discussed in Section 3.7. In order to avoid generation of a contact photovoltage, sample contacts were shielded from the chopped light, as shown in the figure. Approximately the central third of a sample was illuminated.

Figure 2 shows a schematic of the electrical system employed. The sample-under-test is connected in a constant-current circuit ($R >> R_s$), and the steady-state photoconductivity (SSPC) signal, ΔV, due to chopped-light illumination is monitored. Voltage gain is provided by a low-noise transformer (Triad Geoformer G-10) and an operational amplifier (Analog Devices 118A). The signal is phase-sensitively detected by means of an Ithaco Model 353. Using appropriate circuit considerations, the measured signal was related to the signal of interest, ΔV.

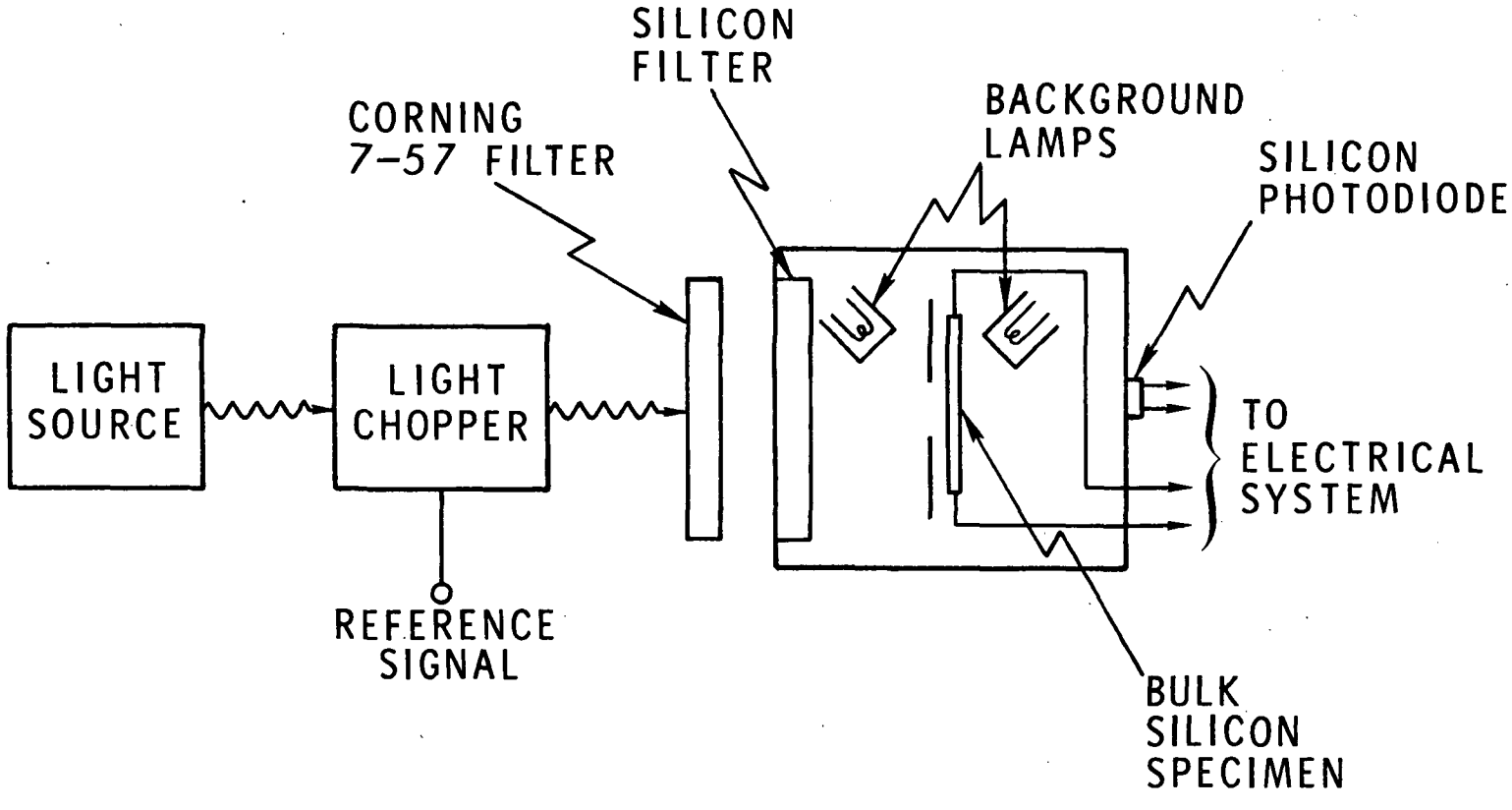

Figure 1. Schematic representation of the steady-state photoconductivity (SSPC) apparatus employed to measure minority-carrier lifetime in bulk silicon specimens.

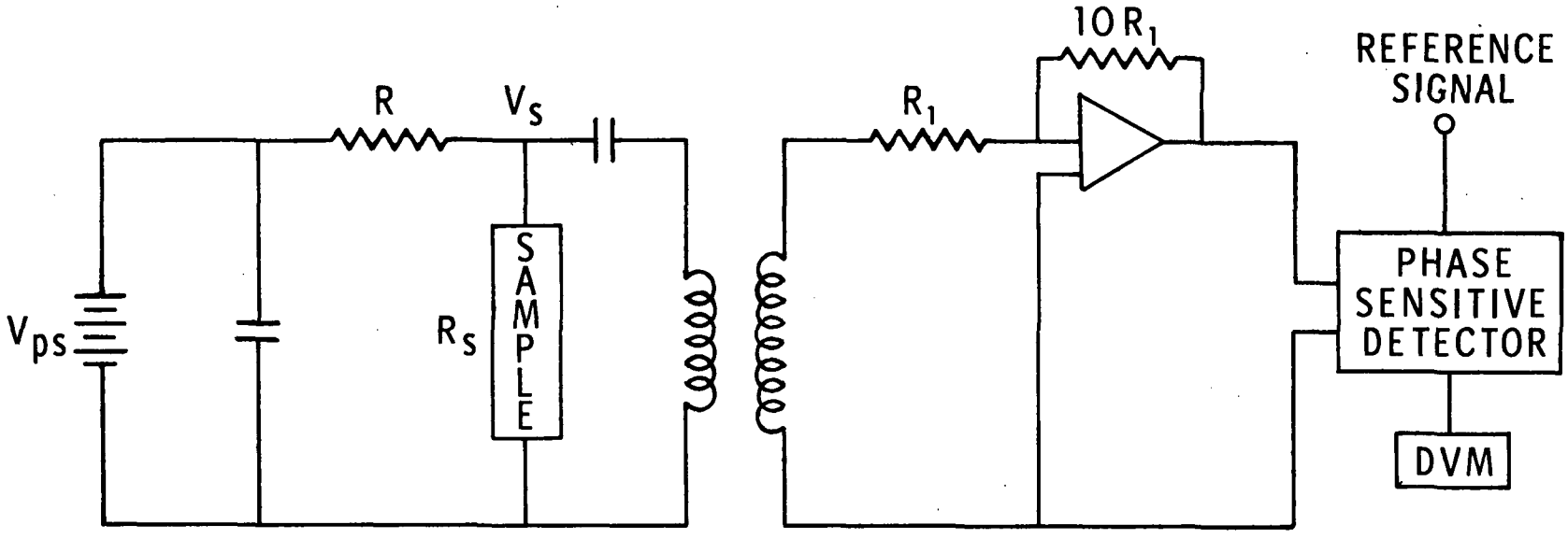

Figure 2. Schematic representation of the measurement system employed in conjunction with the SSPC apparatus to determine minority-carrier lifetime in bulk silicon specimens.

For a constant current circuit, excess minority-carrier density Δn (assuming p-type material) is given by the relation

$$\Delta n = \frac{\Delta V \; p_o \mu_h}{V_o (\mu_e + \mu_h)} = \frac{\Delta V}{e V_o \rho (\mu_e + \mu_h)}, \tag{2}$$

where p_o is equilibrium majority carrier density, ρ is resistivity, V_o is the dc voltage drop across the illuminated portion of the sample, e is the electronic charge, and μ_h and μ_e are hole and electron drift mobilities, respectively. (Equation 2 assumes that $\Delta V << V_o$, a condition that held true for the present study.) Measured excess carrier density from an SSPC experiment is related to minority-carrier lifetime τ by

$$\Delta n = g \tau, \tag{3}$$

where g is carrier generation rate. The generation rate for the SSPC apparatus was determined using a calibration procedure described in Section 3.6. We measured Δn and g was known, thus yielding τ. To obtain diffusion length L, the expression

$$L = (D \tau)^{1/2} \tag{4}$$

was employed. The procedure used to determine diffusivity D is discussed in Section 3.2. All lifetime measurements using the SSPC apparatus were made at room temperature ($25 \pm 5^{\circ}C$).

Measurements of lifetime for several unirradiated specimens were also made using transient photoconducitivity decay techniques. A flash x-ray source was used for carrier excitation; the experimental apparatus employed has been described previously.[3]

Measurements of diffusion length were made for n-on-p Si solar cells using the Co-60 gamma-ray source at Northrop Research and Technology Center. This measurement method has been described by Gremmelmaier,[4] Rosenzweig,[5] and, more recently, by Reynolds and Meulenberg.[6] Measurements of short-circuit current I_{sc} were made and then diffusion lengths were determined using the expression[6]

$$I_{sc} = q A g_{\gamma} L \left[\frac{\cosh(w/L) - 1}{\sinh(w/L)} \right], \tag{5}$$

where A is cell area, w is cell width, and g_{γ} is the carrier generation rate for the Co-60 source. This rate was determined from a series of total dose measurements using CaF thermoluminescent dosimeters. Measured

dose rate in rads(Si)/sec was converted to g_γ using the conversion factor 4.2×10^{13} pairs/cm^3 rad. The result obtained was $g_\gamma = 6.55 \times 10^{14}$ pairs/cm^3 sec.

Equation (5) only holds for the case of an infinite surface recombination velocity (s) at the back surface of a solar cell. We assumed infinite s here. Using a more general expression[6] to calculate L for various values of s reveals that the difference between results for $s = 10^4$ cm/sec and $s = \infty$ is very small. * The assumption of infinite s at an ohmic contact seems quite reasonable. We finally note that employment of Equation 5 to determine L based on measured I_{sc} requires an iterative procedure, and this was accomplished using a programmable desk-top calculator.

Current-voltage characteristics for solar cells were obtained before and after irradiation using the solar simulator at Centralab Semiconductor. Measurements were made under AMO conditions at room temperature (25 to 30°C).

An alternative measurement technique that was considered for employment here is the steady-state surface photovoltage (SPV) method.[7-10] This approach to measuring diffusion length was developed quite a few years ago, but only recently has it begun to receive attention by various research groups. In the present investigation, a comparison was made for several samples of diffusion lengths determined using the SSPC method and the SPV method. **

2.2 Sample Preparation Procedures

Low-resistivity (~0.1 ohm-cm) boron-doped silicon ingots for use in this program were obtained from Dow Corning. Four ingots were obtained, corresponding to the four possible combinations of high and low oxygen concentration and high and low dislocation density. Two ingots were grown by the float-zone method and were expected to have a relatively low oxygen content. The other two ingots were grown by the Czochralski method (relatively high oxygen content). One float-zone crystal and one Czochralski crystal were grown to be

---

* For the interested reader, we note that the general expression referred to here (Equation A9 in Reference 6) appears to have a few typographical errors. It should read (using the present notation):

$$I_{sc} = qAg_\gamma L \left[\frac{D\exp(-w/L) + sL\{\exp(-w/L) - 1\}}{sL\sinh(w/L) - D\cosh(w/L)} + 1 \right] .$$

** SPV measurements were made at the Jet Propulsion Laboratory through the cooperation of R. J. Stirn.

dislocation free, and the other two ingots had a high dislocation density. (Measurements of dislocation density are described in Section 3.4). Studies were also made on higher resistivity material, also grown by Dow Corning. This material was already on hand at Northrop Research and Technology Center at the start of this program.

An important factor in deciding on bulk-silicon test-specimen dimensions was the bombarding particle energies to be employed. Table I shows the energies used and the corresponding particle ranges in silicon.[11] It is desirable to avoid a condition of inhomogeneous damage for the purpose of aiding data interpretation. We selected a sample thickness of 0.3 cm, which is comparable to that employed in conventional solar cells. This thickness is considerably less than the particle ranges under consideration, and thus reasonably uniform damage profiles should result for 1.0- and 2.5-MeV electrons and for 10-MeV protons. For 0.5-MeV electrons, although the range is three times larger than the sample thickness, inhomogeneities are expected to occur because the variation of damage coefficient with particle energy is quite strong near 0.5 MeV. Upon penetrating half the thickness of a 0.3 mm sample, a 0.5-MeV electron loses ~0.057 MeV. The 0.5-MeV-to-0.443-MeV damage coefficient ratio for silicon[12] is ~ 1.45, and thus the amount of damage expected at the center of the sample is ~70% of that at the bombarded surface. (A similar calculation for incident 1.0-MeV electrons yields ~90% at the sample center.)

TABLE I

Electron Energy (MeV)	Electron Range (mm)	Proton Energy (MeV)	Proton Range (mm)
0.5	0.94	10	0.71
1.0	2.3		
2.5	6.2		

Electron and proton ranges in silicon for the bombardment energies employed in this study.

Bulk silicon samples measuring approximately 1 cm x 2 cm x 0.03 cm were fabricated at Centralab from several Northrop-supplied silicon ingots. Centralab also prepared samples for our use from 6 ohm-cm Czochralski material (B-doped) that is conventionally employed in the fabrication of solar cells. Additionally, n-on-p solar cells were fabricated

at Centralab using the same Northrop-supplied ingots employed in the preparation of bulk samples, thus permitting a meaningful device-bulk comparison. Conventional production-line n-on-p cells (Czochralski) were also obtained from Centralab for the purpose of providing a "standard-cell" comparison during the radiation testing.

All bulk-samples were sandblasted at Centralab for the purpose of achieving a high surface recombination velocity. (Surface recombination considerations are discussed in subsequent sections of this report.) Ohmic contacts were prepared at Northrop using ultrasonic soldering techniques. Contacts (two per sample) were narrow (~0.1 cm) stripes prepared on a major face at the ends along the 1-cm dimension. Contacts were checked by making forward and reverse resistance measurements at room temperature. Resistivity was measured for each specimen using conventional four-point-probe techniques.

2.3 Radiation Facilities and Irradiation Procedures

Electron irradiations were performed at 0.5-, 1.0-, and 2.5-MeV using the Dynamitron at the Jet Propulsion Laboratory (JPL), Pasadena, Calif. All bulk specimens and solar cells were illuminated during irradiation at an intensity of 140 mW/cm^2 using the solar simulator at the Dynamitron facility. Test specimens were bombarded while in vacuum at a pressure of ~10^{-6} mm Hg. Samples were attached to an Al plate using Apiezon H vacuum grease to provide a good thermal contact (see grease discussion in Section 3.5). The temperature of the plate was controlled at 25°C. To minimize room-temperature annealing, all irradiated bulk samples and solar cells were stored at dry ice temperature following irradiation, with storage beginning approximately one-half hour after bombardment. Specimens were removed from dry ice for about an additional one-half hour to permit a measurement, then were returned to dry ice until time for the next irradiation. Current-voltage characteristics for solar cells and lifetime measurements for bulk samples were obtained after a total of ~1 hour at room temperature. Diffusion length measurements on selected solar cells using a Co-60 source were made after ~2 hours at room temperature.

At the Dynamitron, a Faraday cup was employed to determine the fluence. The following fluences were utilized at all three electron energies: 3×10^{13}, 10^{14}, 3×10^{14}, 10^{15}, and 3×10^{15} electrons/cm^2. For the first three fluences, the flux was 5×10^{10} electrons/cm^2 sec. At 10^{15} electrons/cm^2, the flux was 10^{11} electrons/cm^2 sec; and at 3×10^{15} electrons/cm^2, it was 2×10^{11} electrons/cm^2 sec. The flux was increased with increasing fluence in order to obtain reasonable exposure times. (The last exposure at a given energy required 2.8 h.)

The 13-MeV Tandem Van de Graaff at the California Institute of Technology, Pasadena, California, was employed for 10-MeV proton irradiations. Bulk samples and solar cells were illuminated during irradiation at an intensity of 140 mW/cm^2 using a Varian VIX-150 Xenon Short-Arc Illuminator. A Coherent Radiation Model 201 Broad Band Power Meter was employed to calibrate the xenon illuminator and map the light-beam profile. At the proton source, because of beam uniformity and beam size considerations only one sample could be irradiated at a time. The xenon lamp could be employed to illuminate a single sample to an intensity of 140 mW/cm^2 to within about ±5% over the specimen surface. Samples were irradiated in vacuum at a pressure of $\sim 10^{-5}$ mm Hg. The light source was external to the vacuum chamber and illumination was accomplished through a fused quartz window (Type 125) in the chamber wall. This window has a transmittance of nearly 100% over the wavelength range from 0.27 to 2.7 μm. Samples were mounted with Apiezon H vacuum grease on a massive, moveable block of Al in the chamber and externally moved into the beam one at a time. *Irradiation times were ⩽30 seconds per sample for all fluences.* The temperature rise of the aluminum block was determined to be less than 1°C during the irradiation of each lot of about 15 samples. Furthermore, the temperature rise of the sample relative to the sample mount was determined to be about 1°C when subjected to the light. In the absence of temperature control mechanisms, the sample holder was, therefore, brought to an initial temperature of 23°C prior to evacuation, giving sample temperatures ranging from 24 to 25°C during irradiation. Fluences employed were the following: $\sim 3 \times 10^{10}$, $\sim 10^{11}$, $\sim 3 \times 10^{11}$, and 1.2×10^{12} p/cm^2.

Fluences were controlled by means of a current integrator which monitored the charge impinging on the sample mount through an aperture of known area. The sample holder was maintained at positive bias to collect secondary electrons. Integrator offset current and leakage current due to finite resistance from sample to ground were balanced out, and the beam currents employed were chosen to be large compared to residual drift in these quantities. A thin wire was scanned past the aperture to measure beam current as a function of position and verify beam uniformity over the aperture. This method of regulating fluence was deemed to be preferable to the use of a Faraday cup since the area of beam uniformity was not much larger than the sample size. A Faraday cup would have had to be removed from the area of interest, and would have had a very small beam aperture, necessitating the measurement of much smaller currents. The fluxes for proton irradiations were as follows: The fluence of 3×10^{10} p/cm^2 was obtained at a flux of about 6×10^9 p/cm^2 sec; the fluence of 10^{11} at $6\text{-}9 \times 10^9$; of 3×10^{11} at 2×10^{10}; and the fluence of 1.2×10^{12} p/cm^2 at a rate of 3.6×10^{10} p/cm^2 sec. The fluxes were chosen so as to keep total time at room temperature within acceptable limits of about 1 h for each group of samples which were mounted in vacuum simultaneously. Dry ice storage was utilized in the same manner as described above for electron irradiations.

2.4 Sample Designation System

As discussed above, a set of bulk samples and solar cells were fabricated from the same silicon ingot to permit a meaningful comparison between device and bulk behavior. This same procedure was followed for a variety of silicon ingots. The sample designation system employed in this report, both in the text and on all figures, provides information concerning growth technique, resistivity, dislocation density, and whether a specimen is a bulk sample or a solar cell. For float-zone material, the abbreviation FZ is employed, and for Czochralski material CZ is used. We employ the shorthand designations HD for samples prepared from material with a high dislocation density and LD for low-dislocation-density units. (These designations only appear for low-resistivity specimens because no dislocation-density determinations were made for higher-resistivity material.) Nominal resistivities are given in ohm-cm and also a number is assigned to each bulk sample and device.

A few examples will serve to illustrate the designation system: a) FZLD 0.1/4: this notation is for a bulk silicon sample (number 4) fabricated from 0.1 ohm-cm (nominal) low-dislocation-density float-zone material; b) CZHD 0.1/SC2: this designation is for a solar cell (SC), device number 2, fabricated from 0.1 ohm-cm high-dislocation-density Czochralski material; c) FZ 13/4: a bulk sample (number 4) fabricated from 13 ohm-cm float-zone material. Bulk samples designated CZ 6/x were fabricated from material typically employed at Centralab for the fabrication of solar cells. Solar cells designated CZ 9/SCx are typical production line cells obtained from Centralab.

Data points on all figures are identified in two ways. Some symbols are associated with measurements on a particular bulk sample or solar cell, and in these cases the sample (or device) number is listed on the figure in a legend. Other symbols represent an average of data obtained for two or more bulk specimens of the same type, and in these cases the legend identifying this type of data point will list the ingot designation only, with no specimen number appearing. For example, a data point identified as CZLD 0.1 represents an average value for identically treated bulk samples from ingot CZLD 0.1.

SECTION 3.0

PRELIMINARY EXPERIMENTS AND ANALYSES

In the course of preparing for irradiations and subsequent determination of damage coefficients, several preliminary experiments were performed. Additionally, analyses were made of certain features of the experiment, including surface recombination effects and other phenomena of interest. This section discusses the various preliminary considerations that were made.

3.1 Analysis of Surface Recombination Effects

The employment in this investigation of thin bulk silicon samples with sandblasted surfaces necessitates accounting for surface recombination effects. (Justification for choosing sandblasted surfaces, along with a description of associated experimental results, is given in Section 3.8.) In general, one measures an effective lifetime τ_{eff} which may or may not be equal to the bulk lifetime τ depending on the degree of surface recombination occurring. An analysis of such effects was performed for the sample geometry used in this study. The sample can be approximated by a thin slab having one finite and two infinite dimensions. The problem is to determine the ratio of τ_{eff} to τ for a given value of bulk diffusion length L and a given surface recombination velocity s.

For a thin slab of thickness 2T under conditions of uniform carrier excitation, the following expression holds:[13]

$$\tau_{eff}/\tau = \left[1 - \frac{(sL/DT)\sinh(T/L)}{(1/L)\sinh(T/L) + (s/D)\cosh(T/L)}\right]. \qquad (6)$$

Calculations appropriate for 0.1 ohm-cm p-type silicon were made using Equation 6 by assuming a diffusivity D of 11.7 cm^2/sec* and a sample half-thickness of 165 μm. Computational results are presented in Figure 3, where τ_{eff}/τ is plotted versus bulk diffusion length with surface recombination velocity as a parameter. Assuming that the pre-irradiation value of L is 100 μm, for the largest values of s measured lifetime will differ from the actual value by as much as a factor of about two. On the other hand, if s is ≤ 100 then the error will be no larger than about 5% before irradiation. Another noteworthy feature of the calculations is that the difference between results for $s = 10^4$ cm/sec and $s = \infty$ is very small. Thus, as long as the condition $s \geq 10^4$ cm/sec holds for specimen samples, differences in s from sample to sample with otherwise identical properties will be only of second-order importance in terms of measured lifetime (τ_{eff}).

*This value of D is employed only to illustrate the calculational procedure. As noted in Section 3.2, a slightly smaller electron diffusivity was utilized in this investigation for all calculations relating to experimental findings.

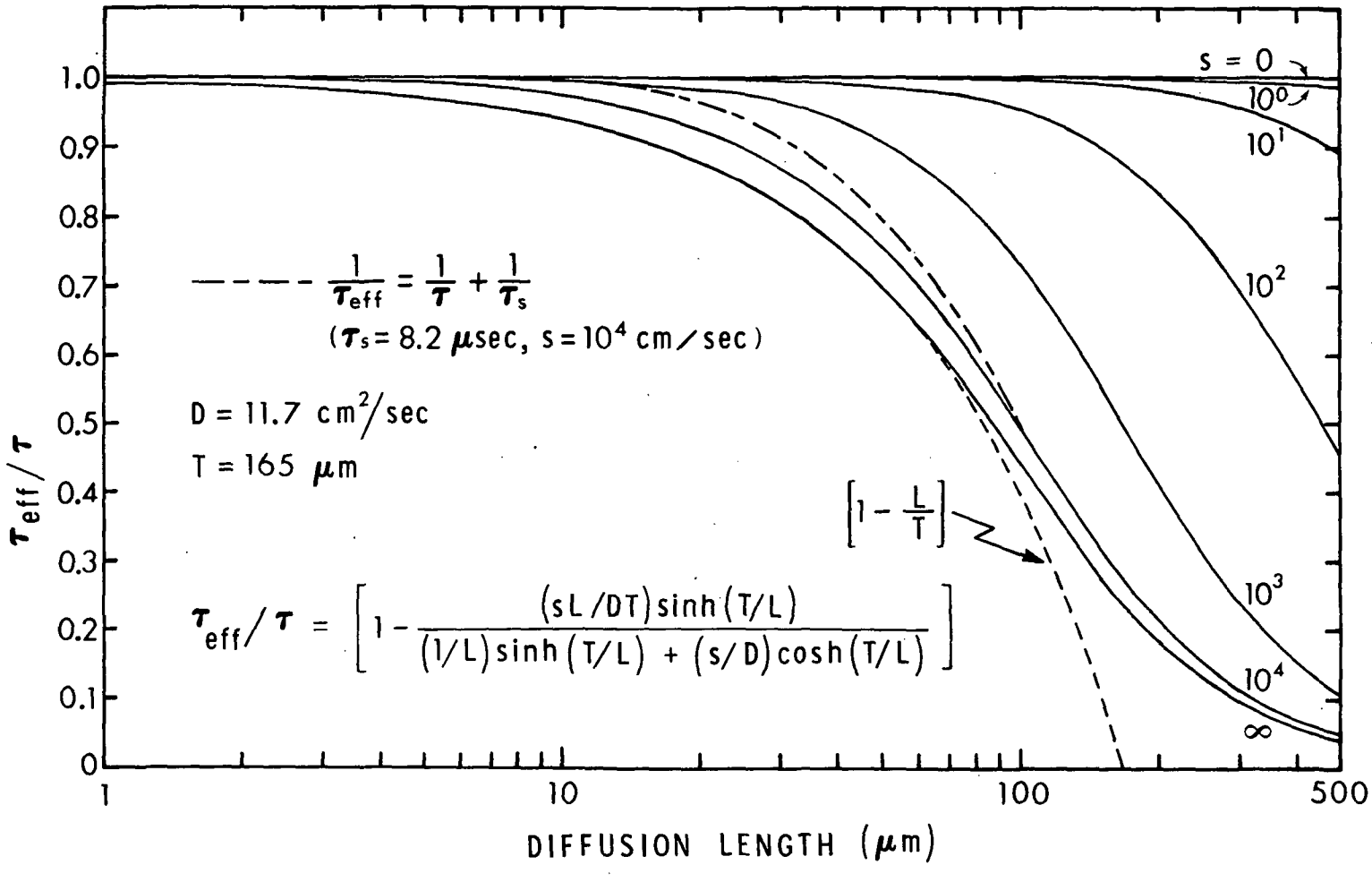

Figure 3. The ratio of effective to actual lifetime versus diffusion length with surface recombination velocity s as a parameter for a thin silicon slab. The solid curves were calculated using the relationship shown along with the listed values of diffusivity D and half-thickness T. The dashed curves were calculated using the two approximations shown (see text for discussion).

Since the variation of τ_{eff}/τ is approximately independent of surface recombination velocity for $s \geq 10^4$, analysis is simplified for samples with such surface properties. Two examples will illustrate this point. First, we note that for $T > L$, $\sinh(T/L) \approx \cosh(T/L)$. If it is further assumed that $sL >> D$, Eq. (6) reduces to

$$\tau_{eff}/\tau \approx \left[1 - \frac{L}{T}\right]. \tag{7}$$

This expression was used to obtain one of the dashed curves in Figure 3, assuming $T = 165$ μm, and agreement with the $s = \infty$ curve is seen to be excellent for $L \leq 100$ μm. The deviation for larger L is due to the deviation of $\sinh(T/L)$ from $\cosh(T/L)$. It is thus seen that for the case of large s the analytical dependence of τ_{eff}/τ on diffusion length assumes a very simple form.

From the standpoint of correcting for surface recombination effects, it is desirable to express τ_{eff} as

$$\frac{1}{\tau_{eff}} = \frac{1}{\tau} + \frac{1}{\tau_s}, \tag{8}$$

where τ_s is "surface" lifetime. Such an expression implicitly assumes a constant value for τ_s. It turns out that this approach is strictly true only for the case of $T \ll L$. For this situation, Eq. (6) yields $\tau_s = T/s$. For our case the inequality $T \ll L$ will certainly not hold. However, Eq. (8) constitutes a very good approximation for the present situation, as seen by the following example.

Consider a sandblasted 0.1 ohm-cm p-type sample with a half-thickness T of 165 μm, a pre-irradiation diffusion length of 100 μm, and a surface recombination velocity of 10^4 cm/sec. Assuming a diffusivity D of 11.7 cm^2/sec, we obtain a pre-irradiation value for τ of 8.5 μsec. From Figure 3, $\tau_{eff}/\tau = 0.49$ for $L = 100$ μm, and therefore $\tau_{eff} = 4.2$ μsec. Equation (8) yields $\tau_s = 8.2$ μsec. We next assume that τ_s remains constant as τ degrades due to irradiation. The second dashed curve in Figure 3 shows the results of calculating τ_{eff}/τ for various L values (≤ 100 μm, normalized to solid $s = 10^4$ curve at 100 μm) by employing Eq. (8) and assuming $\tau_s = 8.2$ μsec. It is seen that the largest deviation of the dashed (approximate) curve from the actual (exact) curve is only on the order of 5%. Therefore, one could accurately employ Eq. (8) to interpret steady-state photoconductivity measurements. The same surface correction that is applied prior to irradiation can be applied following bombardment.

Under the assumption of a constant surface lifetime, τ_s, it is readily shown that if effective values of diffusion length are employed to determine damage coefficients, then Equation 1 takes the form

$$(L^{eff})^{-2} - (L_0^{eff})^{-2} = K_L \phi . \tag{9}$$

If we denote a damage coefficient determined with Equation 9 as K_L^{eff}, then based on the above discussion one would expect K_L^{eff} to be in good agreement with a damage coefficient determined using actual bulk diffusion lengths (K_L). This was found to be the case experimentally. Values for K_L^{eff} were, on the average, ~6% larger than those for K_L (based on data obtained following 1-MeV electron irradiation).

Although we could have employed the above-described effective-diffusion-length approach to determining K_L in the present investigation, the more informative approach of obtaining actual pre- and post-irradiation diffusion lengths was followed. This required that each measured (effective) lifetime be converted to actual bulk diffusion length by properly correcting for the effects of surface recombination. For this purpose, Equation 6 was employed in a slightly different form:

$$\tau_{eff} = \frac{L^2}{D} \left[1 - \frac{(sL/DT) \sinh (T/L)}{(1/L) \sinh (T/L) + (s/D) \cosh (T/L)} \right] . \tag{10}$$

Appropriate values of s and D (both discussed below) were employed and that value of L required to satisfy Equation 10 was then determined by using an iterative procedure on a programmable desk-top calculator.

3.2 Procedure for Determining Diffusivity and Mobility

Determination of diffusion-length damage coefficients was a primary goal of the present study. Because minority-carrier lifetime is the measured quantity, utilization of Equation 4 is required to determine diffusion length, which requires knowledge of diffusivity D. Additionally, determination of lifetime with the SSPC method requires knowledge of drift mobilities. (Of course, μ and D are related through the Einstein relation.) Since lifetime measurements were made as a function of resistivity, and thus D varied, it became necessary to assume reasonable values for diffusivity in a consistent manner (i.e., consistent with measured resistivities). The following approach was employed. Irvin's data[14] was used to determine acceptor concentration N_a from measured resistivity. Next, hole drift mobility μ_h was calculated using the expression

$$\mu_h = 1/\rho e N_a \tag{11}$$

which assumes $N_a = p_o$. Next, Irvin's data was again employed to determine the resistivity of n-type Si with the same impurity concentration as determined above for p-type material. Equation 11 then yields μ_e for the new value of ρ (with donor concentration N_d substituted for N_a). This approach cannot be directly employed for 0.1 ohm-cm material because all impurity atoms are not ionized. We determined the number of ionized impurities, based on the value of N determined from Irvin, in the following manner.

For 0.1 ohm-cm boron-doped silicon, the equilibrium Fermi level E_f is sufficiently close to the acceptor level E_a so that a significant fraction of the acceptor atoms are not ionized at room temperature. The ratio of ionized acceptor concentration N_a^- to the total acceptor concentration N_a is given by[15]

$$\frac{N_a^-}{N_a} = \frac{1}{1 + \beta \exp\left[(E_a - E_f)/kT\right]}, \qquad (12)$$

where β is the impurity level spin degeneracy ($\beta = 4$ for acceptor levels[15]). For 0.1 ohm-cm material, N_a is about 4.8×10^{17} cm^{-3} (from Irvin[14]). Additionally, E_a is located 0.045 eV above the valence band. By considering the variation of E_f with carrier concentration simultaneously with Equation 12, the following results were obtained: E_f is located approximately 0.092 eV above the valence band and about 60% of the acceptor atoms are ionized.

Once the ionized acceptor density is determined by this method, then Equation 11 yields μ_h (substitute N_a^- for N_a). Following this approach yields $\mu_h = 210$ $cm^2/V\text{-sec}$ for 0.1 ohm-cm material. Determination of μ_e for low-resistivity silicon using the above approach presents somewhat of a problem. One would like to determine the electron mobility in p-type material with N_a acceptor atoms, N_a^- of which are ionized. Irvin's plot of ρ vs N for n- and p-type Si has built into it certain assumptions regarding impurity ionization for low-resistivity material (spin degeneracy, impurity level locations, etc.) Without knowledge of these precise assumptions, one hesitates to attempt a detailed calculation for physically equivalent n-type material (equivalent in terms of scattering effectiveness) which would yield, in conjunction with Irvin's graphs, a value for μ_e in 0.1 ohm-cm material. Instead, we have employed the approach of averaging literature values for this quantity. Sze and Irvin[16] give a value of ~ 435 $cm^2/V\text{-sec}$ and Wolfstirn's value[17] is ~ 405 $cm^2/V\text{-sec}$. The average of these two quantities is numerically equal to that given in Neuberger[18], ~ 420 $cm^2/V\text{-sec}$, and hence we employ here this value for μ_e in 0.1 ohm-cm p-type Si. The corresponding electron diffusivity is 10.9 cm^2/sec at 300°K.

It may not be clear yet to the reader why we employed the approach described above for obtaining mobility values in silicon of various resistivities. To determine Δn using Equation 2 mobility values must be assumed. Commonly employed references, such as Sze and Irvin[16], give graphs of mobility vs impurity concentration N. Thus, to use such graphs one must determine N. A common approach is to measure resistivity and then use Irvin's graph[14] to determine N, followed by the obtaining of mobility values from Sze and Irvin. However, built into Irvin's graph are assumed mobility values which are not completely consistent with the mobility graphs of Sze and Irvin. (In fact, there is an apparent plotting error in Sze and Irvin's μ_h curve in that at low impurity concentrations a limiting value of ~600 cm^2/V-sec is approached, as opposed to the accepted value of ~500 cm^2/V-sec.) Hence, for purposes of consistency we decided to employ Irvin's graph alone to determine mobility, as described above, with the exception of the μ_e value for 0.1 ohm-cm material. (This approach removed a considerable amount of scatter initially observed in a comparison of SSPC lifetimes and photoconductivity decay (PCD) lifetimes performed during the generation rate calibration (described below) for the SSPC apparatus.)

As an experimental check on the hole mobility assumed for 0.1 ohm-cm material, Hall mobility measurements were made at room temperature using conventional techniques for one sample from each of the four low-resistivity ingots being studied in this program. Results are shown in Table II, along with calculated drift mobilities. (A Hall-to-drift mobility ratio 0.92 was assumed.[18]) Agreement among the four ingots is good. It is satisfying to note that the average hole drift mobility in Table II (223 cm^2/V sec) is in good agreement (~6% higher) with the value of 210 cm^2/V sec determined above.

TABLE II

Ingot	Hall Mobility (cm^2/V sec)	Drift Mobility (cm^2/V sec)
FZLD 0.1	208	226
FZHD 0.1	194	211
CZLD 0.1	212	230
CZHD 0.1	208	226

Measured Hall mobilities for low-resistivity p-type silicon specimens. Drift mobilities were obtained assuming a Hall-to-drift mobility ratio of 0.92 (Reference 18).

3.3 Resistivity Considerations

During the preliminary stages of this investigation, an apparent discrepancy was observed in some cases between four-point-probe resistivity measurements and resistivity determinations based on potential profiles. In particular, differences between measurements on thick and thin samples were noted. In an attempt to resolve this discrepancy, careful four-point-probe and potential-profile measurements were made on four low-resistivity samples, two of which were relatively thick (0.32 cm) and the other two were relatively thin (~0.03 cm). Results are shown in Table III and it is seen that the two methods yield resistivities that are in excellent agreement for thin specimens. For the thicker samples, four-point-probe values are a factor of 1.07 larger than their potential-profile counterparts. Upon comparing four-point-probe readings for thick and thin samples prepared from the same ingot, values for FZLD 0.1 agree exactly. For CZHD 0.1, the thin-sample value is a factor of 1.07 larger than that for the thick specimen. In view of the fact that the discrepancies noted are rather small and that the two measurement techniques agree for thin samples, we decided to employ resistivities measured using a four-point probe for all of the thin bulk silicon samples under study. The source of observed differences is unknown at present, but determination of this source was considered unimportant for the present investigation.

TABLE III

Sample Designation	Dimensions cm	Resistivity Four-Point Probe Ω-cm	Resistivity Potential Profile Ω-cm	Ratio of Two Methods
CZHD 0.1/689	0.60 x 1.53 x 0.32	0.106	0.099	1.07
CZHD 0.1/2	0.99 x 1.99 x 0.030	0.113	0.113	1.0
FZLD 0.1/686	0.61 x 1.54 x 0.32	0.108	0.101	1.07
FZLD 0.1/10	1.0 x 2.0 x 0.031	0.108	0.111	0.97

Comparison of resistivity measurements made by four-point-probe and potential-profile methods for thick (0.32 cm) and thin (~0.03 cm) low-resistivity bulk silicon specimens.

3.4 Dislocation Density Determinations

Dislocation densities were determined for the four low resistivity silicon ingots using the Sirtl etch method (ASTM Designation F-47-70). A chromic acid etch was employed and two slices from each ingot, designated A and B,

were examined. For a given ingot, the positions of slices A and B were chosen such that all other material to be studied (i. e., material for preparation of bulk samples, solar cells, and slices for determination of oxygen concentration) was situated between them. This approach was employed to obtain an indication of variations in dislocation density over the region under investigation for a particular ingot. Results obtained are shown in Table IV. Measurements made by Dow Corning are shown for comparison.

TABLE IV

Dislocation Densities for Four Low Resistivity Silicon Ingots

Ingot Designation	Dow Corning Ingot No.	Dislocation Density (cm^{-2}) Slice A	Slice B	Dow Corning
FZHD 0.1	S73-5277	2.5×10^4	2.8×10^4	1.5 to 3×10^4
FZLD 0.1	S71-1305	0*	0*	0
CZHD 0.1	S73-5278	3.9×10^3	2.9×10^3	3 to 6×10^3
CZLD 0.1	S73-5276	0	0	0

* For FZLD 0.1, a swirl pattern of etch pits was observed which apparently is not associated with the presence of dislocations. See text for discussion.

Ingot FZLD was grown by Dow Corning to be dislocation free. However, we observed a swirl pattern of etch pits for slices A and B. These swirls covered about 30% of the slice surface, with the remainder of the surface being free of etch pits. The local etch pit density in a swirl was $\sim 1.3 \times 10^4$ cm^{-2}, and the average density (entire area) for both slices was $\sim 4 \times 10^3$ cm^{-2}. Etch pit patterns such as those noted here have been observed in dislocation-free float-zone silicon by de Kock[19,20] and Ciszek[21] and have been attributed to vacancy clustering at a vacancy-oxygen complex.[19] Thus, the presence of etch pits does not necessarily indicate the presence of dislocations. Based on the dislocation density given by Dow Corning for this ingot (Table IV) and on the close correspondence of our observations of etch pits with those of others[19-21] on dislocation-free-material, we conclude that ingot FZLD most likely is free of dislocations.

3.5 Vacuum Grease Experiments

For the irradiations performed in this study, it was necessary to insure that bulk samples and solar cells were in good thermal contact with a heat sink to prevent unwanted temperature rises during bombardment. As mentioned above, specimens were attached to a heat sink by using a small amount of Apiezon H vacuum grease. (This approach had previously been employed with success at JPL for solar cell irradiations). However, the question arose as to whether the grease could be completely, and readily, removed from a sandblasted surface. Additionally, we wished to determine whether this grease would affect the measured steady-state photoconductivity signal by changing the surface electrical and/or optical properties. We performed experiments which addressed these two questions. The following procedure was found to quickly, and apparently completely, remove Apiezon H: a sample with grease on it was dipped for a few seconds in a beaker of trichloroethylene contained in an ultrasonic cleaner; this treatment was followed by a few seconds in acetone, then methyl alcohol, and finally deionized water, all three of which were also in the ultrasonic cleaner. Examination under a microscope revealed no grease on the sample surface. To examine the effect of Apiezon H on photoconductivity signal, three 0.3 mm thick samples were measured in the SSPC apparatus both before application of grease and after application of grease and subsequent cleaning of the surface using the above procedure. The average post-cleaning photoconductivity signal was found to be within a few per cent of the corresponding pre-grease measurement, and we concluded that Apiezon H can be employed to attach specimens to a heat sink without having a detrimental effect on subsequent lifetime measurements.

3.6 Generation Rate Calibration for the SSPC Apparatus

Measurement of steady-state photoconductivity signal ΔV for a given specimen yields excess carrier density Δn through Equation 2. Lifetime is then obtained through Equation 3 assuming knowledge of the carrier generation rate g. Absolute determination of diffusion lengths, and thus damage coefficients, depends on the accuracy to which g is known for the SSPC apparatus. A careful series of experiments were performed for this purpose, and the procedure followed and results obtained are briefly described in this section.

Thirteen bulk silicon samples, listed in Table V, were employed in the calibration, all of which were prepared in the usual manner (see Section 2.2). As a first step, photoconductivity decay techniques were used to determine low-level carrier lifetimes (designated τ_{pcd} in Table V). Injection ratios at which PCD measurements were made ranged from $\sim 10^{-5}$ for low-resistivity samples to $\sim 5 \times 10^{-5}$ for higher resistivity specimens. In most cases, particularly for CZ 2.5 samples and FZLD 0.1 samples,

SAMPLE DESIGNATION	RESISTIVITY ohm-cm	τ_{ss} μsec	τ_{pcd} μsec	$\frac{\tau_{ss}}{\tau_{pcd}}$
CZ 2.5/9	2.58	3.59	3.59	≡ 1.0
CZ 2.5/10	2.54	3.64	3.58	1.02
FZ 2.5/1	2.51	3.82	3.60	1.06
FZ 13/5	14.9	3.44	3.75	0.92
FZ 13/6	12.4	3.77	3.75	1.01
CZ 2.5/1	2.52	3.71	3.67	1.01
CZ 2.5/2	2.54	3.90	3.66	1.07
FZ 13/3	12.8	3.30	3.64	0.91
FZ 13/4	13.2	3.34	3.54	0.94
FZLD 0.1/2	0.106	6.85	6.83	1.00
FZLD 0.1/3	0.104	7.36	7.16	1.03
FZHD 0.1/2	0.099	5.44	5.67	0.96
FZHD 0.1/3	0.099	5.72	5.95	0.96

TABLE V

Measured resistivities and effective minority carrier lifetimes for bulk silicon specimens. Resistivity measurements were made using a four-point probe and lifetimes were measured using both steady-state-photoconductivity (τ_{ss}) and photoconductivity-decay (τ_{pcd}) techniques.

trapping effects were small. In a few cases (particularly for FZ 13), long-time-constant trapping effects were noted. Because lifetimes were much shorter than trapping times, a baseline shift occurred in the photoconductivity decay; recombination time constants were readily extracted from observed signals of this type.

PCD lifetime measurements for CZ 2.5 were judged to be the most accurate and we thus employed one of these samples (CZ 2.5/9) as a standard for determining g. Steady-state measurements were then made in the SSPC apparatus at a constant chopped light intensity under a traps-filled condition (achieved with the aid of background lamps--see Section 3.7). A measurement of Δn was made for the standard sample, and generation rate was determined through the relation

$$g = \Delta n / \tau_{pcd} . \qquad (13)$$

The quantity Δn was also measured for the other samples using SSPC, and steady-state lifetime, τ_{ss}, then determined using the value of g obtained from the standard specimen. (Injection ratios due to chopped light in the steady-state measurements ranged from 1 to 3×10^{-6} for low resistivity samples and from 1 to 5×10^{-4} for higher resistivity specimens.) The ratio of steady-state lifetime obtained in this fashion to τ_{pcd} is listed in Table V for each sample and it is seen that all values lie close to the ideal ratio of unity. With the exception of samples FZ 13/3 and FZ 13/5, all ratios are within 7% of 1.0. Note that the quantity τ_{ss}/τ_{pcd} was determined for a resistivity range covering more than two orders of magnitude. The favorable results obtained suggest that our measurements of ΔV, V_o and ρ are quite accurate over the range studied and also that the assumed mobility values are consistent with measured resistivities.

The steady-state lifetime measurements listed in Table V were made at a generation rate (due to chopped light) of 1.5×10^{17} pairs/cm^3-sec, as were all other SSPC lifetime measurements in this investigation. With the present experimental set-up, the highest generation rate that can be achieved is a factor of $\sim$2.5 larger than this quantity.

In calibrating the SSPC apparatus in terms of generation rate, it was necessary to exercise extreme care in the relative placement of all parts of the system (sample, filters, light source, etc.). In particular, a considerable amount of time was spent in constructing a sample holder that would allow repeatable and reliable placement of a specimen with respect to the filters and the chopped light source. A slight rotational placement error, for example, results in an appreciable change in generation rate. Additionally, calibration of the SSPC apparatus was periodically checked with a set of unirradiated samples to ensure that g remained invariant during the course of the investigation.

It was considered desirable to check the calibration of the SSPC apparatus against an independent measurement method. Diffusion-length determinations by the steady-state surface photovoltage method were made on several samples, and results of the SSPC--SPV comparison are discussed in Section 4.4.

3.7 Trapping Effects

Measurements of relative lifetime versus injected-carrier density were made on representative bulk silicon samples with sandblasted surfaces upon receipt from Centralab (prior to the generation-rate calibration) to determine whether steady-state photoconductivity measurements were affected by minority-carrier trapping. The shape of lifetime-versus-excess-density curves at low injection levels reveals whether trapping is important.[22,23] The SSPC apparatus was employed for these measurements in the following way. Excess density Δn, due to chopped-light illumination, was determined in the usual manner (Section 2.1). We can express Δn as

$$\Delta n = g\tau = g'I\tau , \qquad (14)$$

where g' is a generation constant and I is illumination intensity. A signal proportional to I was measured using a silicon photodiode (refer to Figure 1), and relative lifetime then determined by dividing Δn by this signal.

Rather strong trapping effects were observed for all four low-resistivity ingots. Trapping was also noted for 2.5 and 13 ohm-cm samples.* These results, particularly for 0.1 ohm-cm material, were surprising to us and were not expected based on our previous observations. We have generally observed in the past that trapping effects become less important as resistivity decreases. Additionally, relatively thick Northrop-fabricated 2.5 ohm-cm samples with sandblasted surfaces had been observed earlier to exhibit relatively slight trapping. This observation suggested that the noted trapping effects were associated with surface properties.

A few experiments were performed for the purpose of attaining insight into the nature of the observed trapping effects. Figure 4 shows measured relative lifetime versus excess carrier density for sample FZHD 0.1/1 under three conditions: a) original (as received from Centralab); b) after etching the surfaces with CP-4; c) after sandblasting the etched surfaces. Data are normalized to unity relative lifetime at an injected-carrier density of 3×10^{12} cm^{-3} for convenience of comparison. It is seen that etching enhanced trapping whereas a subsequent sandblasting diminished trapping effects compared to the original sample. The same experiment was performed for a 2.5 ohm-cm sample and a similar result was obtained. There are at least two relevant statements that can be made based on these findings: a) Observed trapping effects are surface related since changing surface properties changes trapping behavior; b) Results obtained following sandblasting

*The observation of relatively strong trapping effects in SSPC measurements as compared to PCD can be explained plausibly in terms of significantly fewer filled traps in the transient measurement case.

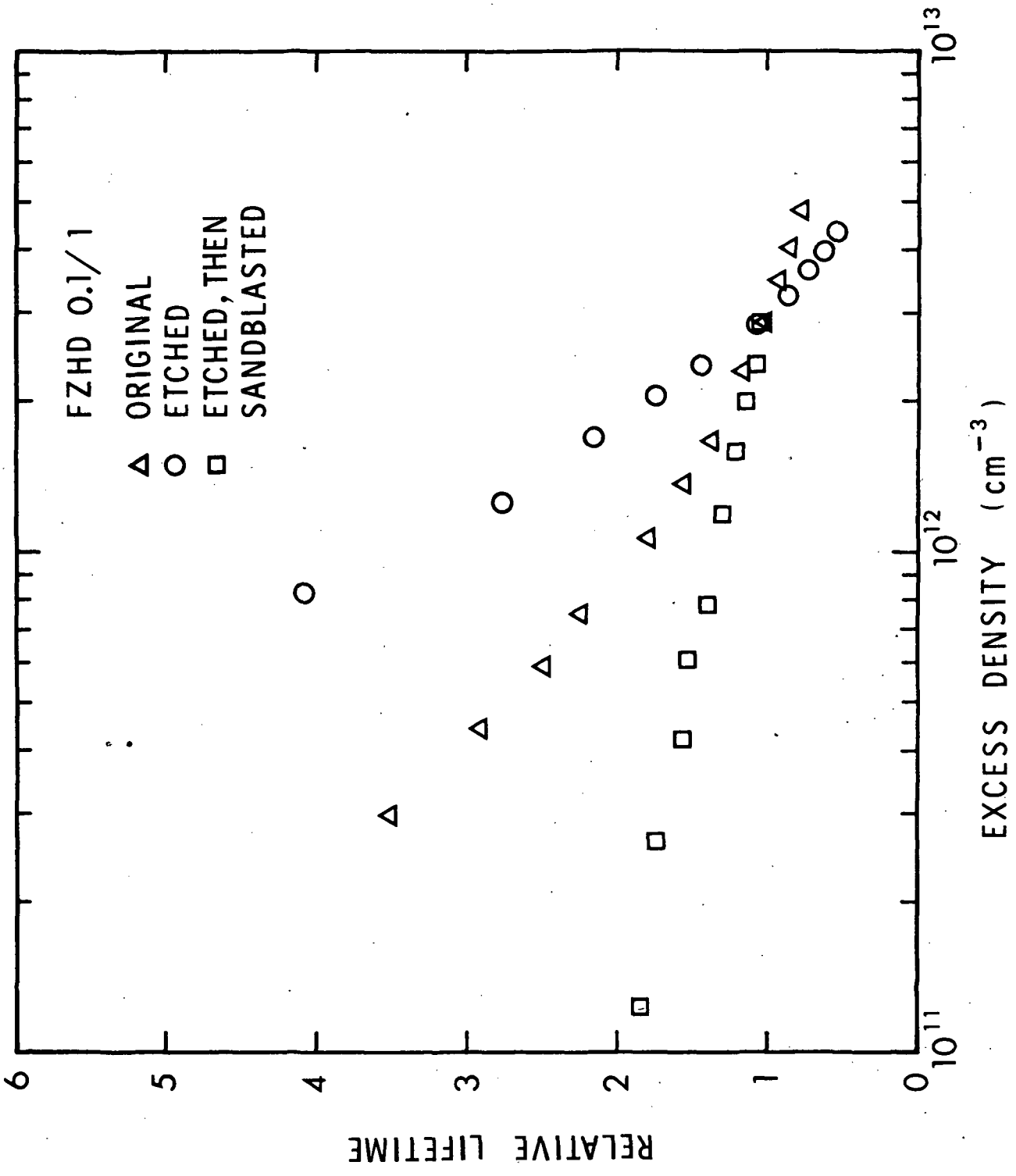

Figure 4. Relative lifetime vs excess carrier density for a 0.1 ohm-cm FZ Si sample after various surface treatments. (The "original" case refers to a Centralab-fabricated sample.)

(after etching) are consistent with findings on Northrop-fabricated sandblasted samples in which trapping effects were observed to be considerably less important than for Centralab samples. Regarding the latter statement, an experiment was performed on sample CZLD 0.1/1 in which lifetime versus excess density curves were obtained before and after a Northrop sandblasting (no etching). Results are shown in Figure 5 and it is seen that Northrop sandblasting did not alter the amount of trapping but merely decreased the amount of light absorbed in this Centralab-fabricated sample by about a factor of two due to reflectivity changes.

The experiments described above aimed at determining the nature and origin of observed trapping effects are obviously incomplete. Further study was beyond the scope of the present work (particularly in view of the successful use of non-penetrating light to fill traps in Centralab-fabricated samples as described below). One might argue that all samples could be etched and then sandblasted to reduce trapping. However, it would be very difficult to control such processing so that surface optical properties had the required sample-to-sample uniformity that is necessary in making accurate measurements of lifetime using the SSPC apparatus. It is quite likely that Centralab-fabricated samples have the required uniformity although they also have the trapping problem. We decided to employ unmodified Centralab bulk Si samples (in conjunction with non-penetrating light) to measure lifetimes and subsequently obtain damage coefficients.

A common approach to separating trapping and recombination is to employ a background (unchopped) light to keep the traps filled which then permits observation of steady-state photoconductivity signals that are not influenced by trapping. As traps are filled by an increasingly intense background light, the observed signal will decrease until a saturation is reached which corresponds to the low-injection-level value of carrier lifetime. Further increases of background lamp intensity beyond this saturation point will not result in further changes in the photoconductivity signal. (Eventually, at excess densities higher than under consideration here, lifetime will become injection-level dependent and the above statement will no longer hold.) Our first approach to filling traps was to employ penetrating background illumination (i.e., unchopped filtered light). However, it was found that at the highest available background lamp intensity all the traps were not yet filled. With an increasingly intense lamp, there is the problem of heating the Si filter. Bandgap changes with temperature will alter the spectrum of transmitted light, which is an undesirable effect. Assuming that observed trapping was surface related, then the utilization of non-penetrating light to fill surface traps is appropriate. It was decided that non-penetrating light was probably the best solution to the trapping problem, and to implement this approach several small lamps were installed near the sample holder in the SSPC apparatus (see Figure 1). Light from these lamps does not pass through the Si filter and is thus highly absorbed

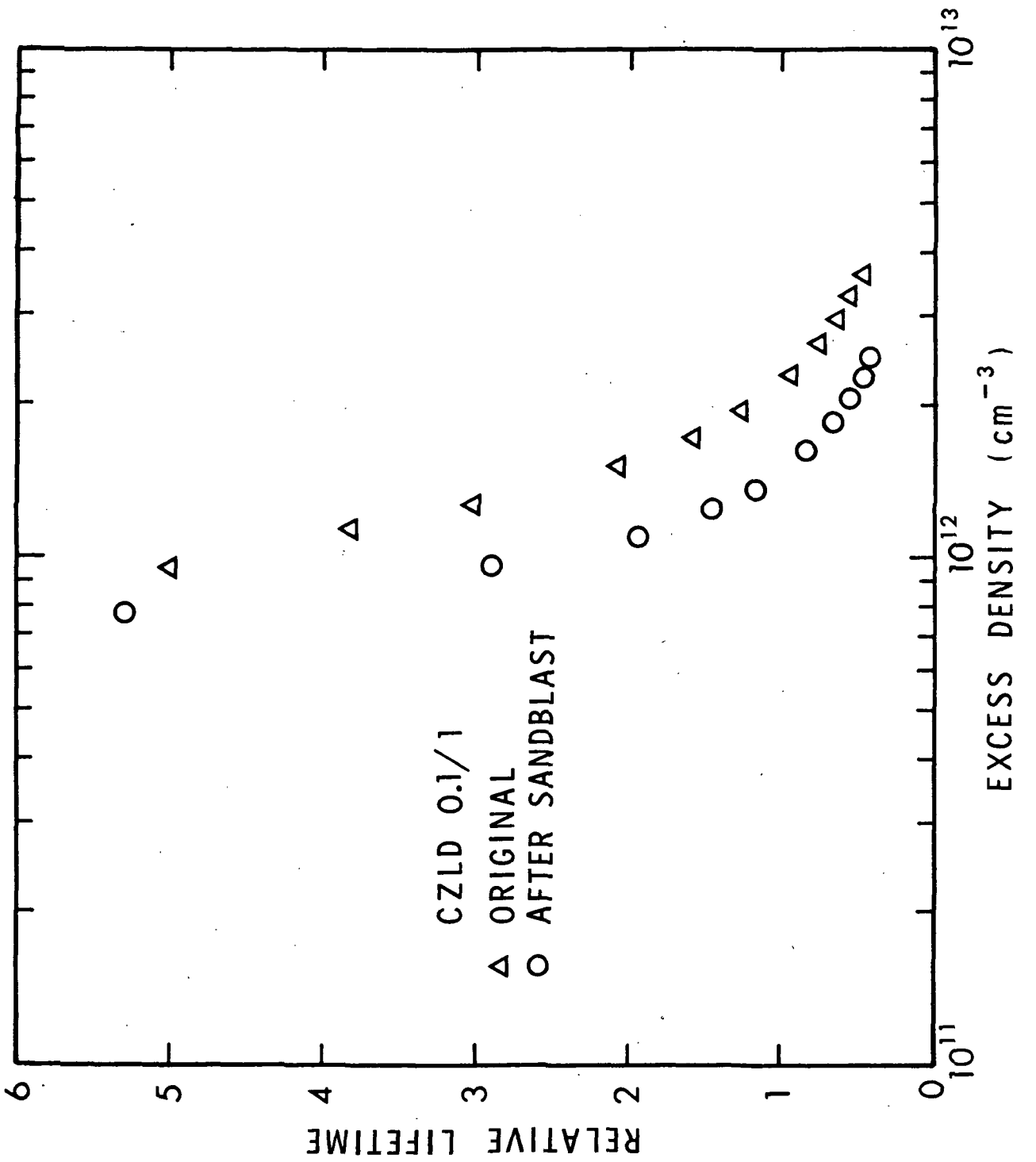

Figure 5. Relative lifetime vs. excess carrier density for a 0.1 ohm-cm CZ Si sample before and after Northrop sandblasting. (The "original" case refers to a Centralab-fabricated sample.)

near the surface of a bulk Si sample. The placement of the background lamps was such that uniform illumination of the front and rear surfaces of a given sample resulted.

Steady-state photoconductivity measurements were then made for one unirradiated sample of each type to determine whether the background lamps could fill traps completely. For all samples examined, a saturation condition was reached in which further increases in background (unchopped) lamp intensity did not cause a change in the chopped-light signal. This experiment demonstrated that nonpenetrating light can be used to separate trapping and recombination, thus permitting measurement of pre-irradiation lifetime for all specimens.

In the course of examining background light effects, it was observed that the lamp intensities required to completely fill traps resulted in sample heating. Heating occurred rather slowly ($\sim 1^{\circ}$ per min for the first few minutes), and we therefore adopted the approach of performing photoconductivity measurements in a time ≤ 1 min after the background lamps were turned on. Taking data in this manner presented no problem and allowed the undesirable effects of a sample temperature rise to be avoided.

Upon discovering the unexpectedly strong trapping effects for bulk samples, it became apparent to us that even if trapping and recombination could be separated before irradiation using an appropriate background lamp, this would possibly be difficult to accomplish after irradiation. This situation would not arise, however, if the following reasoning holds. If it is assumed that the traps in question are located at the surface, that the surface recombination velocity is infinite, and that any increase in surface trap concentration due to irradiation is negligible compared to that already present, then the lamp intensity required to fill surface traps will be invariant with irradiation. This will be true since the lifetime at the surface is assumed to be zero and thus that portion of the excess carrier density at the surface that is available for filling traps will not be affected by irradiation (surface lifetime cannot experience a further decrease). If the above model is not an accurate description of the physical situation for the samples in question, then it is possible that an increasingly intense background lamp would be required following irradiation to fill traps. This situation would occur if the fraction of injected carriers available for trapping at a given lamp intensity decreases as bulk lifetime decreases due to irradiation. In this case, one quickly reaches experimental limitations imposed by the choice of an appropriate background lamp.

To assess our ability following irradiation to separate recombination and trapping using background lamps, a trial 1.0-MeV electron irradiation was performed to a fluence of 3×10^{14} electrons/cm^2. A careful post-irradiation examination of bulk silicon specimens revealed that with the

background-lamp set-up described above all traps could be filled, even though lifetimes were significantly degraded, thus permitting measurement of post-irradiation lifetime. Somewhat more intense illumination was required to fill traps compared to the pre-irradiation situation. It now appeared that we could separate trapping and recombination and accurately measure lifetimes in irradiated bulk samples. (As discussed in Section 4.0, for certain cases in subsequent irradiations measured diffusion lengths appeared to saturate at high fluences, and this behavior is attributed to radiation-induced trapping effects.)

3.8 Surface Recombination--Experimental Considerations

The employment of a high surface recombination velocity as a boundary condition for bulk silicon specimens was selected on the basis of reproducibility and stability of surface properties. Although techniques for producing low-s surfaces exist, it was felt that a considerable technical effort would have been necessary to ensure that a selected technique would repeatably produce surfaces with a very low surface recombination velocity that did not vary with time. On the other hand, sandblasting is known to produce high-s surfaces and, as shown in Section 3.1, s can vary from $\sim 10^4$ cm/sec to infinity without significantly affecting measured photoconductivity signal. In this section, we describe a few preliminary experiments relating to surface recombination effects and also discuss considerations regarding the s-value employed for Centralab-fabricated bulk samples.

3.8.1 Simulation of Zero and Infinite Surface Recombination Velocity with a Diffused Sample

During the course of deciding on an appropriate boundary condition for bulk samples, an approach was suggested by NASA-Lewis personnel which, in principle, would allow one to achieve a condition of either $s = 0$ or $s = \infty$ on the same sample. Figure 6 shows a schematic representation of such a specimen. The diffused region between the ohmic contacts wraps around to the other side of the specimen and covers most of the non-contacted surface area. The sample is assumed to be prepared from p-type starting material with an n^+ diffusion. With lead A grounded, minority carriers created in the p-type material by illumination will be collected at the n^+-p junction if they are within a diffusion length of it. Since the junction acts as a minority-carrier sink, a condition of $s = \infty$ is simulated. With lead A open-circuited, a condition of $s = 0$ is simulated.

The above approach was experimentally examined using the SSPC apparatus. Centralab fabricated five n-on-p samples for us with the geometry shown in Figure 6. They utilized 10 ohm-cm p-type material for these specimens. Measurement of the steady-state photoconductivity signal was made with

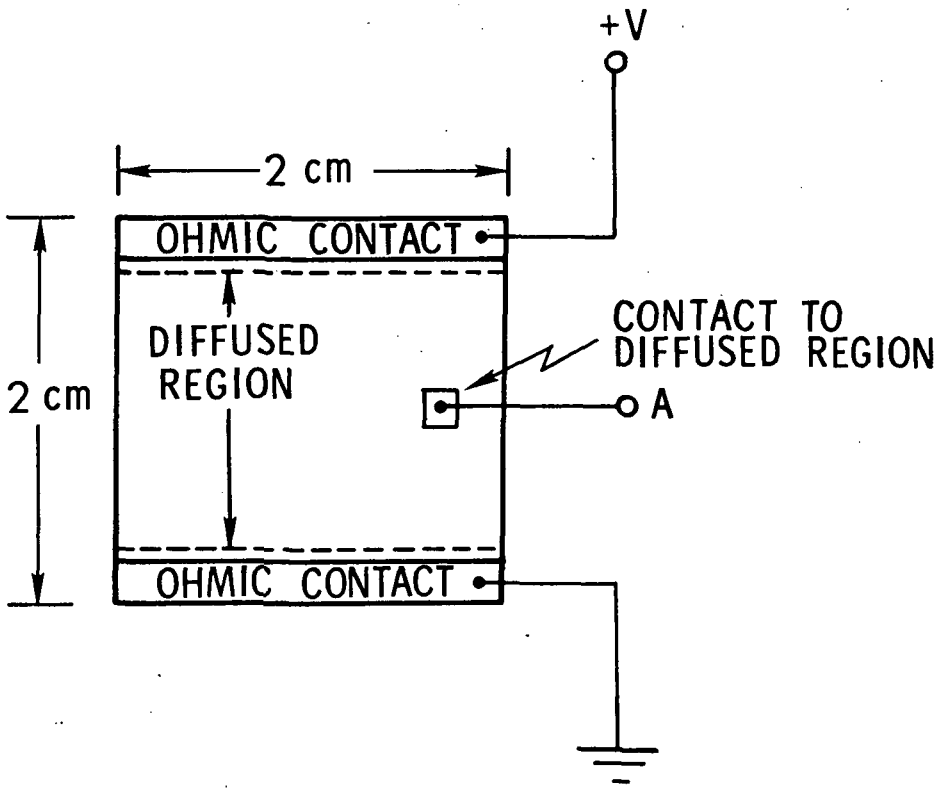

Figure 6. Schematic representation of a diffused sample used to simulate conditions of s = 0 and s = ∞.

the diffused region open-circuited and with this region grounded for all five units. The following open-circuit-to-grounded photoconductivity-signal ratios were obtained for samples 1 through 5 respectively: 5.4, 3.0, 1.1, 3.1, and 2.1. The larger open-circuit signal observed is consistent with the expectation of a low surface recombination velocity for such a configuration.

Considering the result for sample #1, Figure 3 reveals that a value for τ_{eff}/τ of 0.19 (= 1/5.4) occurs for a bulk diffusion length of ~190 μm (using the s = 0 and s = ∞ curves). For 10 ohm-cm p-type material, a pre-irradiation diffusion length of 190 μm is reasonable for a solar cell, which suggests that the sample structure employed can be effectively utilized to simulate conditions of s = 0 and s = ∞. However, it is obvious that additional study, both experimental and analytical, would be necessary before one could have confidence in such an approach to steady-state lifetime measurements on thin samples. In particular, a detailed analysis of the open-circuit condition is needed to demonstrate how closely a zero surface recombination velocity is approximated. We conclude that the diffused-sample approach to simulating conditions of s = 0 and s = ∞ appears promising, but additional work would be required to raise our level of understanding of this method to the point where it could be confidently employed in steady-state lifetime measurements.

3.8.2 Measurement of the Thickness Dependence of Lifetime for a Sandblasted Bulk Sample

An experiment was performed to examine the thickness dependence of measured minority-carrier lifetime in a bulk silicon sample with sandblasted surfaces. The purpose of this study was to compare theory with experimental findings and thus evaluate the accuracy with which we could correct for surface recombination effects during steady-state-photoconductivity measurements of lifetime on solar-cell-size bulk silicon samples with sandblasted surfaces. A sample was prepared from ingot CZ 2.5 (actual sample resistivity = 2.7 ohm-cm) and measured 30.2 x 6.89 x 6.82 mm after lapping to remove saw damage and subsequent sandblasting of all surfaces with 320 mesh silicon carbide. Ohmic contacts were prepared on the end faces using ultrasonic soldering techniques. Forward and reverse resistance measurements indicated no rectification at room and dry ice temperatures. Lifetime was measured using photoconductivity decay. The observed decay was exponential, yielding a value of 44 μsec, and no trapping effects were observed. Such a situation is ideal for transient measurements of lifetime. Steady-state photoconductivity measurements were also made, as discussed below.

Figure 7 shows measured lifetime (PCD) versus sample thickness. The original sample was cut into two pieces which were 4.1 and 2.4 mm thick after lapping to remove saw damage and then sandblasting. Lifetime for

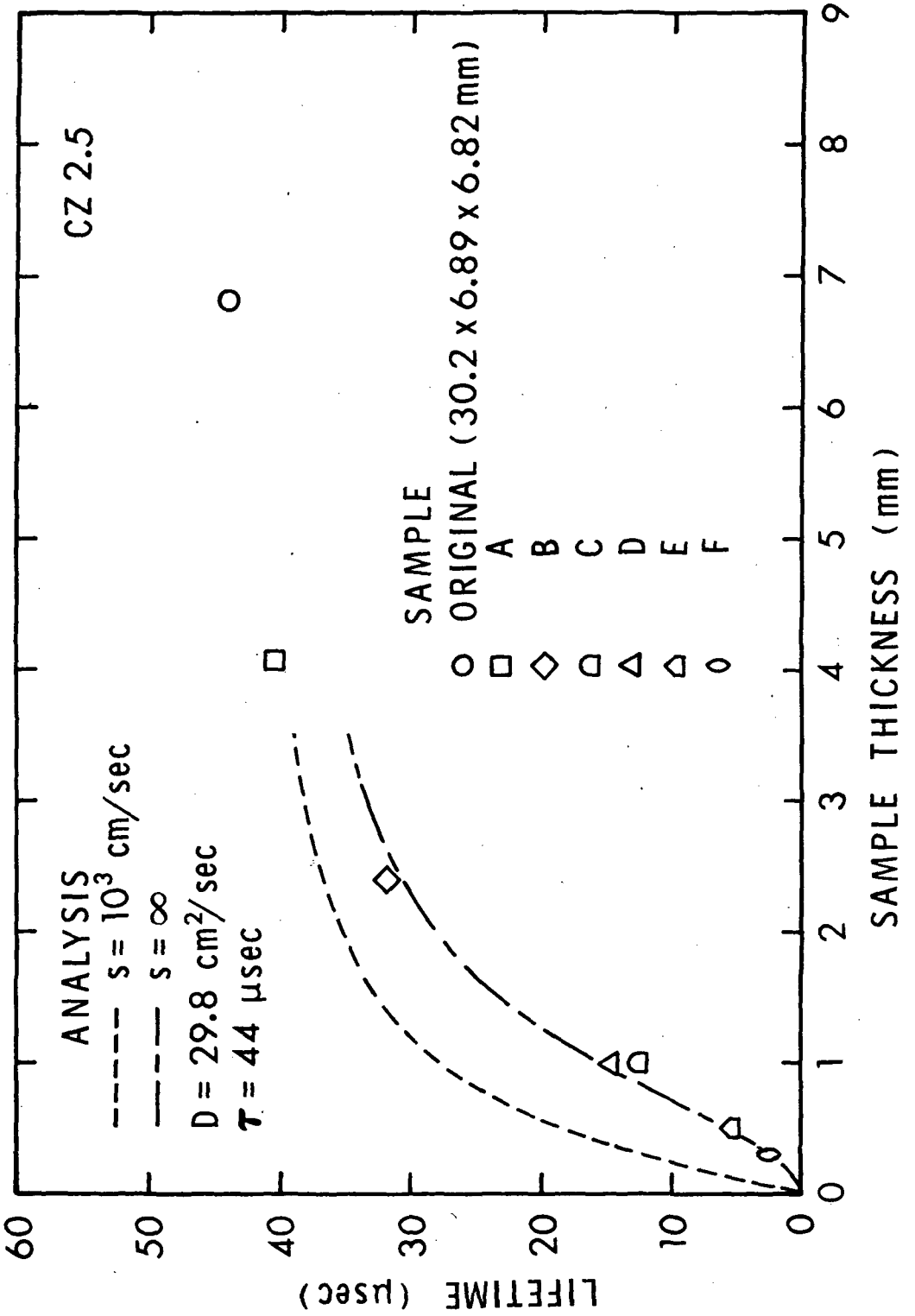

Figure 7. Measured lifetime (PCD) versus sample thickness for a 2.7 ohm-cm boron-doped silicon sample. Shown for comparison are analytical results for two values of surface recombination velocity using a one-dimensional model.

sample A (4.1 mm) was measured on two consecutive days to check repeatability. A slight difference was observed (~6%) which probably reflects experimental error or possibly a small temperature difference. To obtain samples C and D, sample B was cut into two equal-thickness pieces. As shown in Figure 7, measured lifetimes for these samples are in reasonable agreement. To obtain sample E, sample C was lapped down to half its original thickness and then sandblasted. Sample F was obtained by lapping sample E. Following lapping and a light sandblasting of the surfaces, the sample thickness was 0.31 mm, which is nearly the same as the thickness of bulk samples prepared by Centralab and utilized here for damage coefficient determinations. To examine for possible changes in effective lifetime due to changes in surface properties with time, lifetime measurements were repeated five weeks later for several samples (A, D, and E). Within a few per cent, lifetime was found to be invariant over this time period.

For purposes of analysis, Equation 6 was employed. Because this expression is one-dimensional (i.e., assumes two of the sample dimensions are large compared to the third), it does not apply for large sample thicknesses, and this point should be kept in mind when comparing experimental and analytical results (Figure 7). A value for electron mobility of 1150 $cm^2/V\text{-}sec$ was assumed, yielding a D value of 29.8 cm^2/sec. For bulk lifetime τ, the value measured for the original sample (44 μsec) was employed, resulting in a bulk diffusion length of 362 μm. Effective lifetime was calculated as a function of sample thickness for two values of surface recombination velocity, and results are shown in Figure 7. For $s = \infty$, agreement with experiment is good for 0.31, 0.5, 1, and 2.4 mm specimens. For the thicker samples, Equation 6 is not applicable. Note that the measured lifetime at 0.31 mm is only 6% of that for the original sample, and for $s = \infty$ the theory predicts a value for effective lifetime that is in excellent agreement. For $s = 10^3$ cm/sec, however, the predicted value at 0.31 mm is a factor of ~5 too large. The assumed bulk value of 44 μsec could possibly be too small due to surface effects even on the largest sample. However, a larger value of τ would result in an even greater discrepancy between theory and experiment for $s = 10^3$ cm/sec. Consideration of experimental results and analysis leads us to conclude that the surface recombination velocity for a sandblasted surface is indeed large, as expected, and that measurements agree closely enough with theory to allow a reasonably accurate correction for surface recombination effects in the present investigation.

Steady-state photoconductivity measurements were also made versus sample thickness using the SSPC apparatus. For these measurements, the thickness of the Si filter was 2.5 mm. Since this filter thickness is $\leq$ the sample thickness for the original sample and for samples A and B, a nonuniform excess carrier density results in these samples, which

complicates data interpretation. Therefore, measurements on relatively thin samples (C through F) are more readily interpretable. Upon comparing [relative τ (1 mm)/relative τ (0.5 mm)] for steady-state measurements with the corresponding absolute quantity for transient data (Figure 7), reasonable agreement (within ~15%) was found. Once again, the indication is that the experimental situation is understood well enough to be able to apply the theory directly in accounting for the effects of surface recombination.

3.8.3 Surface Recombination Velocity for Bulk Specimens

As discussed in Section 3.1, Equation 10 was employed to correct measured effective lifetimes for the effects of surface recombination. An iterative procedure was utilized with this equation to obtain actual bulk diffusion length. As a starting point, we assumed $s = \infty$ and then substituted various values of L into Equation 10. This procedure did not work for any of the Centralab-fabricated bulk samples; no finite value of L would yield a value for τ_{eff} as large as those measured, assuming infinite s. This result suggested that s was actually less than infinite for Centralab-fabricated samples. As discussed above, measurements of lifetime versus sample thickness for a CZ 2.5 specimen with Northrop-sandblasted surfaces were made, and excellent agreement was found between analysis and experiment when infinite s was assumed. This finding strongly indicated that the Northrop surface treatment results in an infinite surface recombination velocity. Centralab also sandblasted sample surfaces after preparation, but subsequently it became apparent that there were differences between the surface optical properties of Northrop-sandblasted samples and Centralab samples. At a given light intensity, measured excess carrier density was significantly larger in the Centralab case, indicating more energy absorption in the sample bulk. This observation is also consistent with less recombination of excess carriers at the surface for Centralab samples (fewer surface recombination centers) and thus a smaller s. More concrete evidence for a smaller s was sought, along with an appropriate method for determining s for Centralab samples. The procedure followed is now described.

Samples from three higher-resistivity Northrop-supplied ingots were also fabricated by Centralab (FZ 2.5, CZ 2.5, and FZ 13). For these ingots, we had on hand accurate (negligible trapping effects) PCD lifetime measurements for large bulk samples where surface effects can be neglected. For FZ 2.5 and FZ 13, we had fabricated a large number of bulk samples on another program three years ago and then measured pre-irradiation values of τ. These existing data were used to obtain an average bulk lifetime for each of the two ingots under consideration. Next, all measured pre-irradiation values of τ_{eff} for each of these ingots were averaged, as were sample thicknesses, resistivities, and assumed mobilities. This procedure thus yielded average values for the following quantities for each of two ingots based on a rather large number of samples: τ_{eff}, τ (and

hence L), T, and D. Next, these average values were employed in Equation 10 and the value of s that would then satisfy the equation was then determined. For FZ 2.5 and FZ 13, we obtained $s = 8.3 \times 10^3$ cm/sec and $s = 8.0 \times 10^3$ cm/sec, respectively. The same procedure was followed for ingot CZ 2.5 except that only one bulk lifetime value was available ($\tau = 44$ μsec). Using average values for τ_{eff}, T, and D along with this value of τ, a value of $s = 8.5 \times 10^3$ cm/sec resulted. The evidence thus strongly indicated that the surface recombination velocity for Centralab-fabricated samples is slightly less than 10^4 cm/sec. Referring to Figure 3, it is seen that the difference between analytical results for $s = 10^4$ and $s = \infty$ is relatively small. However, in attempting to correct values of τ_{eff} for the effects of surface recombination in the present investigation, one cannot employ $s = \infty$ for Centralab samples. Based on the above results, a value of $s = 8.3 \times 10^3$ cm/sec was assumed for all bulk silicon samples under study, and τ was determined using Equation 10 in the manner described above. As discussed above, in terms of obtaining K_L it is not necessary to perform a correction for surface effects. This correction is obviously necessary, however, if one wishes to determine actual pre-irradiation lifetimes and diffusion lengths.

3.9 Determination of Oxygen Concentration

An attempt was made to determine oxygen concentration in the four 0.1 ohm-cm silicon ingots employed in this investigation by using the infrared absorption method (ASTM Designation F-121-70 T). To perform this measurement for FZ material, a specimen with negligible oxygen concentration is required as a reference. A piece of oxygen-free material was supplied to us by Dow Corning and this piece, along with four low-resistivity slices (one per ingot) were mechanically polished according to specified ASTM procedures. For comparison, a slice from ingot CZ 2.5 was also prepared for determination of oxygen content. Initial measurements were made using Beckman IR-4 and IR-20A spectrophotometers. Subsequently, a Beckman Model 4250 IR spectrophotometer was employed.

Measurements at room temperature on CZ 2.5 revealed the expected absorption peak at 9 μm due to oxygen. However, in room temperature measurements on all four low-resistivity slices no transmission was observable for wavelengths ≥ 5 μm, thus preventing the observation of 9-μm absorption. Comparison of these negative results with the findings for CZ 2.5 suggests that the problem with measurements on 0.1 ohm-cm material is lack of transmission due to free carrier absorption. According to ASTM Designation F-121-70 T, free carrier absorption should not be a problem for resistivities greater than 0.01 ohm-cm in the method being employed. We also made measurements on low-resistivity Czochralski material at liquid nitrogen temperature for the purpose of freezing out majority carriers and thus decreasing free carrier absorption. Per cent transmission

increased at wavelengths considerably less than 9 μm, but once again no transmission was observed at 9 μm. Other workers have also been unable to observe transmission through 0.1 ohm-cm silicon slices and were thus unsuccessful in determining oxygen content.[24]

It was subsequently learned[25] that the ASTM statement regarding applicability of the method for resistivities ≥0.01 ohm-cm is in error and should actually be ≥0.1 ohm-cm. Measurements on 0.1 ohm-cm Czochralski material are quite difficult and apparently are not possible on float-zone material of that resistivity. To make measurements on Czochralski material, one apparently must violate ASTM procedures and make the test specimen thin enough (≤0.5 mm) to permit transmission. Additionally, the slit on the spectrophotometer should be opened as wide as permissible, given the 32 cm^{-1} room temperature line width, scale expansion should be employed, and a slow scan should be performed.

The above approach was employed to measure the oxygen concentration in a thin (0.35 mm) polished CZHD 0.1 slice using a Beckman Model 4250 dual-beam spectrophotometer. Transmission was observed at 9 μm, and the oxygen absorption was a small perturbation on the free carrier absorption of about 50 cm^{-1}. The observed absorption coefficient of 0.9 cm^{-1}, corrected for lattice band absorption, corresponds to an oxygen concentration of about 4×10^{17} cm^{-3}. The observed linewidth exceeded the expected 32 cm^{-1} by 40%, however, so that the observed peak absorption is an underestimate in view of the excessive slitwidth having been employed.

3.10 Pre-irradiation Properties of Bulk Samples and Solar Cells

Table VI lists bulk silicon samples employed in the present investigation. Shown are resistivities and pre-irradiation values for effective lifetime, actual lifetime, and actual diffusion length. Also listed are irradiating particle energies for each sample and additional information regarding special conditions for certain specimens. As indicated, post-irradiation annealing studies were performed for selected samples at either room temperature (RT) or 60°C. Additionally, two samples were irradiated in the dark with 10-MeV protons to examine the effect of illumination on K_L.

Table VII lists pre-irradiation properties of solar cells obtained using a solar simulator. Cells with the designation "dose monitor" were irradiated for the purpose of obtaining a rough check on fluences received by comparing cell degradation with that expected based on previous findings (such as Reference 11). For the cells listed in Table VII, solar-simulator current-voltage characteristics were obtained following each bombardment, and data are presented in Section 4.0. Also in that section are results of diffusion length measurements (using a Co-60 source) for these cells and other units.

Sample Designation	Pre-Irradiation Resistivity ohm-cm	τ_{eff} μsec	τ μsec	L μm	Irradiating Particle Energy, MeV	Comments / Special Condition
FZLD 0.1/1	0.106	7.21	37.1	201	0.5	RT anneal
4	0.110	7.09	25.5	167	"	-
5	0.105	7.55	46.5	225	"	-
6	0.105	7.54	37.1	201	"	-
8	0.108	7.22	27.0	172	1.0	RT anneal
10	0.108	7.08	34.2	193	"	60°C anneal
11	0.109	7.26	27.5	173	"	-
12	0.108	7.49	34.2	193	"	-
13	0.105	7.60	52.9	240	"	-
14	0.107	7.43	36.2	199	2.5	RT anneal
15	0.109	6.71	22.7	157	"	-
16	0.105	7.25	40.6	210	"	-
17	0.105	7.12	30.5	182	"	-
18	0.107	7.38	41.5	213	10	RT anneal
19	0.110	6.90	24.0	162	"	60°C anneal
20	0.105	7.30	42.4	215	"	-
21	0.107	6.96	33.5	191	"	-
22	0.105	7.56	54.3	243	"	-
FZHD 0.1/4	0.100	5.69	15.3	129	10	-
5	0.095	6.03	19.1	146	0.5	RT anneal
6	0.097	5.97	20.0	148	"	-
7	0.096	5.93	20.4	149	"	-
8	0.099	5.87	18.7	143	"	-
11	0.099	5.99	20.7	149	1.0	RT anneal
12	0.096	5.93	20.4	149	"	60°C anneal
13	0.093	6.37	25.9	168	10	unilluminated
14	0.096	6.14	21.9	155	1.0	-
15	0.097	5.73	17.7	139	"	-
16	0.099	5.92	19.6	146	"	-
17	0.096	5.85	18.5	142	2.5	RT anneal
18	0.095	5.99	21.0	151	"	-
19	0.096	6.24	23.0	158	"	-
20	0.094	6.02	21.4	153	"	-
21	0.095	6.03	20.7	150	10	RT anneal
22	0.095	6.17	22.2	156	"	60°C anneal
23	0.094	6.10	22.3	156	"	-
24	0.094	6.08	21.2	152	"	-
25	0.097	5.73	18.3	141	"	-

TABLE VI

Pre-irradiation lifetimes and diffusion lengths for bulk silicon specimens of various resistivities.

Sample Designation	Resistivity ohm-cm	Pre-Irradiation τ_{eff} μsec	Pre-Irradiation τ μsec	Pre-Irradiation L μm	Irradiating Particle Energy, MeV	Comments / Special Condition
CZLD 0.1/3	0.117	1.45	1.84	44.7	0.5	RT anneal
5	0.112	1.62	2.15	48.4	"	-
6	0.111	1.46	1.89	45.4	"	-
7	0.113	1.52	1.98	46.5	"	-
8	0.110	2.00	2.76	54.8	10	-
9	0.112	1.66	2.16	48.5	1.0	RT anneal
10	0.111	1.74	2.30	50.0	"	60°C anneal
11	0.114	1.76	2.34	50.5	"	-
12	0.116	1.60	2.10	47.8	"	-
13	0.114	1.78	2.36	50.7	"	-
14	0.110	1.86	2.54	52.6	2.5	RT anneal
15	0.113	1.65	2.17	48.6	"	-
16	0.115	1.68	2.19	48.8	"	-
17	0.115	1.82	2.42	51.3	"	-
18	0.114	1.83	2.48	52.0	10	RT anneal
19	0.112	1.66	2.21	49.0	"	60°C anneal
22	0.113	1.73	2.30	50.0	"	-
23	0.112	1.68	2.21	49.0	"	-
24	0.111	1.51	1.96	46.2	"	-
CZHD 0.1/1	0.112	2.38	3.53	62.0	0.5	RT anneal
5	0.108	2.33	3.59	62.5	"	-
6	0.111	2.20	3.25	59.5	"	-
7	0.109	2.04	2.98	57.0	"	-
8	0.108	2.45	3.85	64.8	1.0	RT anneal
9	0.105	2.75	4.74	71.8	"	60°C anneal
10	0.109	2.18	3.26	59.6	"	-
11	0.103	2.49	4.00	66.0	"	-
12	0.108	2.74	4.63	71.0	"	-
13	0.109	2.38	3.63	62.8	2.5	RT anneal
14	0.109	2.01	2.90	56.2	"	-
15	0.112	2.04	2.93	56.5	"	-
16	0.112	2.08	3.00	57.2	"	-
17	0.111	2.00	2.88	56.0	10	RT anneal
18	0.112	2.04	2.90	56.2	"	60°C anneal
19	0.109	2.45	3.74	63.8	"	-
20	0.108	2.48	4.06	66.5	"	-
21	0.112	2.02	2.90	56.3	"	-

TABLE VI (continued)

Sample Designation	Resistivity ohm-cm	Pre-Irradiation τ_{eff} μsec	Pre-Irradiation τ μsec	Pre-Irradiation L μm	Irradiating Particle Energy, MeV	Comments/ Special Condition
FZ 2.5/2	2.57	3.63	25.1	288	0.5	-
4	2.56	3.70	42.6	375	"	-
5	2.43	3.95	73.2	485	1.0	-
6	2.34	4.16	140	670	"	-
7	2.47	3.77	38.2	353	2.5	-
8	2.50	3.97	72.1	485	"	-
9	2.60	3.82	46.1	390	10	-
10	2.43	3.55	48.6	407	"	-
11	2.46	4.01	87.7	535	"	-
CZ 2.5/3	2.57	3.77	24.6	285	0.5	-
4	2.54	3.91	30.4	315	"	-
5	2.57	3.78	26.3	295	1.0	-
7	2.60	3.95	37.1	350	"	-
8	2.53	3.76	24.5	283	2.5	-
11	2.39	4.30	40.4	360	10	-
12	2.38	4.55	63.1	450	"	-
13	2.41	4.16	116	610	2.5	-
15	2.45	4.00	86.1	530	10	-
16	2.53	4.04	99.6	570	"	-
CZ 6/1	6.49	3.98	11.4	198	0.5	-
2	5.57	4.30	14.4	226	1.0	-
3	5.90	4.35	15.5	234	2.5	-
4	5.93	3.29	7.27	157	10	-
5	6.63	3.69	9.32	177	"	unilluminated
6	5.93	4.46	16.9	239	"	-
FZ 13/2	13.5	3.65	48.6	411	0.5	-
7	15.4	3.92	117	638	"	-
8	13.7	3.47	29.5	320	1.0	-
9	12.6	3.76	56.8	440	"	-
10	12.5	3.55	48.6	407	10	-
11	13.6	3.64	87.3	551	"	-
13	13.4	3.69	131	675	2.5	-
14	12.6	3.78	126	655	"	-
15	12.7	3.76	55.5	435	10	-
18	12.3	3.82	119	630	"	-

TABLE VI (continued)

Solar Cell Designation	Pre-Irradiation I_{sc} mA	V_{oc} mV	P_{max} mW	Irradiating Particle Energy, MeV	Comments
FZLD 0.1/SC2	65.0	617	28.8	1.0	1 cm x 2 cm
4	64.5	615	28.0	10	"
FZHD 0.1/SC1	61.2	612	27.5	1.0	"
2	62.5	613	28.4	10	"
CZLD 0.1/SC2	53.7	605	23.3	1.0	"
3	54.2	600	22.0	10	"
CZHD 0.1/SC2	58.5	605	24.9	1.0	"
3	58.2	605	25.5	10	"
CZ 2.5/SC2	65.4	578	27.6	1.0	"
3	66.5	578	28.1	10	"
CZ 9/SC2	144	548	57.2	0.5	2 cm x 2 cm (dose monitor)
3	145	550	57.5	1.0	"
4	145	550	57.2	2.5	"
CZ 2.5/SC4	67.2	578	28.5	10	1 cm x 2 cm) (dose monitor)

TABLE VII

Pre-irradiation electrical properties of n-on-p silicon solar cells of various base resistivities (AMO, 140 mW/cm^2, ~27°C).

SECTION 4.0

RESULTS

In this section, experimental results of this investigation are presented. Included are data showing the degradation of diffusion length for electron- and proton-irradiated bulk samples and solar cells of various resistivities. Damage coefficients are determined as a function of resistivity and device and bulk behavior are compared. Results of annealing studies on irradiated bulk specimens are given. Degradation with irradiation of solar cell parameters obtained using a solar simulator is presented. A comparison is made of data obtained using both steady-state photoconductivity and steady-state surface photovoltage methods.

4.1 Results of Electron Irradiations

Tables VIII through X list diffusion length as a function of fluence for bulk silicon samples irradiated with 0.5-, 1.0-, and 2.5-MeV electrons, respectively. For the purpose of determining damage coefficients the quantity $(L^{-2} - L_0^{-2})$ was plotted versus fluence, and a unity slope fit to data on a log-log plot yields a value for K_L (refer to Equation 1).

4.1.1 0.5-MeV Electrons

Figure 8 presents data for 0.5-MeV electron-irradiated specimens of various resistivities. With the exception of data for CZ 6/1 and CZ 9/SC2, all data points shown are averages for samples of a given type (refer to Table VIII). Unity-slope lines fit most of the data, with a few exceptions. Data for CZLD 0.1 and CZHD 0.1 at the lowest fluence appear to be inaccurate, which is probably attributable to experimental error since only a very slight degradation in L occurred at this fluence. At the highest fluences, a saturation is beginning to occur for CZLD 0.1 and CZHD 0.1. (This effect was more markedly observed at higher energies, and these findings are discussed below.) Data for FZ 13 cannot be fit with a line of unity slope. The reason for this is unknown, but is possibly attributable to experimental errors associated with the relatively small amount of damage introduced or to an error in measured L_0. To obtain K_L for FZ 13 samples, values of $(L^{-2} - L_0^{-2})$ at the highest fluence were employed since these values are the least affected by errors in L_0. For other resistivities, K_L corresponds to the dashed-line fits in Figure 8.

Figure 9 presents K_L vs resistivity for 0.5-MeV electron-irradiated specimens. It is seen that the bulk data fall into two groups and both can be fit with a line of slope equal to -0.67. The fit for CZLD 0.1, CZHD 0.1, and CZ 6 yields values of K_L that are larger by a factor of ~ 3 than those obtained from the fit for FZLD 0.1, FZHD 0.1, FZ 2.5, CZ 2.5, and FZ 13 if com-

Sample	Pre-irradiation	3×10^{13} e/cm^2	1×10^{14}	3×10^{14}	10^{15}	3×10^{15}
FZLD 0.1/1	201 μm	163 μm	118 μm	76.5 μm	-	-
4	167	162	115	74.6	43.8 μm	28.6 μm
5	225	175	124	77.0	46.0	29.1
6	201	162	126	79.0	46.4	29.8
FZHD 0.1/5	146	126	106	-	-	-
6	148	131	112	73.2	43.1	29.0
7	149	132	110	75.2	47.0	29.8
8	143	132	108	72.0	46.4	29.4
CZLD 0.1/3	44.7	42.8	-	-	-	-
5	48.4	49.1	42.4	36.3	28.7	25.0
6	45.4	44.8	41.5	34.9	28.8	24.3
7	46.5	46.8	41.4	36.1	27.8	24.0
CZHD 0.1/1	62.0	56.5	48.6	38.2	28.2	-
5	62.5	55.8	50.5	39.4	30.0	24.9
6	59.5	52.0	48.5	38.1	28.6	24.0
7	57.0	52.6	47.0	37.5	29.9	24.9
FZ 2.5/2	288	293	264	189	126	83.9
4	375	363	292	232	137	85.0
CZ 2.5/3	285	282	247	183	118	71.2
4	315	310	282	196	122	79.2
CZ 6/1	198	193	172	134	93.8	62.7
FZ 13/2	411	379	260	216	161	129.5
7	638	600	305	249	189	151.1

TABLE VIII

Diffusion length as a function of fluence for 0.5-MeV electron-irradiated bulk silicon specimens.

Sample	Pre-irradiation	3×10^{13} e/cm^2	1×10^{14}	3×10^{14}	10^{15}	3×10^{15}
FZLD 0.1/8	172 μm	76.8 μm	42.6 μm	27.7 μm	-	-
10	193	80.4	44.6	27.6	-	-
11	173	82.0	44.2	28.4	23.0 μm	22.0 μm
12	193	83.4	49.5	29.1	22.4	23.4
13	240	88.0	47.3	30.4	23.9	23.3
FZHD 0.1/11	149	78.1	47.0	-	-	-
12	149	74.5	46.3	-	-	-
14	155	76.2	45.0	28.4	23.3	22.9
15	139	73.9	43.5	28.7	21.9	23.8
16	146	71.5	43.5	28.9	23.7	22.9
CZLD 0.1/9	48.5	36.8	-	-	-	-
10	50.0	37.8	-	-	-	-
11	50.5	37.4	30.7	24.3	21.9	20.4
12	47.8	36.2	30.0	23.5	21.2	21.3
13	50.7	39.5	33.1	24.5	20.8	21.3
CZHD 0.1/8	64.8	47.7	34.2	25.4	23.4	-
9	71.8	51.0	33.6	27.8	23.7	-
10	59.6	45.0	33.4	25.3	22.7	22.0
11	66.0	46.3	33.4	26.8	24.1	22.7
12	71.0	48.5	33.6	25.1	22.8	22.6
FZ 2.5/5	485	217	128	72.0	42.6	27.6
6	670	150	138	77.2	45.2	29.7
CZ 2.5/5	290	179	120	71.3	42.2	29.6
7	350	193	124	72.5	43.8	30.1
CZ 6/2	226	156	104	66.0	38.5	24.8
FZ 13/8	320	226	170	113	78.3	52.2
9	440	305	188	120	79.4	54.7

TABLE IX

Diffusion length as a function of fluence for 1.0-MeV electron-irradiated bulk silicon specimens.

Sample	Pre-irradiation	3×10^{13} e/cm^2	1×10^{14}	3×10^{14}	10^{15}	3×10^{15}
FZLD 0.1/14	199 μm	39.5 μm	26.7 μm	23.6 μm	-	-
15	157	39.9	25.8	23.7	22.3 μm	22.2 μm
16	210	41.3	27.4	24.6	23.1	22.0
17	182	39.8	26.4	24.4	22.4	22.0
FZHD 0.1/17	142	39.5	26.9	-	-	-
18	151	39.9	26.7	24.9	23.8	23.3
19	158	42.3	27.1	25.9	24.0	23.3
20	153	41.8	28.4	24.9	23.6	23.3
CZLD 0.1/14	52.6	31.0	-	-	-	-
15	48.6	29.7	24.4	22.3	21.6	21.9
16	48.8	30.1	24.5	21.7	21.0	20.6
17	51.3	29.8	24.2	22.1	21.3	21.2
CZHD 0.1/13	62.8	32.7	24.5	23.7	22.7	-
14	56.2	32.0	24.9	23.7	23.1	22.5
15	56.5	30.2	23.9	23.0	22.3	22.1
16	57.2	31.2	23.9	22.7	22.0	22.0
FZ 2.5/7	353	102	61.4	39.7	24.8	20.1
8	485	103	61.7	39.7	25.4	20.3
CZ 2.5/8	283	94	58.9	37.6	24.5	20.5
13	610	102	62.7	40.9	25.7	21.6
CZ 6/3	234	101	63.6	39.9	24.4	17.1
FZ 13/13	675	184	112	73.3	42.5	29.8
14	655	193	115	71.4	42.6	30.0

TABLE X

Diffusion length as a function of fluence for 2.5-MeV electron-irradiated bulk silicon specimens.

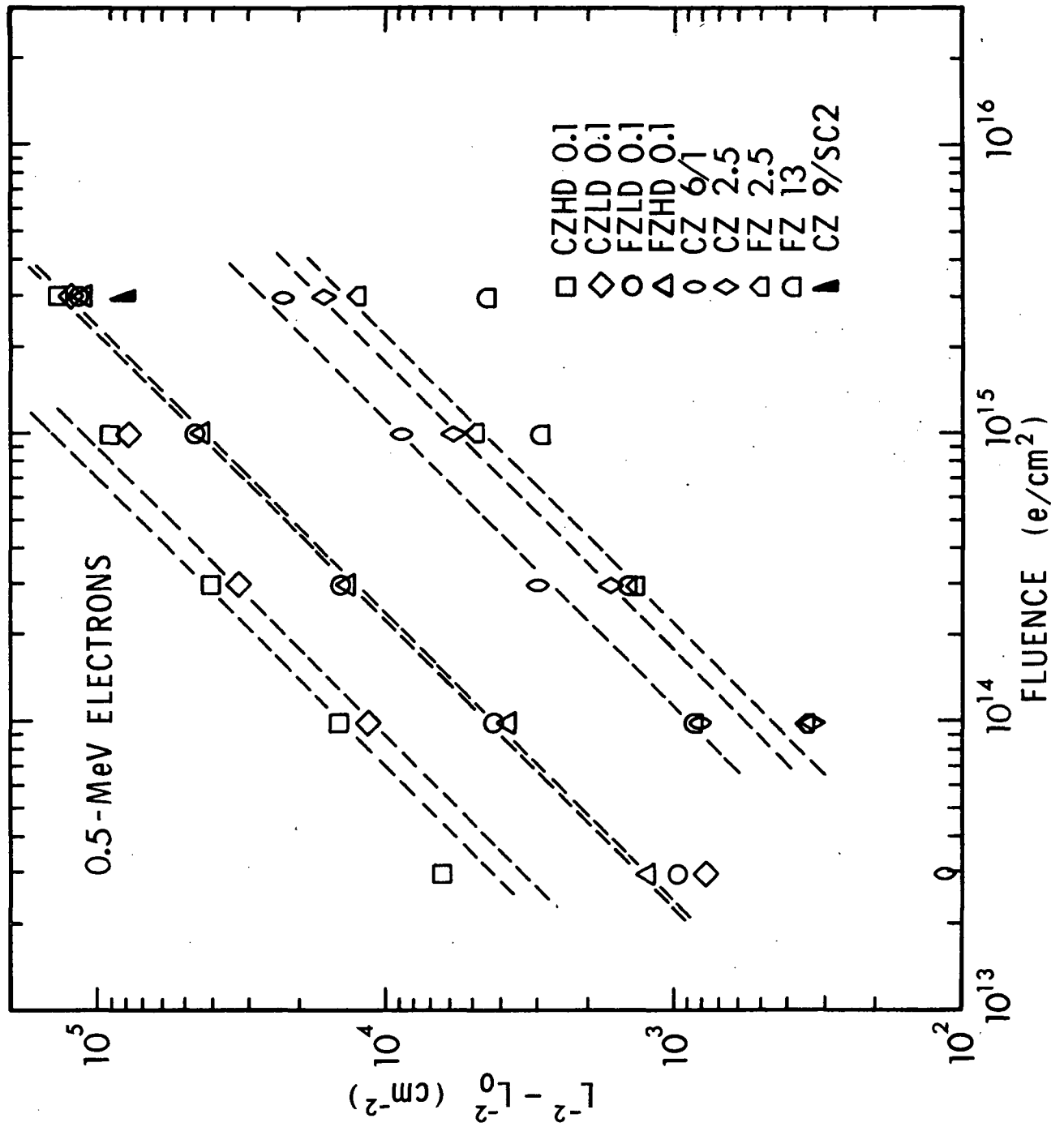

Figure 8. The quantity ($L^{-2} - L_0^{-2}$) vs fluence for 0.5-MeV electron-irradiated bulk silicon specimens. A data point obtained from an irradiated solar cell is also shown.

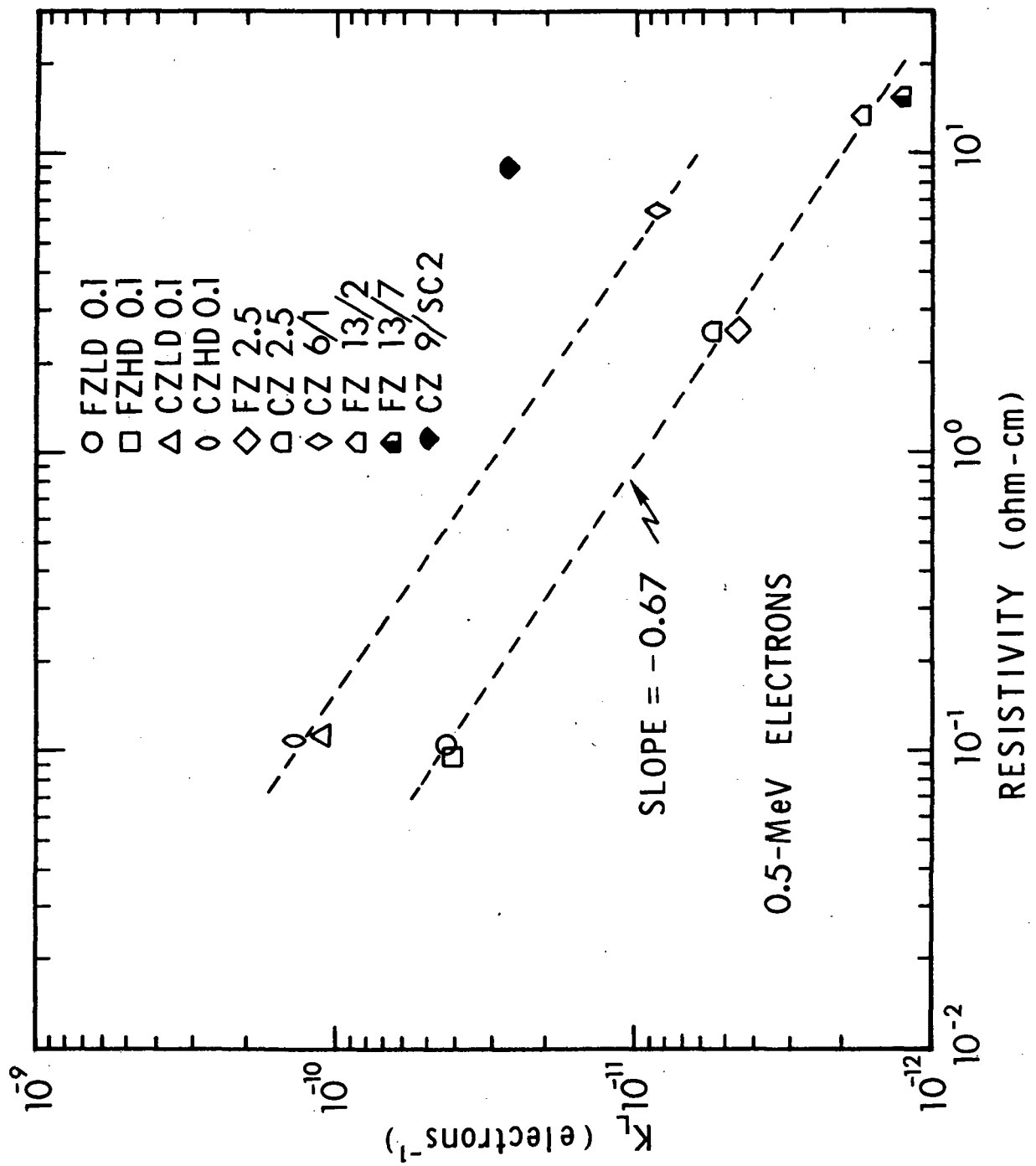

Figure 9. Damage coefficient vs. resistivity for 0.5-MeV electron-irradiated specimens.

parison is made at a given resistivity. Except for the CZ 2.5 result, these findings are consistent with observations of others[26,27] that FZ solar cells are more tolerant of electron irradiation than are CZ units. (This observation and others presented below for different energies lead us to suspect that ingot CZ 2.5 was actually FZ material. However, infrared absorption measurements on a sample from this ingot revealed an absorption peak at 9 μm, which is characteristic of a large oxygen content. Thus, ingot CZ 2.5 appears to be CZ material. It is not clear at present why damage coefficients for specimens from this ingot exhibited behavior consistent with that for FZ material.) A larger K_L for CZ material indicates that the presence of oxygen enhances production of those defects primarily responsible for diffusion-length degradation.

Figure 9 reveals that K_L-values for FZLD 0.1 and FZHD 0.1 are nearly identical. Damage coefficient values for CZLD 0.1 and CZHD 0.1 are also in good agreement with each other. This observation indicates that there is no significant dependence of K_L on dislocation density for 0.1 ohm-cm material bombarded with 0.5-MeV electrons. (Additional discussion relating to this point is given in the Appendix.)

One solar cell data point is shown in Figure 9. It is seen that the K_L value for CZ 9/SC2 is a factor of ~ 4 larger than that expected on the basis of findings for CZ bulk samples. Further comparisons of solar-cell and bulk findings are discussed below.

As discussed in Section 2.2, an incident 0.5-MeV electron degrades in energy to ~ 0.44 MeV by the time it reaches the center of a bulk sample with a thickness of 0.3 mm. Thus, the bulk damage effects presented above are more appropriately associated with an average electron energy of ~ 0.44 MeV rather than the incident particle energy. (This consideration can account for a portion of the difference between solar cell and bulk material damage coefficients (at 0.5 MeV) because the SSPC measurement technique samples damage throughout the entire test specimen whereas solar cell measurements are presumably only affected by damage within a diffusion length of the n^+p junction).

4.1.2 1.0-MeV Electrons

Figure 10 presents data for 1.0-MeV electron-irradiated bulk samples and solar cells. Low-resistivity specimens exhibit linear degradation with fluence at low fluences, but exhibit saturation at high fluences (i.e., an apparent sharply decreased defect introduction rate). We defer additional discussion of observed saturation effects to Section 4.3. Higher resistivity samples also indicate a deviation from linearity at high fluences. (At the highest fluence, the onset of carrier removal was noted for the higher resistivity specimens. The resistivity increase in FZ 13 samples was ~ 7% and was ~ 3% for FZ 2.5 and CZ 2.5.) Data for several solar cells (FZLD 0.1/SC1 and SC2, CZLD 0.1/SC1 and SC2) were obtained at two fluences and the observed degradation with fluence is close to linear for these two cell types. However, the two

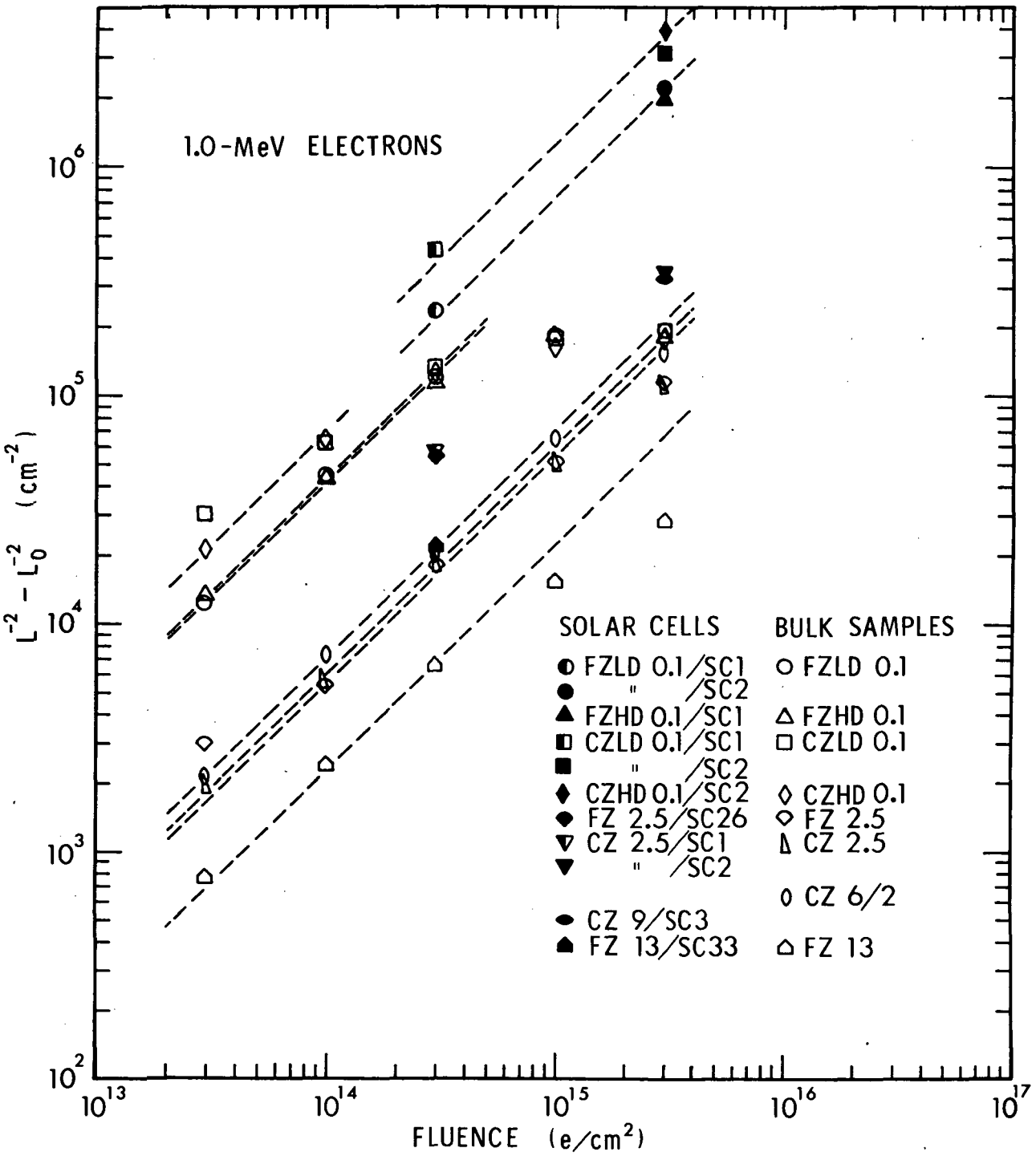

Figure 10. The quantity ($L^{-2} - L_0^{-2}$) vs. fluence for 1.0-MeV electron-irradiated bulk silicon specimens and silicon solar cells.

solar-cell data points for ingot CZ 2.5 (SC1 and SC2) cannot be fit with a unity-slope line. The degradation rate is apparently lower at the higher fluence examined. This result is qualitatively consistent with the observations of Meulenberg and Treble[28] who noted a fluence dependence of K_L for 1.0-MeV electron-irradiated solar cells (~ 9 ohm-cm).

Data corresponding to linear degradation regions (i.e., good fits to unity-slope lines in Figure 10) were used to determine damage coefficients for bulk samples and Figure 11 presents the results along with comparison data (for solar cells) obtained by other workers.[28-30] For the present solar-cell findings, data in Figure 11 represent K_L-values obtained at a single fluence. A line with a slope of -0.63 fits several groups of data points well. Findings for FZ bulk samples, and also CZ 2.5, are fit well by such a line. Bulk data for CZLD 0.1, CZHD 0.1, and CZ 6 are fit well by a parallel line. FZ material is again observed to be more radiation resistant than CZ, with the bulk CZ-to-FZ K_L ratio being ~ 1.9, as compared to ~ 3 for 0.5-MeV electron irradiation.

Two data points taken from solar cell findings of Meulenberg and Treble[28] are shown in Figure 11. They observed a fluence-dependent K_L value, and both high- and low-fluence values are given in the figure. It is seen that this range of values overlaps the present solar cell data and bulk sample data. We further note that the fluence dependence of K_L presently observed for CZ 2.5 cells (SC1 and SC2) encompasses a variation of K_L by a factor of ~ 1.7, whereas the variation of K_L for data of Meulenberg and Treble is a factor of ~ 3. This difference is presumably attributable to the fact that their observations were made over a wider fluence range than that examined here.

Also shown in Figure 11 are four data points obtained from the work of Downing et al.[29] The dashed-line fit shown through their data also fits a number of the solar cell data points obtained in the present investigation. Data of Faith[30] are also presented, and the resistivity dependence of K_L is seen to be about the same as for other data in Figure 11, although his K_L-values are somewhat larger.

Low-resistivity solar cell data in Figure 11 are observed to be consistent with their bulk-sample counterparts in that values of K_L for CZ cells are a factor of ~ 1.9 larger than those for FZ units. Additionally, as was the case for 0.5-MeV electron-irradiated specimens, there appears to be no significant dependence of K_L on dislocation density for low-resistivity bulk samples or sclar cells. We further note that K_L-values for low-resistivity solar cells are a factor of ~ 1.8 larger than their bulk-material counterparts. For the higher-resistivity cases, solar-cell-to-bulk-material K_L ratios range from ~ 2 to ~ 3.2.

4.1.3 2.5-MeV Electrons

Data for 2.5-MeV electron-irradiated specimens are shown in Figure 12, and saturation effects are observed at all resistivities. This phenomenon is particularly strong for low-resistivity specimens, and to determine K_L for such samples we employed the values of $(L^{-2} - L_0^{-2})$ obtained at the lowest

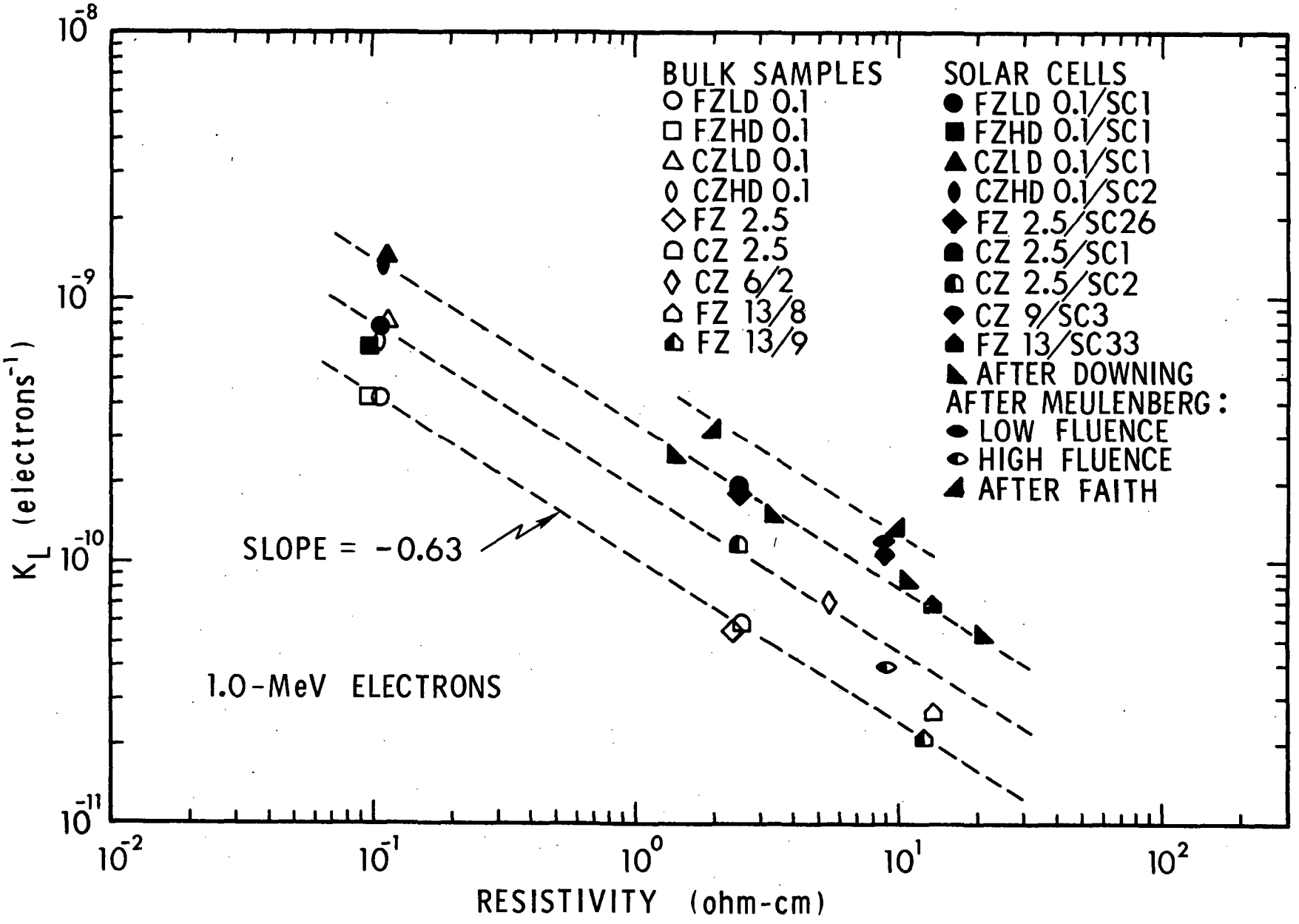

Figure 11. Damage coefficient vs. resistivity for 1.0-MeV electron-irradiated bulk silicon specimens and silicon solar cells.

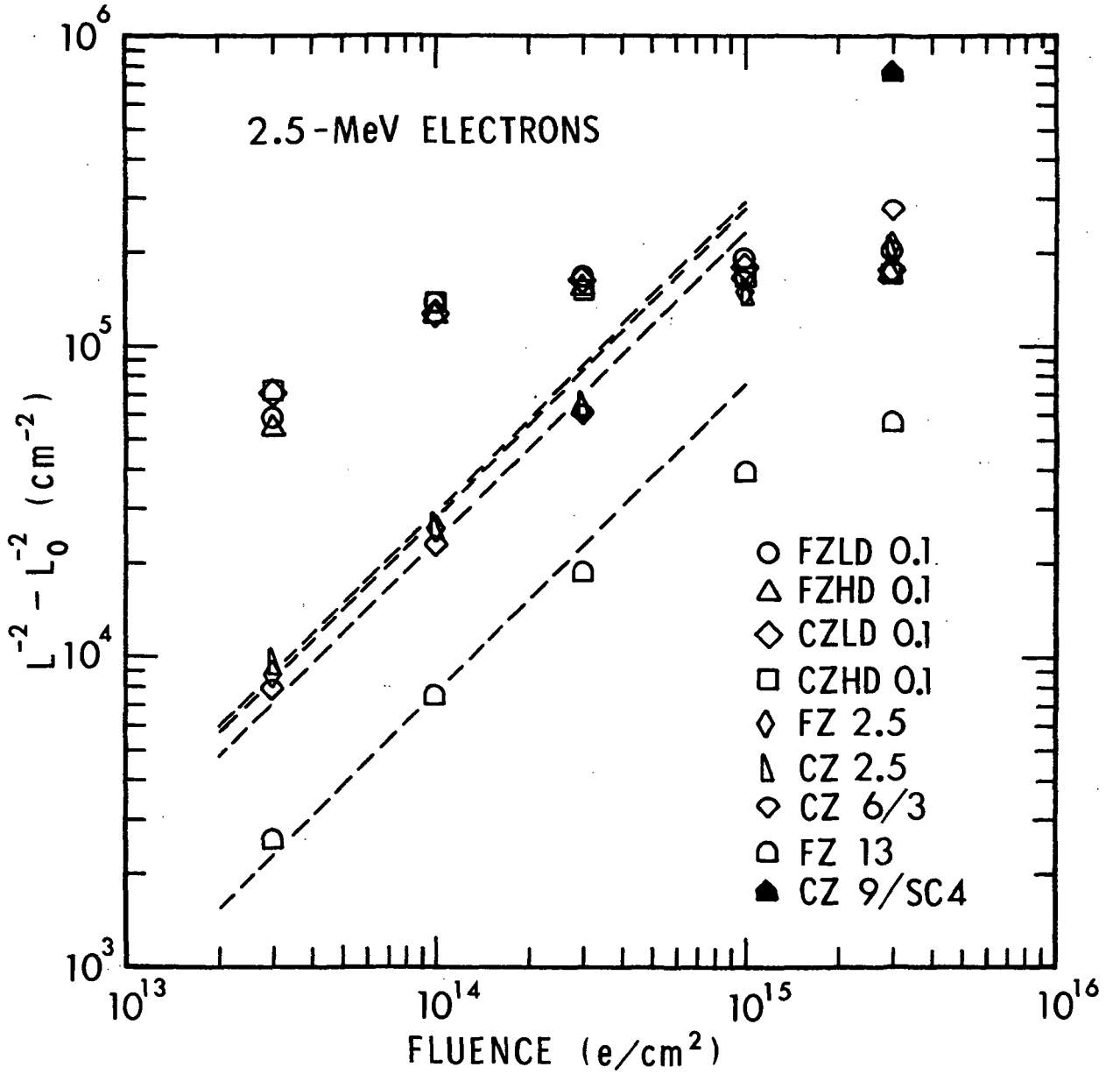

Figure 12. The quantity ($L^{-2} - L_0^{-2}$) vs. fluence for 2.5-MeV electron-irradiated bulk silicon specimens. A data point obtained from an irradiated solar cell is also shown.

fluence (3×10^{13} e/cm^2). Damage coefficients obtained in this manner can be considered lower limits to actual values. As was the case for 1.0-MeV electron irradiation, carrier removal was observed here also. At the highest fluence, resistivity increases of ~25% for FZ 13 and ~ 6% for FZ 2.5 and CZ 2.5 were noted.

Figure 13 presents damage coefficient vs resistivity and it is seen that most of the data are fit well by a line with a slope of -0.67. Based on the CZ 6/3 data point, a CZ-to-FZ K_L ratio of ~ 1.6 is obtained. Low-resistivity samples do not exhibit such a ratio, but those data are most likely influenced somewhat by the saturation effect. As observed in Figures 8 and 10, differences between FZ and CZ material diminish as saturation is approached. We further note that the one solar cell data point in Figure 13 (CZ 9/SC4) would yield a solar-cell-to-bulk-material K_L ratio of ~ 1.4 if one were to extrapolate a line of -0.67 slop through the CZ 6/3 data point to 9 ohm-cm. (It is probably inappropriate to compare K_L for the CZ cell with the straight-line fit for higher-resistivity FZ material.)

4.1.4 Electron Energy Dependence of Damage Coefficient

Average damage coefficients for three resistivities are shown in Figure 14 for the three electron energies utilized in this study. (Data labeled FZ 0.1 represent an average for both FZLD 0.1 and FZHD 0.1 samples.) For comparison, findings of Downing et al.[29] for 3.3 ohm-cm solar cells are also presented. Upon comparing their data with the present FZ 2.5 findings, it is seen that the solar-cell-to-bulk-material K_L ratio tends to decrease with increasing electron energy. We also note that K_L falls off more sharply with decreasing energy for the present data than for that of Downing, and thus our findings deviate more strongly than his from theoretical predictions[29] of the energy dependence of K_L.

4.2 Results of 10-MeV Proton Irradiations

Data for 10-MeV proton-irradiated bulk samples and solar cells are listed in Table XI and shown in Figures 15 and 16. In Figure 15, saturation effects are again evident, particularly for low-resistivity samples (discussed in Section 4.3). Additionally, a fluence dependence of the degradation rate is evident for solar cells. Also shown are data obtained at 9×10^{11} p/cm^2 for two unilluminated bulk specimens. These data indicate slightly lower K_L values for unilluminated samples, but more data are required before a more definitive statement can be made.

The first 10-MeV proton irradiation was performed at a fluence of ~ 10^{11} p/cm^2, followed by ~ 3×10^{11} (cumulative) and 1.2×10^{12} p/cm^2. Carrier removal effects were negligible at this fluence for all resistivities examined. At this point, saturation effects were quite evident and thus it did not appear to be informative to irradiate the original group of bulk samples to an even higher fluence. However, it was obvious that data for fluences lower than 10^{11} p/cm^2 would be beneficial for the purpose of obtaining damage coefficients, particularly for low resistivity specimens. A subsequent

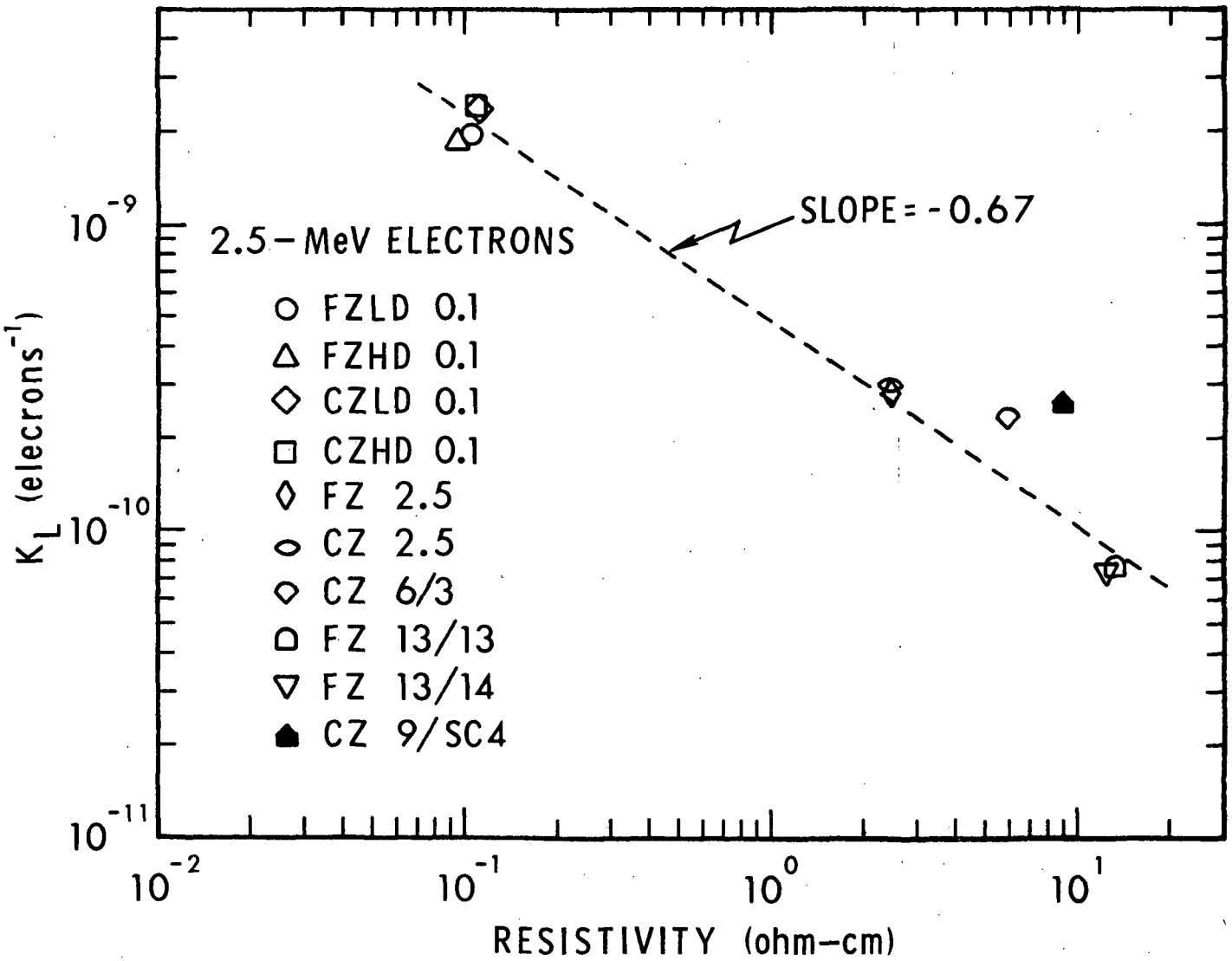

Figure 13. Damage coefficient vs. resistivity for 2.5-MeV electron-irradiated specimens.

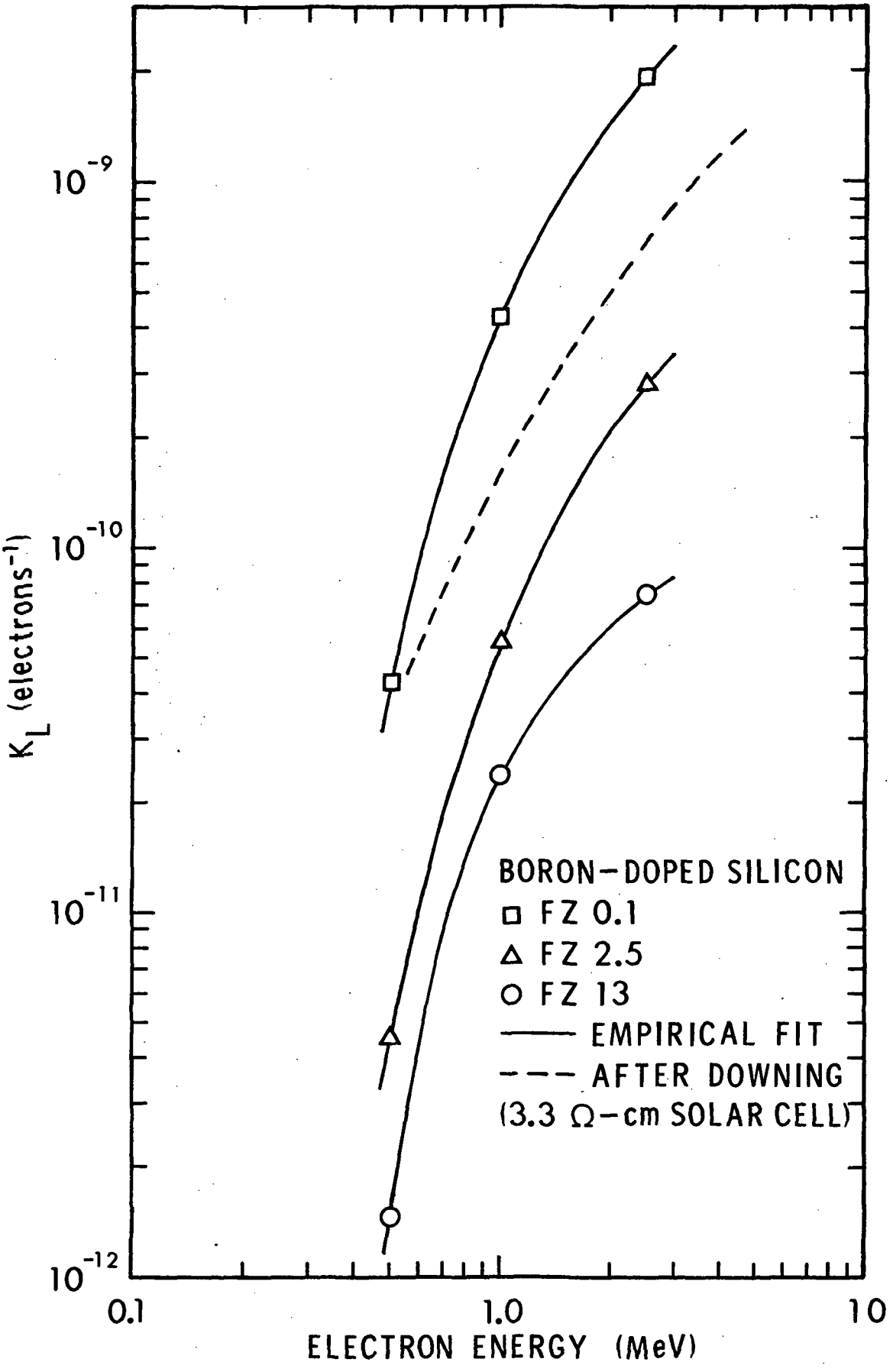

Figure 14. Damage coefficient vs. electron energy for electron-irradiated boron-doped silicon.

Sample	Pre-irradiation	L(μm) @ 2.97×10^{10} p/cm^2	L(μm) @ ϕ (p/cm^2)		L(μm) @ ϕ (p/cm^2)		L(μm) @ ϕ (p/cm^2)	
FZLD 0.1/18	213 μm	-	31.9	9.79×10^{10}	23.1	2.96×10^{11}	22.7	1.20×10^{12}
19	162	-	31.1	1.02×10^{11}	22.2	2.95×10^{11}	21.9	"
20	215	-	30.3	9.91×10^{10}	23.7	2.92×10^{11}	23.3	1.19×10^{12}
21	191	-	29.0	9.91×10^{10}	22.8	"	24.5	"
22	243	-	32.4	1.02×10^{11}	23.3	2.95×10^{11}	22.9	1.20×10^{12}
FZHD 0.1/ 4	129	36.9 μm	-	-	-	-	-	-
13	168	-	-	-	-	-	24.9	9.0×10^{11}
21	150	-	28.8	1.02×10^{11}	24.2	2.95×10^{11}	-	-
22	156	-	29.6	9.94×10^{10}	24.2	2.92×10^{11}	-	-
23	156	-	30.1	1.02×10^{11}	24.5	2.95×10^{11}	24.4	1.20×10^{12}
24	152	-	29.0	9.91×10^{10}	24.2	2.92×10^{11}	23.8	1.19×10^{12}
25	141	-	28.7	1.02×10^{11}	23.7	2.95×10^{11}	23.8	1.20×10^{12}
CZLD 0.1/ 8	54.8	35.3	-	-	-	-	-	-
18	52.0	-	27.6	8.14×10^{10}	-	-	-	-
19	49.0	-	26.2	9.91×10^{10}	-	-	-	-
22	50.0	-	26.6	1.02×10^{11}	21.8	2.95×10^{11}	21.1	1.20×10^{12}
23	49.0	-	25.7	"	22.3	"	21.7	"
24	46.2	-	26.7	"	22.2	"	22.4	"
CZHD 0.1/17	56.0	-	28.4	9.91×10^{10}	22.3	2.92×10^{11}	21.8	1.19×10^{12}
18	56.2	-	26.9	"	21.4	"	22.1	"
19	63.8	-	27.5	1.02×10^{11}	22.1	2.95×10^{11}	22.3	1.20×10^{12}

TABLE XI

Diffusion length as a function of fluence for 10-MeV proton-irradiated bulk silicon specimens.

Sample	Pre-irradiation	L(μm) @ 2.97×10^{10} p/cm^2	L(μm) @	φ (p/cm^2)	L(μm) @	φ (p/cm^2)	L(μm) @	φ(p/cm^2)
CZHD 0.1/20	66.5	-	27.9	1.02×10^{11}	23.8	2.95×10^{11}	23.3	1.20×10^{12}
21	56.3	-	26.2	9.91×10^{10}	23.5	2.92×10^{11}	22.1	1.19×10^{12}
FZ 2.5/ 9	390	-	58.2	"	30.8	"	18.7	"
10	407±	-	-	-	-	-	-	-
11	535	-	64.3	1.02×10^{11}	32.1	2.95×10^{11}	18.2	1.20×10^{12}
CZ 2.5/11	360	104	-	-	-	-	-	-
12	450	111	-	-	-	-	-	-
15	530	-	46.2	8.04×10^{10}	30.3	2.73×10^{11}	20.9	1.17×10^{12}
16	570	-	66.4	1.02×10^{11}	34.4	2.95×10^{11}	19.4	1.20×10^{12}
CZ 6/4	157	81.0	-	-	-	-	-	-
5	177	-	-	-	-	-	21.0	9.0×10^{11}
6	239	-	58.4	8.16×10^{10}	30.5	2.75×10^{11}	17.4	1.18×10^{12}
FZ 13/10	407	150	-	-	-	-	-	-
11	551	162	-	-	-	-	-	-
15	435	-	85.1	1.02×10^{11}	41.9	2.95×10^{11}	24.2	1.20×10^{12}
18	630	-	71.3	9.87×10^{10}	41.1	2.92×10^{11}	24.7	1.19×10^{12}

TABLE XI (continued)

Diffusion length as a function of fluence for 10-MeV proton-irradiated bulk silicon specimens.

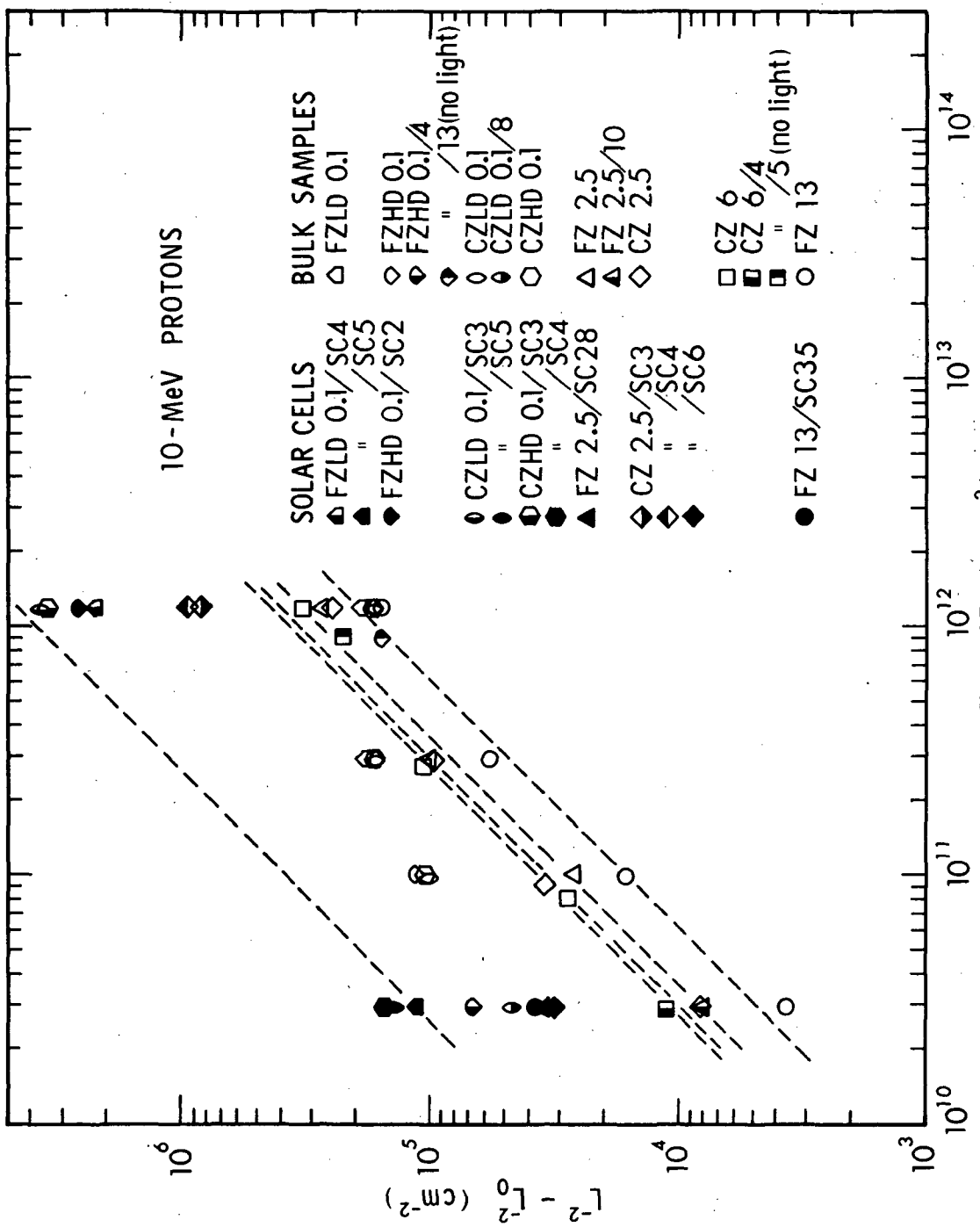

Figure 15. The quantity ($L^{-2} - L_0^{-2}$) vs. fluence for 10-MeV proton-irradiated bulk silicon specimens and silicon solar cells.

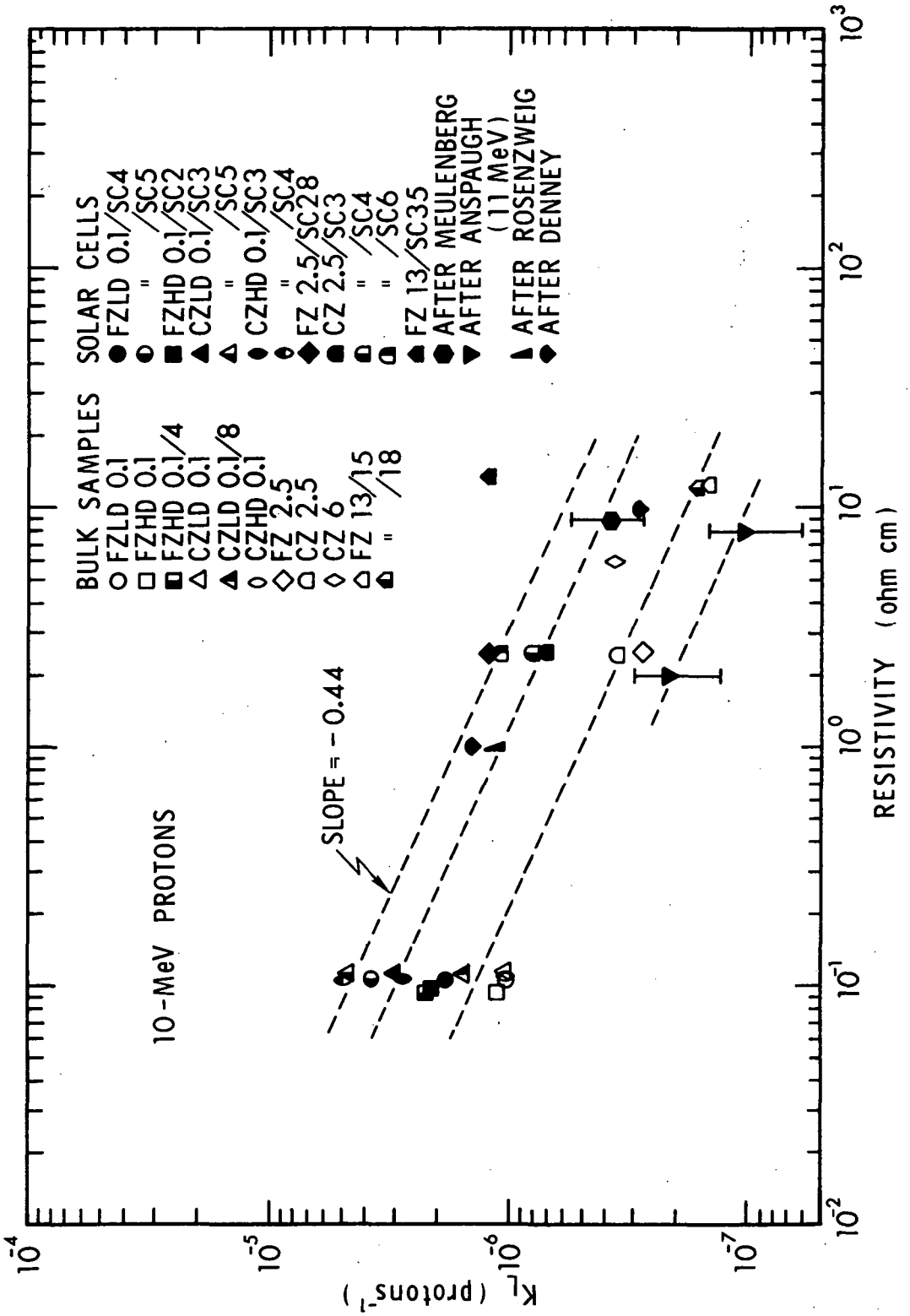

Figure 16. Damage coefficient vs. resistivity for 10-MeV proton-irradiated bulk silicon specimens and silicon solar cells.

irradiation was performed at ~3 x 10^{10} p/cm^2. As seen in Table XI, the number of bulk samples irradiated at this fluence was small. Additional irradiations at relatively low proton fluences on a larger group of low-resistivity bulk samples would clearly have been useful in subsequent K_L determinations.

In Figure 16, K_L is shown vs. resistivity. Values shown for low-resistivity bulk samples are for the two lowest fluences, and the effects of the onset of saturation are evident (lower K_L for the higher fluence). A line with a slope of -0.44 provides a reasonable fit to several groups of data points. Shown for comparison are data obtained by other workers.[28, 31-33] The 11-MeV data of Anspaugh and Carter[31] are somewhat lower than all other K_L values. (The bars shown correspond to the range of values given in Reference 31.) However, their measurements of diffusion length were made at a high injection level, and thus one expects a larger L, and hence a smaller K_L, due to the injection-level dependence of diffusion length. Data of Meulenberg and Treble[28] are also shown, and the bar shown corresponds to the fluence dependence of K_L that they observed. Data obtained by Rosenzweig[33] agree well with the straight-line fit through several of the present solar-cell data points and also data of Meulenberg and Treble. Findings of Denny and Downing[32] are also presented in Figure 16.

Because of observed saturation effects for bulk samples and fluence-dependent K_L-values for solar cells, one must exercise caution when comparing device and bulk damage coefficients in Figure 16. At the lowest fluence, the solar-cell-to-bulk-material K_L ratio for CZ 0.1 is ~3, and this ratio for FZ 0.1 is ~1.7. Upon comparing solar-cell K_L-values obtained at the lowest fluence with bulk material damage coefficients obtained from unity-slope fits to the data (Figure 15), the following ratios result: for FZ 2.5, ~ 4.1; for CZ 2.5, ~ 3.4; for FZ 13, ~ 7.5. The latter value is anomalously high. As seen in Figure 16, K_L for FZ 13/SC35 does not agree with other solar cell data presented; the reason for this discrepancy is unknown at present.

Because of the paucity of low-resistivity data for bulk samples at the lowest fluence and because of saturation effects observed at higher fluences, no conclusion can be reached regarding the effect of dislocation density on K_L for proton-irradiated bulk specimens. However, for low-resistivity solar cells, data for CZLD 0.1 units and CZHD 0.1 devices are in good agreement (Figure 15), which suggests that dislocation density is an unimportant factor for 10-MeV proton damage. (A similar statement can be made for FZLD 0.1/SC4 and FZHD 0.1/SC2.) Regarding differences between FZ and CZ material, Figures 15 and 16 reveal once again that FZ solar cells are more radiation tolerant than their CZ counterparts. For example, the CZ-to-FZ K_L ratio for 0.1 ohm-cm cells at 1.2 x 10^{12} p/cm^2 is ~1.5. For bulk material, upon comparing the K_L value for CZ 6 in Figure 16 with a straight-line fit to data for FZ 2.5 and FZ 13, a ratio of ~ 1.7 is obtained.

4.3 Discussion of Saturation Effects

Saturation effects were observed for irradiated bulk silicon samples in which a departure from linearity was noted in plots of the quantity $(L^{-2} - L_0^{-2})$ versus fluence. Examination of Tables VIII through XI and Figures 8, 10, 12, and 15 reveals that the onset of saturation begins in all cases when L is degraded to a value on the order of 30 μm. Continued irradiation reduces the apparent diffusion length somewhat to a lower limit of ~ 20 μm, and no further degradation is noted. Although such saturation behavior has been previously observed,[34, 35] this effect is clearly not a manifestation of a saturation in the production of recombination centers because solar cells continued to degrade at high fluences while bulk samples saturated.

We have had experimental indications that saturation is attributable to the effects of radiation-induced trapping centers. For heavily degraded samples, it was difficult to achieve a traps-filled condition using background lamps. That is, a slight decrease in observed SSPC signal was noted as the background lamp intensity was increased from about one-half of the maximum value up to the maximum. This was not the case for samples in the linear degradation region. Additionally, photoconductivity-decay lifetime measurements were made for two CZ 2.5 samples: one that had exhibited saturation and another that had not. Distinct differences in behavior were noted for the two samples. The saturation sample exhibited strong trapping behavior consistent with the presence of several types of centers. These centers possessed a range of trapping time constants, including times comparable to and also considerably longer than the lifetime. For this sample, because of trapping effects we were unable to extract a meaningful lifetime value from the observed decay even when a background lamp was employed. On the other hand, for the nonsaturation sample only slight trapping effects were noted. An exponential decay was readily extracted from the observed signal, and the lifetime thus obtained was in good agreement with that determined using the SSPC apparatus.

The above observations suggest that in a heavily irradiated bulk specimen, i.e., one in which L has degraded to ~ 30 μm, traps introduced by radiation begin to have an effect on the SSPC signal. If trapping time constants are comparable to the lifetime, and the number of traps present is appreciable, then the SSPC method will not yield an accurate lifetime value. It will be erroneously high due to trapping, and background illumination does not provide a practical solution to this problem. For the present experiments, in most cases a region of linear degradation of L was observed at lower fluences, which enabled the determination of damage coefficients. Additional study would be necessary to gain a more detailed understanding of observed saturation effects. However, such an understanding is not required to achieve the technical goals of the present investigation.

4.4 Comparison of Steady-State Photoconductivity and Steady-State Surface Photovoltage Measurements

A comparison was made of diffusion lengths measured by two techniques:

steady-state photoconductivity and steady-state surface photovoltage. Four irradiated bulk samples were examined. Following SSPC measurements, sample surfaces were prepared for the SPV technique in the following manner. Surfaces were lapped (6 μm) then polished with Lustrox 1000. After this, surfaces were etched with CP4A followed by HF-H_2O (1:4). Photon intensity vs. reciprocal wavelength is presented in Figure 17 for the four bulk specimens. Extrapolated least-squares fits to the data intercept the abscissa at points numerically equal to bulk diffusion lengths. Table XII compares SSPC and SPV measurements for these specimens.

TABLE XII

Sample	SPV	SSPC	Predicted SSPC L-values based on an extrapolated unity-slope fit
FZLD 0.1/1	97.4 μm	76.5 μm	(not applicable)
CZ 2.5/3	76.4	71.2	"
FZ 13/18	14.4	24.7	20.8 μm
CZHD 0.1/8	6.2	23.4	12.0

Comparison of diffusion lengths measured by SSPC and SPV techniques.

It is seen that agreement between the two methods is reasonably good for long diffusion lengths but is rather poor at short diffusion lengths. However, the two SSPC short diffusion-length values were measured on samples that were heavily irradiated and exhibited saturation in plots of the quantity $(L^{-2} - L_0^{-2})$ vs. fluence. As discussed above, such behavior is most likely due to trapping effects. In an attempt to make a more appropriate SSPC-to-SPV comparison, linear-degradation behavior observed at low fluences was extrapolated to the fluence of interest and an expected value of L (i.e., in the absence of saturation) then calculated. These predicted L-values are also listed in Table XII. Agreement between SSPC and SPV values improves using this procedure, but significant differences still occur, particularly for CZHD 0.1/8.

In Sections 4.1 and 4.2, differences between damage coefficients for solar cells and bulk samples were noted. A comparison is made here of SPV and SSPC findings for the purpose of attempting to account for these K_L differences. Figure 18 compares SSPC and SPV data for FZLD 0.1/1 in a plot of the quantity $(L^{-2} - L_0^{-2})$ vs fluence. Also shown is a similar comparison for CZ 2.5/13. It is seen that SSPC and SPV data agree quite well for CZ 2.5/13. The solar cell data point for CZ 9/SC4 in Figure 18 indicates the rather large device-vs-bulk discrepancy that needs to be accounted for. For sample FZLD 0.1/1, the SPV data point yields

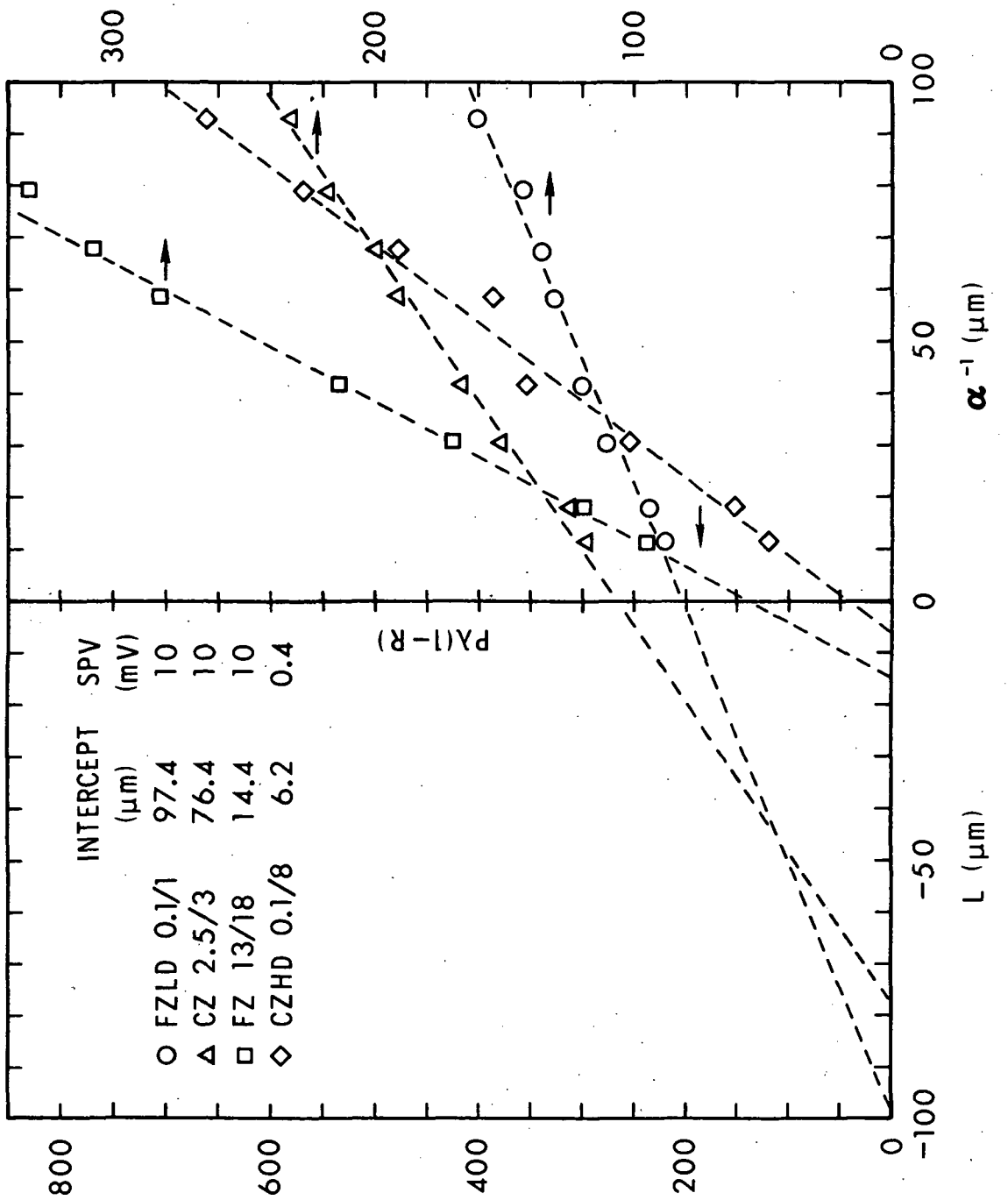

Figure 17. Photon intensity (arbitrary units) vs. reciprocal absorption coefficient for irradiated bulk silicon specimens. Data shown were obtained by the steady-state surface photovoltage method for determining diffusion length. Dashed lines are least-squares fits, and the intercepts yield diffusion lengths.

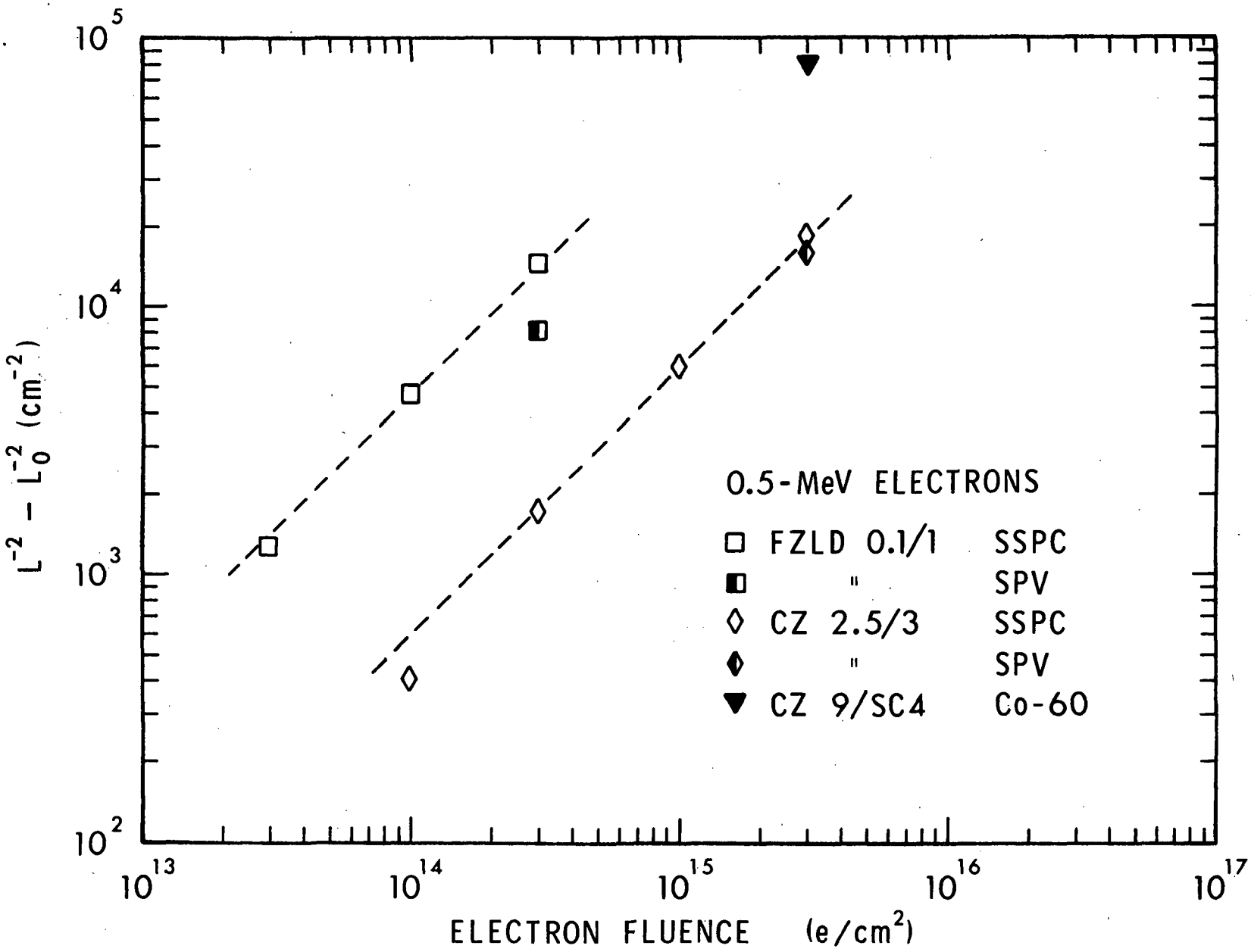

Figure 18. The quantity ($L^{-2} - L_0^{-2}$) vs. electron fluence for 0.5-MeV electron-irradiated silicon specimens. A comparison is made of data obtained by steady-state photoconductivity measurements and by surface photovoltage measurements.

a K_L value even smaller than that for SSPC, and such behavior is in a direction opposite to that required to account for differences between solar cells and bulk material.

Figure 19 presents a similar comparison for the two short-diffusion-length samples of Table XII. For FZ 13/18, the SPV data point lies between the extrapolated SSPC value and that expected for a solar cell. To make this comparison, it is necessary to extrapolate linearly the behavior for FZ 13/SC35 to a fluence of 1.2×10^{12} p/cm^2. (A fluence-dependent damage coefficient would invalidate this comparison, however.) For sample CZHD 0.1/8, it is seen that the SPV result will give a K_L value considerably larger than that expected for CZ 0.1 solar cells at the fluence in question.

It is encouraging that SSPC and SPV L-values are in reasonable agreement for the two longer-diffusion-length cases examined. However, the disagreement noted for the two shorter-L samples indicates that additional comparisons of the two techniques in question, along with comparisons among other measurement approaches, will be required before observed differences between solar-cell and bulk-material damage coefficients can be resolved.

4.5 Annealing Study for Low-Resistivity Samples

An annealing study was performed for selected bulk silicon samples that had been irradiated at different energies to different fluences. One group of samples was annealed at room temperature following irradiation, and a second group was annealed at 60°C. Determinations of diffusion length using SSPC measurements were made for each sample at various times during the annealing period. Data were analyzed in terms of an unannealed fraction, defined through the relation

$$\text{Unannealed Fraction} = \frac{(1/L_t^2) - (1/L_0^2)}{(1/L_{post}^2) - (1/L_0^2)} \quad . \qquad (15)$$

In this expression, L_0 is pre-irradiation diffusion length, L_{post} is post-irradiation diffusion length measured after ~1 h at room temperature, and L_t is post-irradiation diffusion length measured at room temperature after a time t at the annealing temperature. Thus, a value of unity for the unannealed fraction occurs by definition at 1 h after irradiation.

Room-temperature annealing data for twelve samples are shown in Figures 20 and 21. Very little annealing occurred during 500 h at room temperature for most of the samples. Sample FZHD 0.1/5, however, exhibited a significant amount of recovery. This sample was irradiated with 0.5-MeV electrons to a fluence of 1×10^{14} e/cm^2. It is interesting to note that

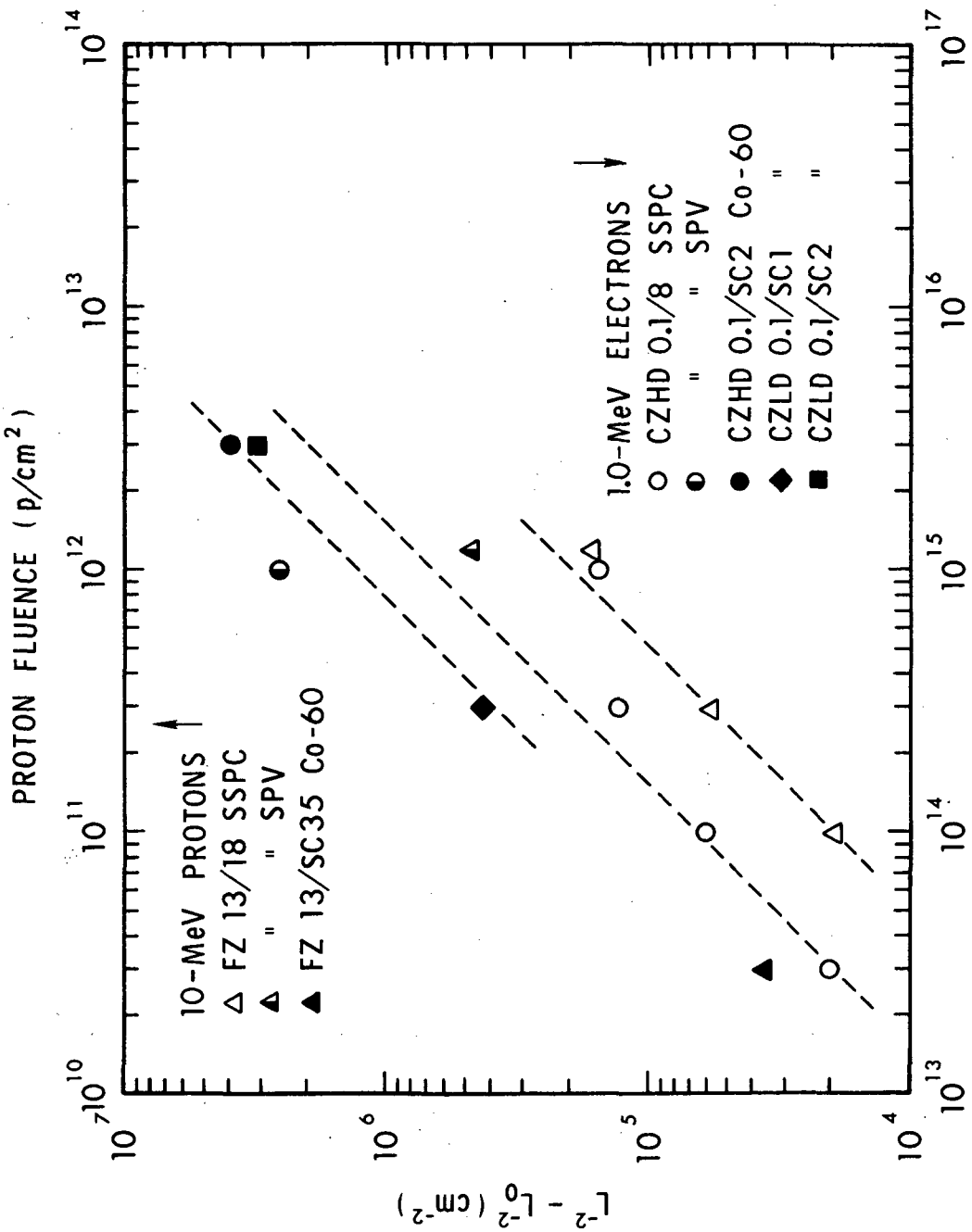

Figure 19. The quantity ($L^{-2} - L_0^{-2}$) vs. fluence for 10-MeV proton- and 1.0-MeV electron-irradiated bulk silicon specimens and silicon solar cells. A comparison is made of SSPC, SPV, and Co-60 data.

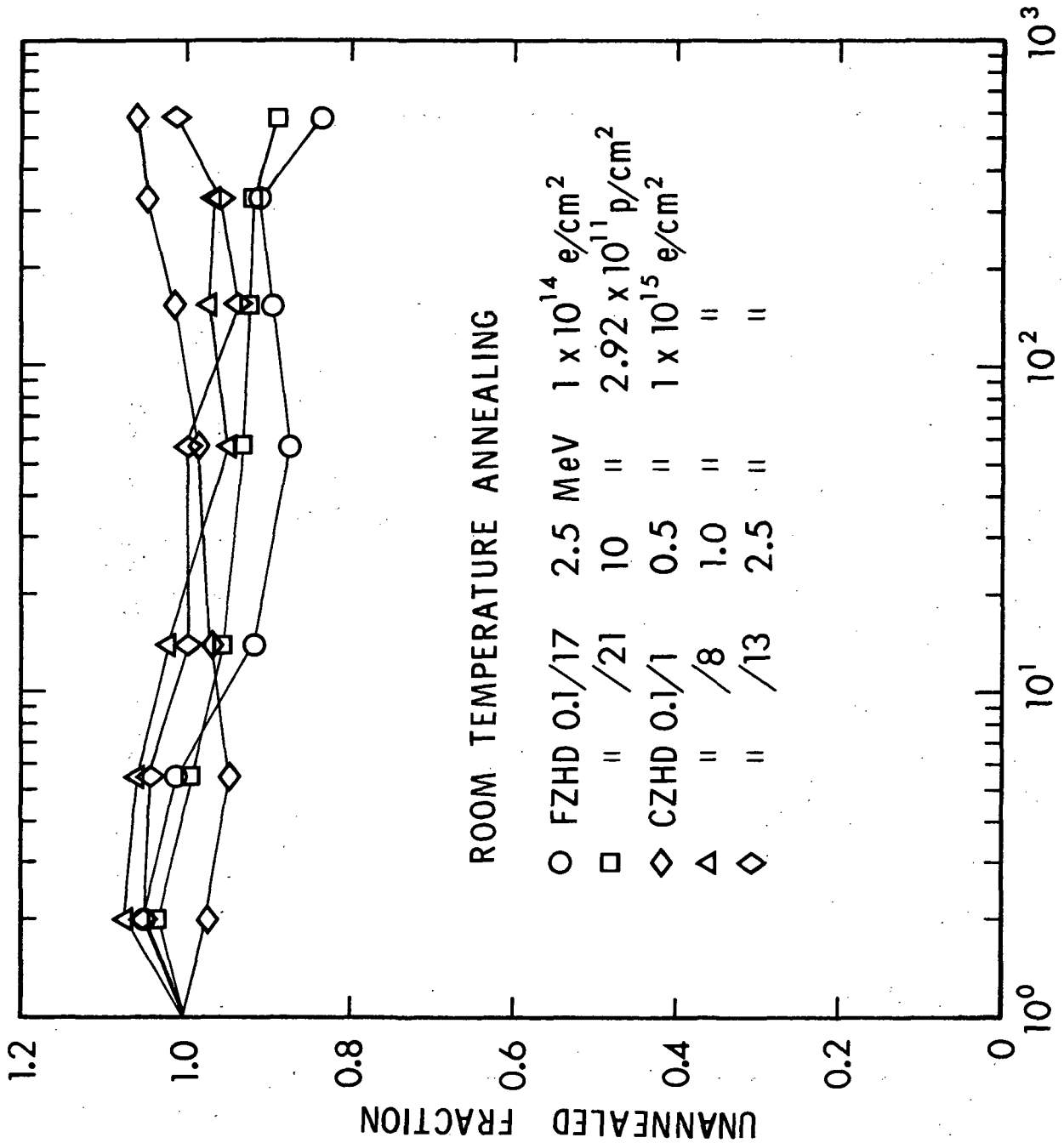

Figure 20. Unannealed fraction vs. time at room temperature for irradiated bulk silicon specimens.

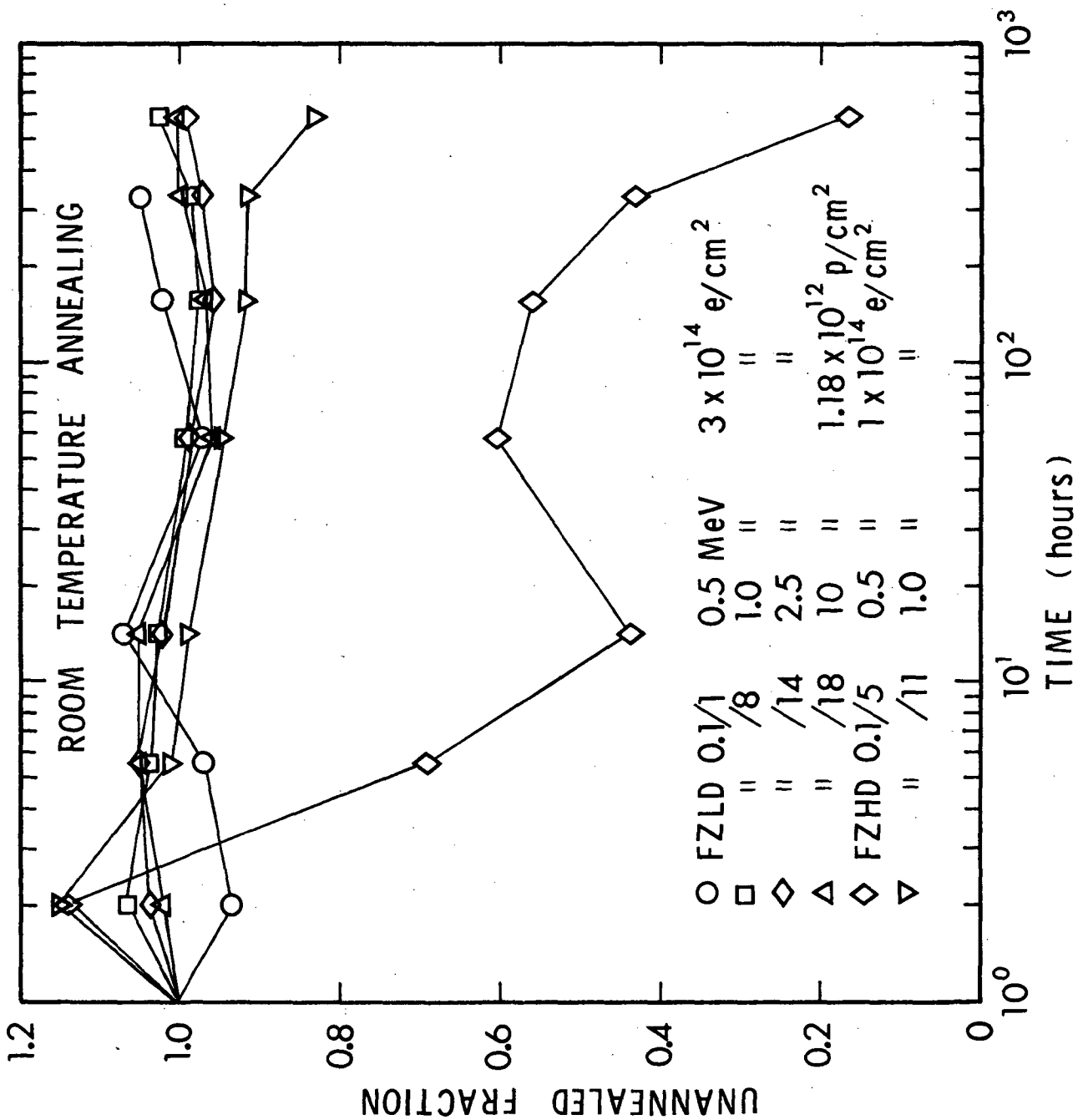

Figure 21. Unannealed fraction vs. time at room temperature for irradiated bulk silicon specimens.

the three other FZHD 0.1 specimens studied exhibited more recovery at 500 h than the other material types. Very little reverse annealing was observed.

Figure 22 presents data for samples annealed at 60°C. After 500 h, six out of the seven samples have recovered somewhat, with an FZHD 0.1 sample once again exhibiting the most annealing. Reverse annealing was evident for one specimen (CZLD 0.1/10).

It should be noted that data in Figures 20 through 22 are for samples with differing irradiation histories. For certain samples, a plot of the quantity $(L^{-2} - L_0^{-2})$ versus fluence would reveal that irradiations for these specimens were discontinued at a fluence in a region of linear degradation. For other samples, irradiation was discontinued in a saturation region and measured diffusion length was most likely influenced by trapping (see Section 4.3). In spite of these sample differences, with only one exception strong variations in annealing behavior among the eighteen samples of Figures 20 through 22 are not apparent.

4.6 Solar Simulator Results for Irradiated Cells

Figure 23 presents data showing the degradation with fluence of short-circuit current (I_{sc}), open-circuit voltage (V_{oc}), and maximum power output (P_{max}) for a 0.5-MeV electron-irradiated 9 ohm-cm CZ solar cell. Data were obtained using a solar simulator, as discussed in Section 2.1, and are normalized to pre-irradiation values (I_{sco}, V_{oco}, and P_{maxo}) of the cell parameters obtained from current-voltage characteristics. Pre-irradiation cell properties are given in Table VII. The cell thickness for CZ 9/SC2 was 0.0285 cm. Downing's data[29] indicate that a 1-MeV electron is ~3.7 times as effective in degrading an n-on-p solar cell as a 0.5-MeV electron. Upon referring to the Solar Cell Radiation Handbook,[11] it is seen that for a 7-13 ohm-cm cell of the thickness employed here, I_{sc} degrades to ~86% of its pre-irradiation value at a fluence of 8.1×10^{14} 1-MeV electrons/cm^2 (refer to Figure 3.11 of Reference 11). At a fluence of 3×10^{15} 0.5-MeV electrons/cm^2, which is 3.7 times the 1-MeV fluence just given, Figure 23 reveals that I_{sc} has degraded to 85% of its initial value. This agreement between data given in Reference 11 and the present findings suggests that the fluence measurements for 0.5-MeV electron irradiations were accurate in the current investigation. (Good agreement is also found when the above calculation is performed for V_{oc} and P_{max}.)

Figure 24 presents data exhibiting the degradation of short-circuit current with fluence for 1-MeV electron-irradiated solar cells of several resistivities. Corresponding plots for open-circuit voltage and maximum power output are shown in Figures 25 and 26, respectively. The thickness of

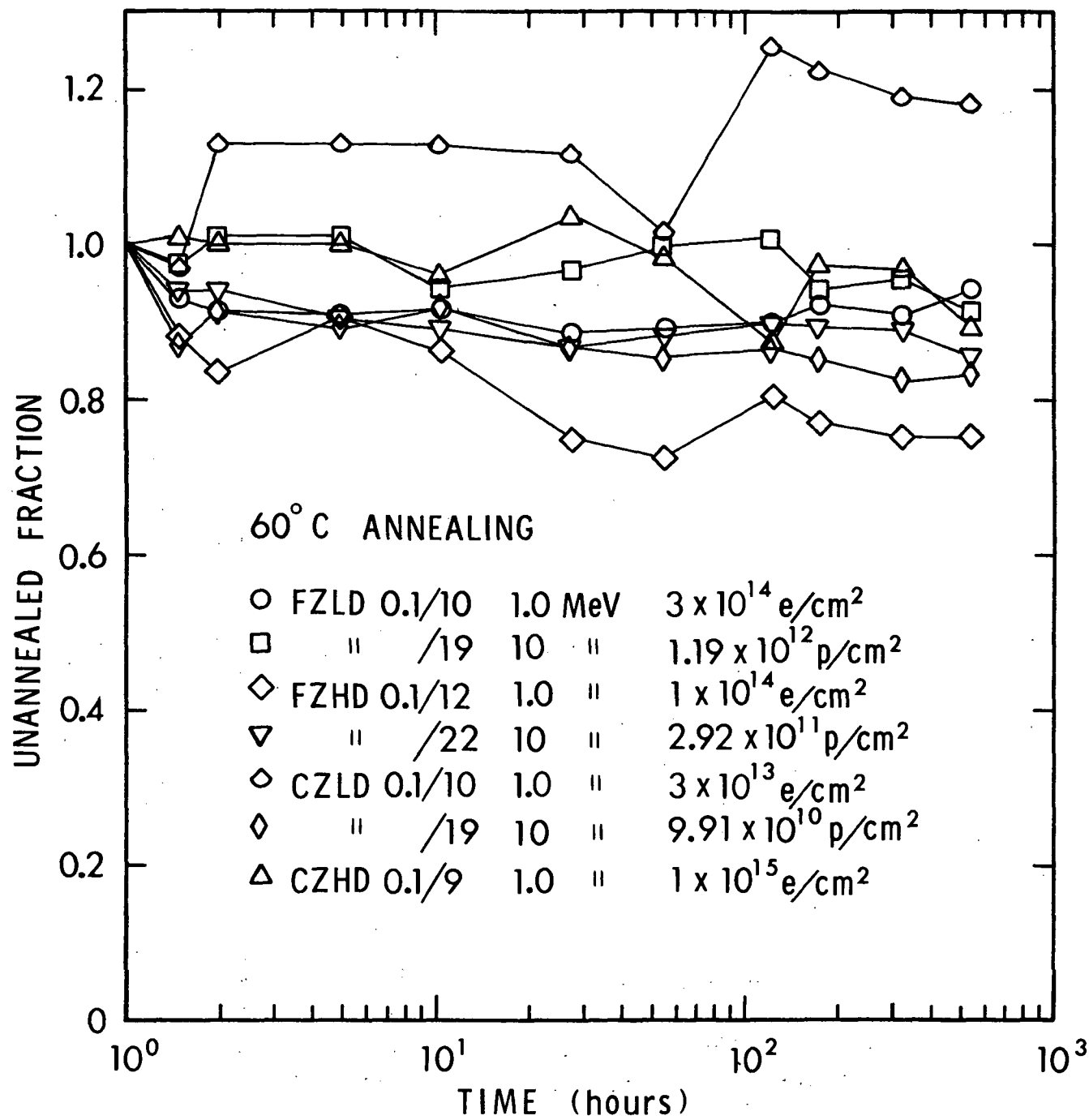

Figure 22. Unannealed fraction vs. time at 60°C for irradiated bulk silicon specimens.

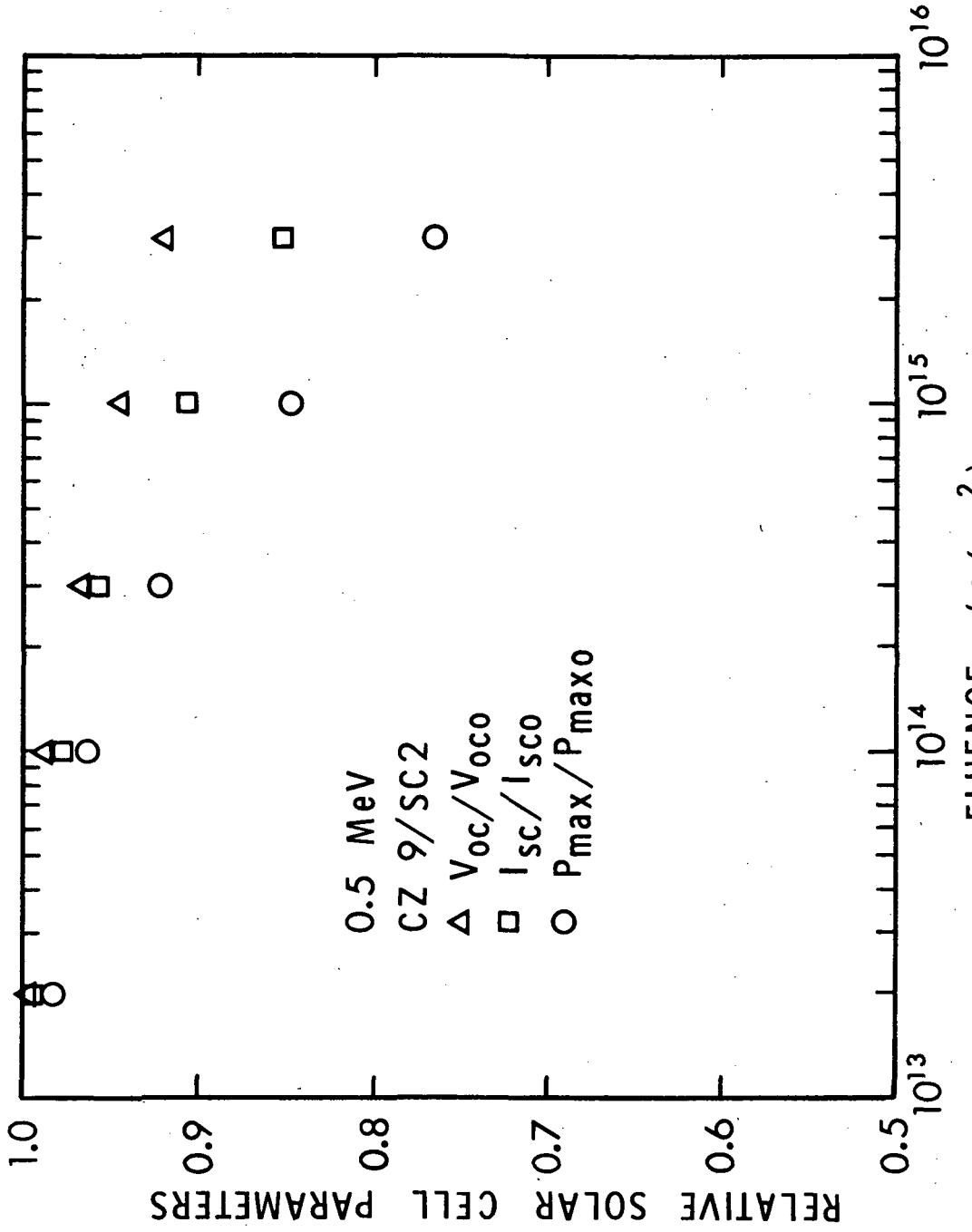

Figure 23. Relative solar cell parameters vs. fluence for a 0.5-MeV electron-irradiated unit.

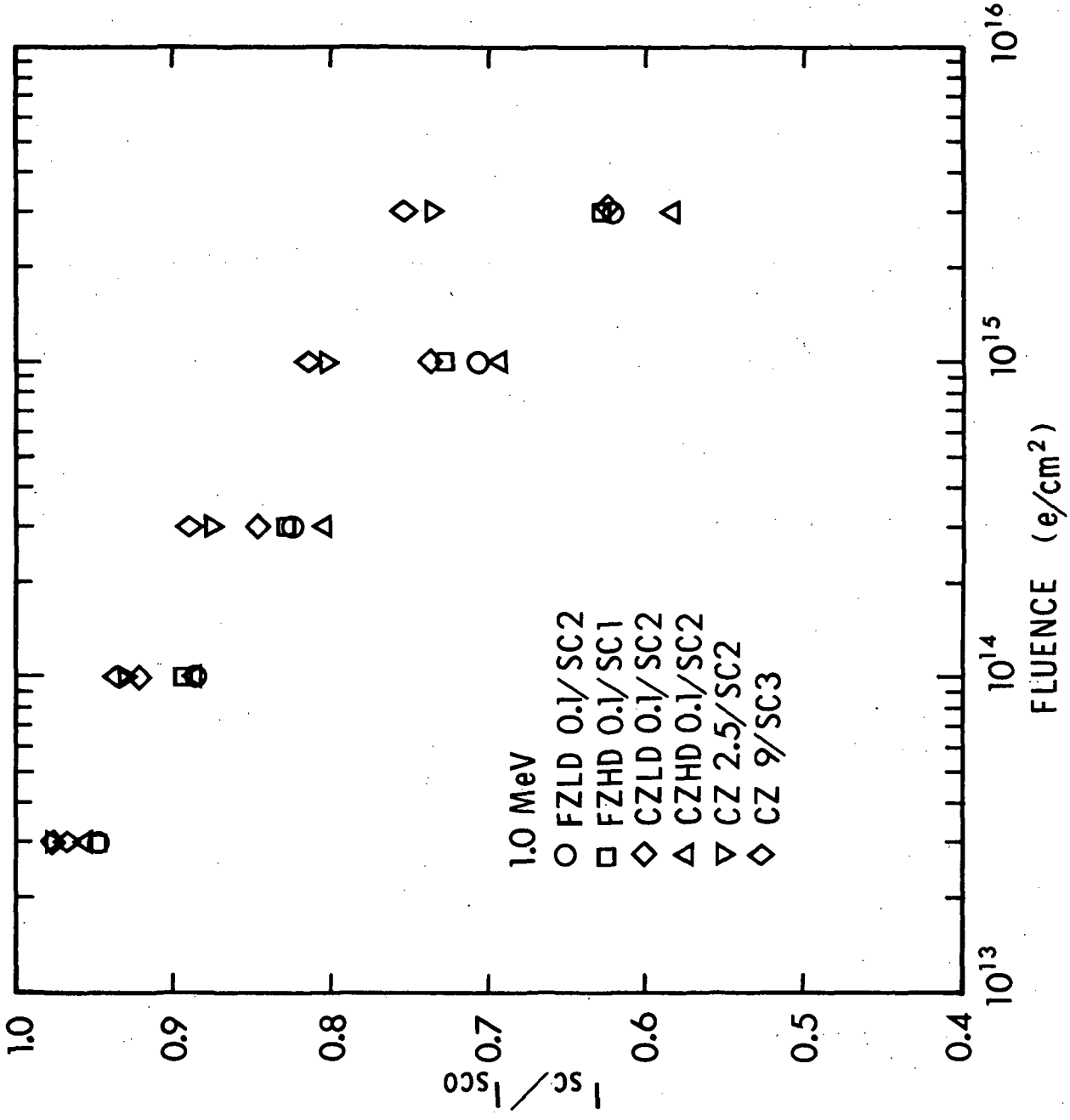

Figure 24. The quantity I_{sc}/I_{sco} vs. fluence for 1.0-MeV electron-irradiated silicon solar cells.

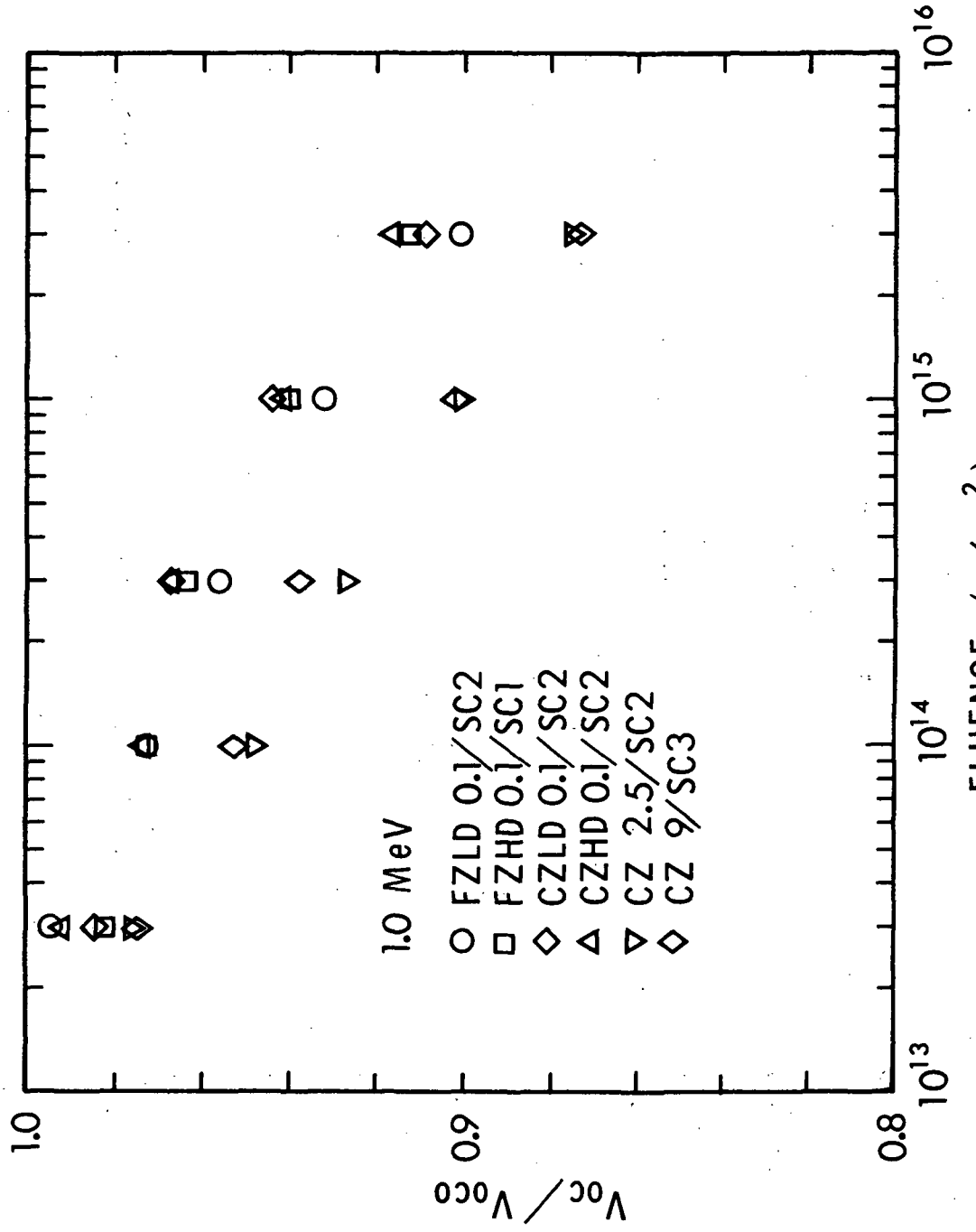

Figure 25. The quantity V_{oc}/V_{oco} vs. fluence for 1.0-MeV electron-irradiated silicon solar cells.

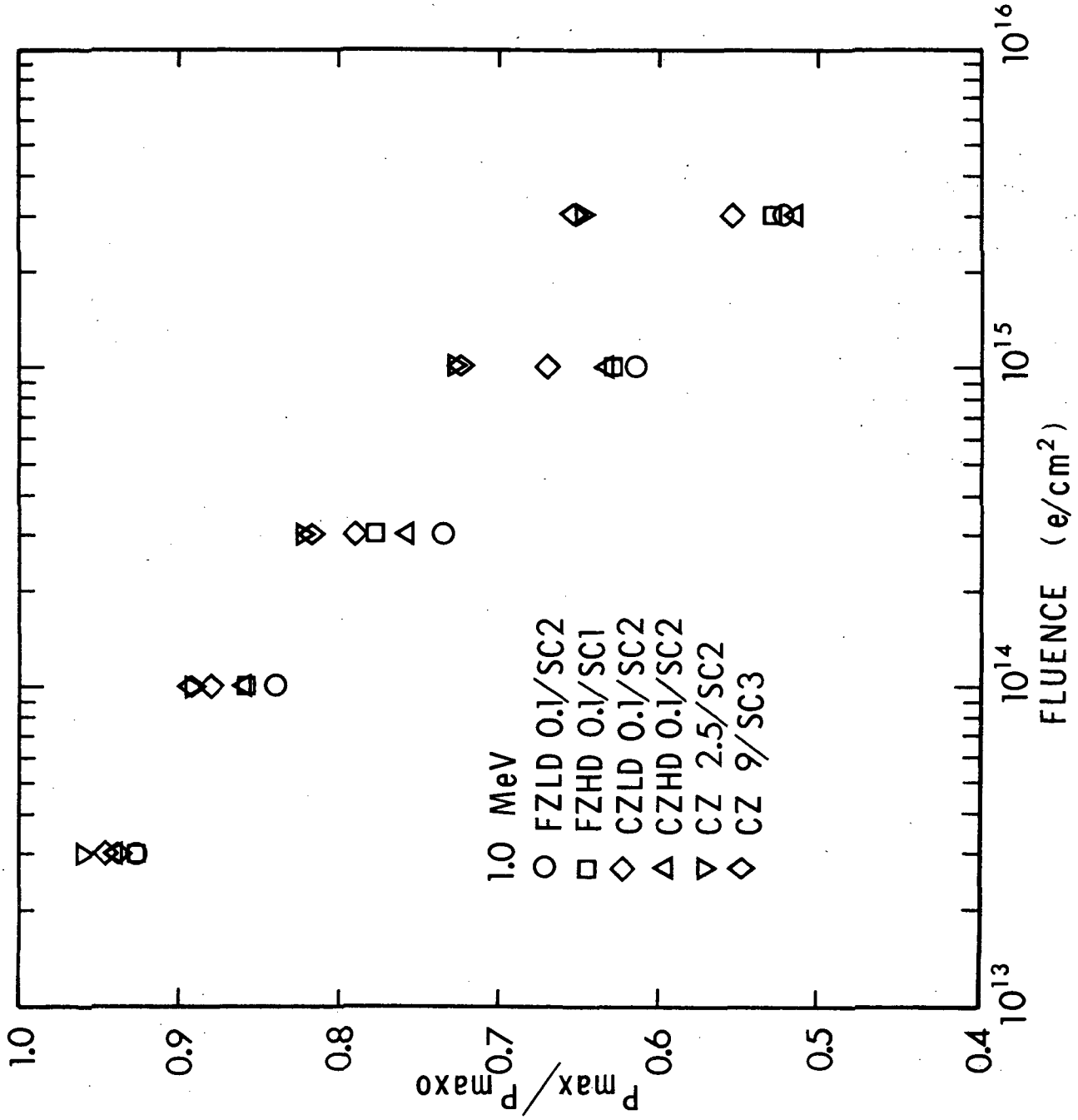

Figure 26. The quantity P_{max}/P_{maxo} vs. fluence for 1.0-MeV electron-irradiated silicon solar cells.

device CZ 9/SC3 is 0.0307 cm, and by comparing the present findings with expected behavior for cells irradiated with 1-MeV electrons,[11] good agreement is found, which once again suggests that fluence measurements were accurate. Figure 24 reveals that I_{sc} degraded to ~62% of its pre-irradiation value at 3×10^{15} e/cm^2 for 0.1 ohm-cm cells, as compared to ~75% for higher-resistivity units. For low-resistivity devices, no dependence of I_{sc} degradation on dislocation density is apparent.

Figure 25 shows that V_{oc} degraded to ~ 88% of its initial value for CZ 2.5 and CZ 9 cells at 3×10^{15} e/cm^2, whereas the corresponding value for low-resistivity cells is ~ 91%. In Figure 26, it is seen that in terms of normalized maximum power output higher resistivity cells are superior. For such units, at 3×10^{15} e/cm^2 $P_{max}/P_{max_0} = 0.65$, whereas the low resistivity value is ~ 0.53. (The one CZLD 0.1 cell tested appears to be slightly superior to the other 0.1 ohm-cm cells; however, in terms of absolute power output, this unit is actually inferior to the others.) Thus, solar simulator findings are consistent with damage coefficient determinations reported above in that low-resistivity solar cells are inferior to higher resistivity units in terms of radiation tolerance.

Figure 27 presents degradation of solar cell parameters with fluence for a 2.5-MeV electron-irradiated 9 ohm-cm device with a thickness of 0.0302 cm. Downing's data[29] indicate that a 2.5-MeV electron is ~4.1 times as effective in degrading an n-on-p cell as a 1.0-MeV electron. Upon taking this difference into account and then comparing the data of Figure 27 with that in the Radiation Handbook[11] in a manner similar to that employed above for 0.5-MeV electrons, good agreement is found. This agreement again suggests accurate dosimetry for the present electron irradiations.

Figure 28 presents the degradation of short-circuit current with fluence for 10-MeV proton-irradiated solar cells of two resistivities (0.1 and 2.5 ohm-cm). Corresponding plots for open-circuit voltage and maximum power output are shown in Figures 29 and 30, respectively. As a check on fluence accuracy, consider data for 2.5 ohm-cm cells. Data in the Radiation Handbook[11] (see Figure 3.6 of this reference) indicate that a 10-MeV proton fluence of 3×10^{11} p/cm^2 will degrade I_{sc} by the same amount as a 1-MeV electron fluence of 2×10^{15} e/cm^2. From Figure 28, we find that I_{sc} for CZ 2.5 cells degrades to ~0.79 of its initial value at 3×10^{11} p/cm^2. From Figure 24, interpolation yields ~0.76 for this same quantity at 2×10^{15} e/cm^2 for a 1.0-MeV electron-irradiated CZ 2.5 cell. This agreement suggests that fluence determinations for 10-MeV proton irradiations were accurate.

Figure 28 indicates that normalized I_{sc} degrades more severely for 0.1 ohm-cm cells than for higher-resistivity units. However, as shown in Figure 29, the opposite is true for V_{oc} degradation. In Figure 30, it is seen that

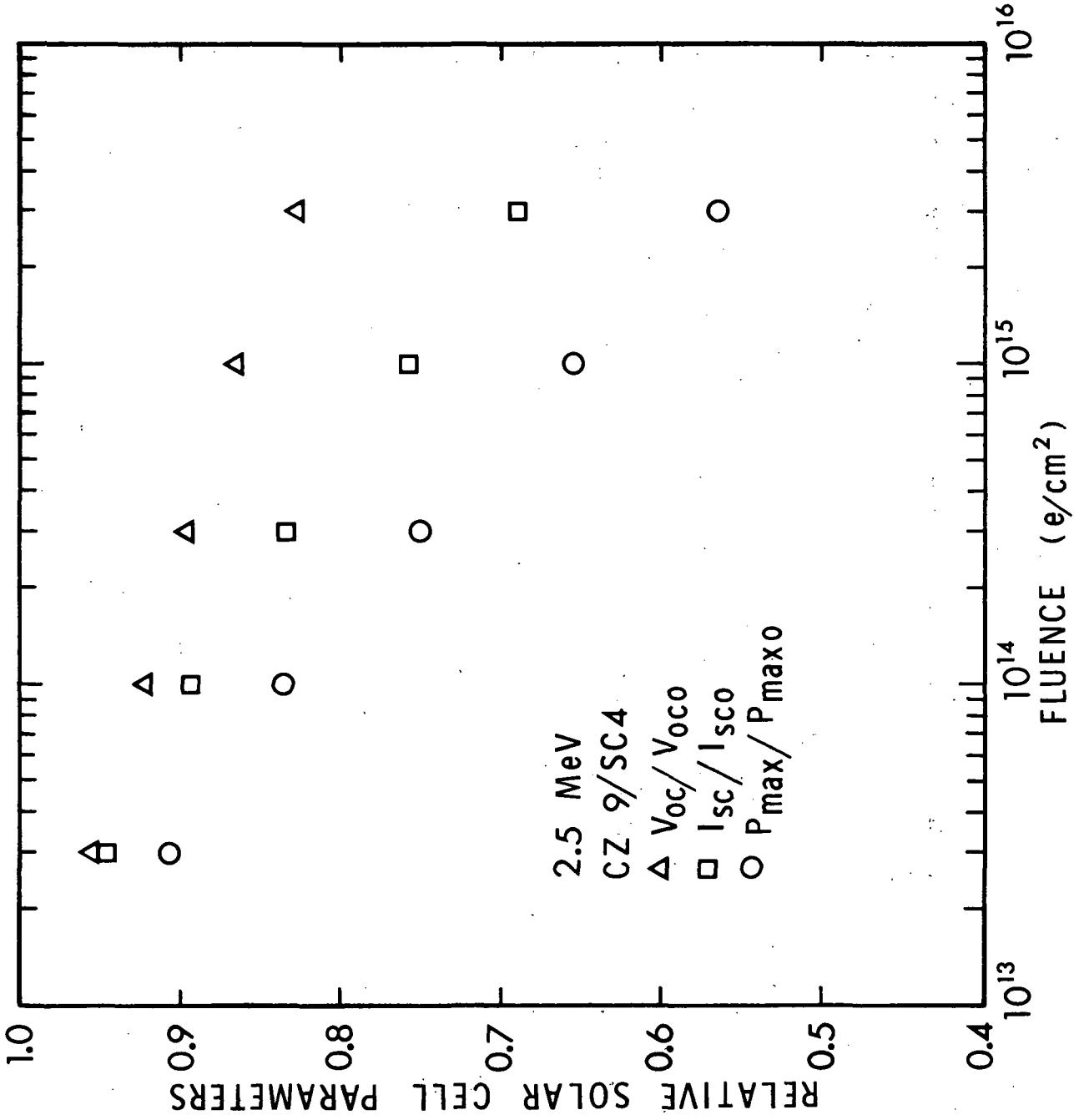

Figure 27. Relative solar cell parameters vs. fluence for a 2.5-MeV electron-irradiated unit.

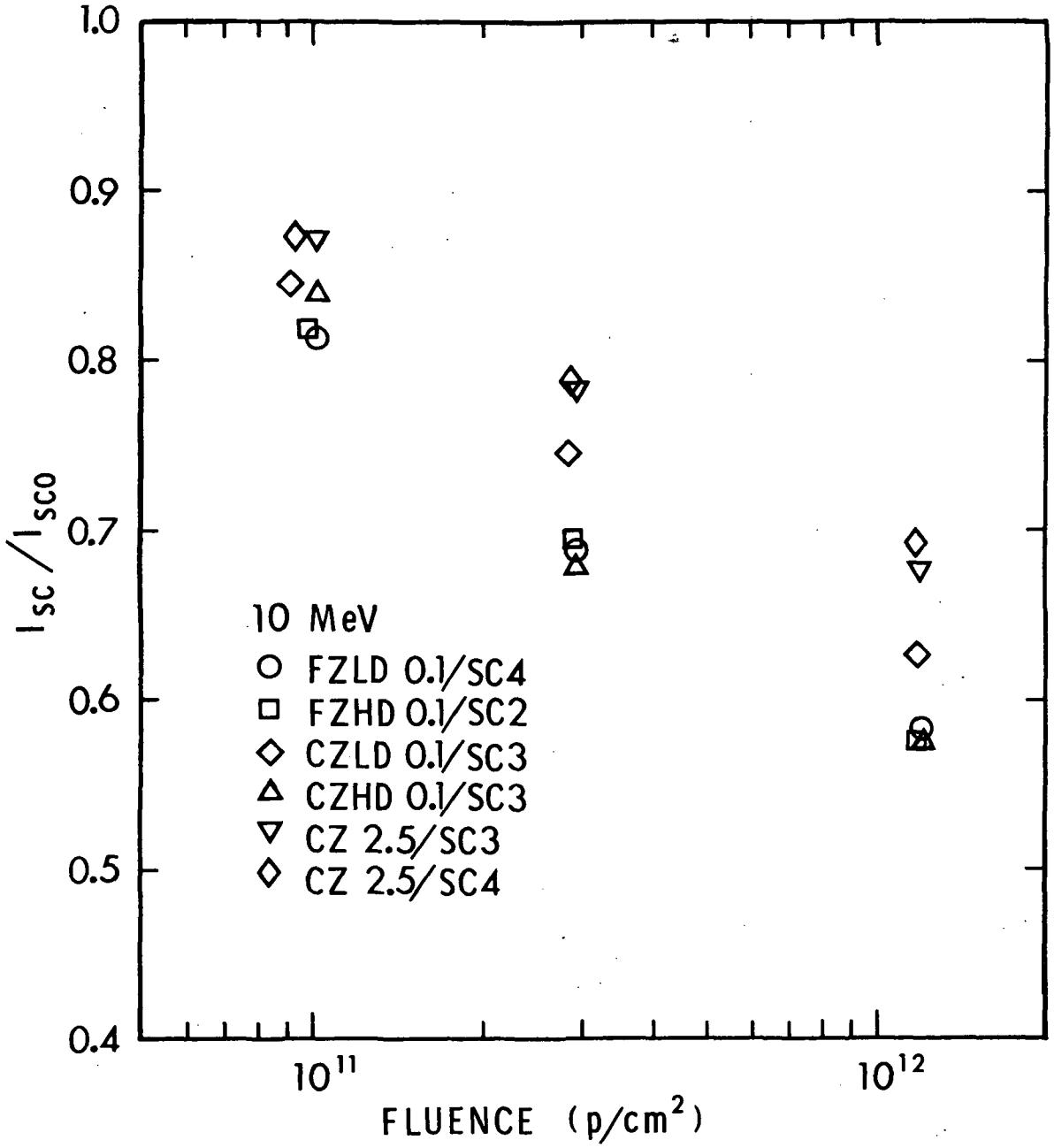

Figure 28. The quantity I_{sc}/I_{sco} vs. fluence for 10-MeV proton-irradiated silicon solar cells.

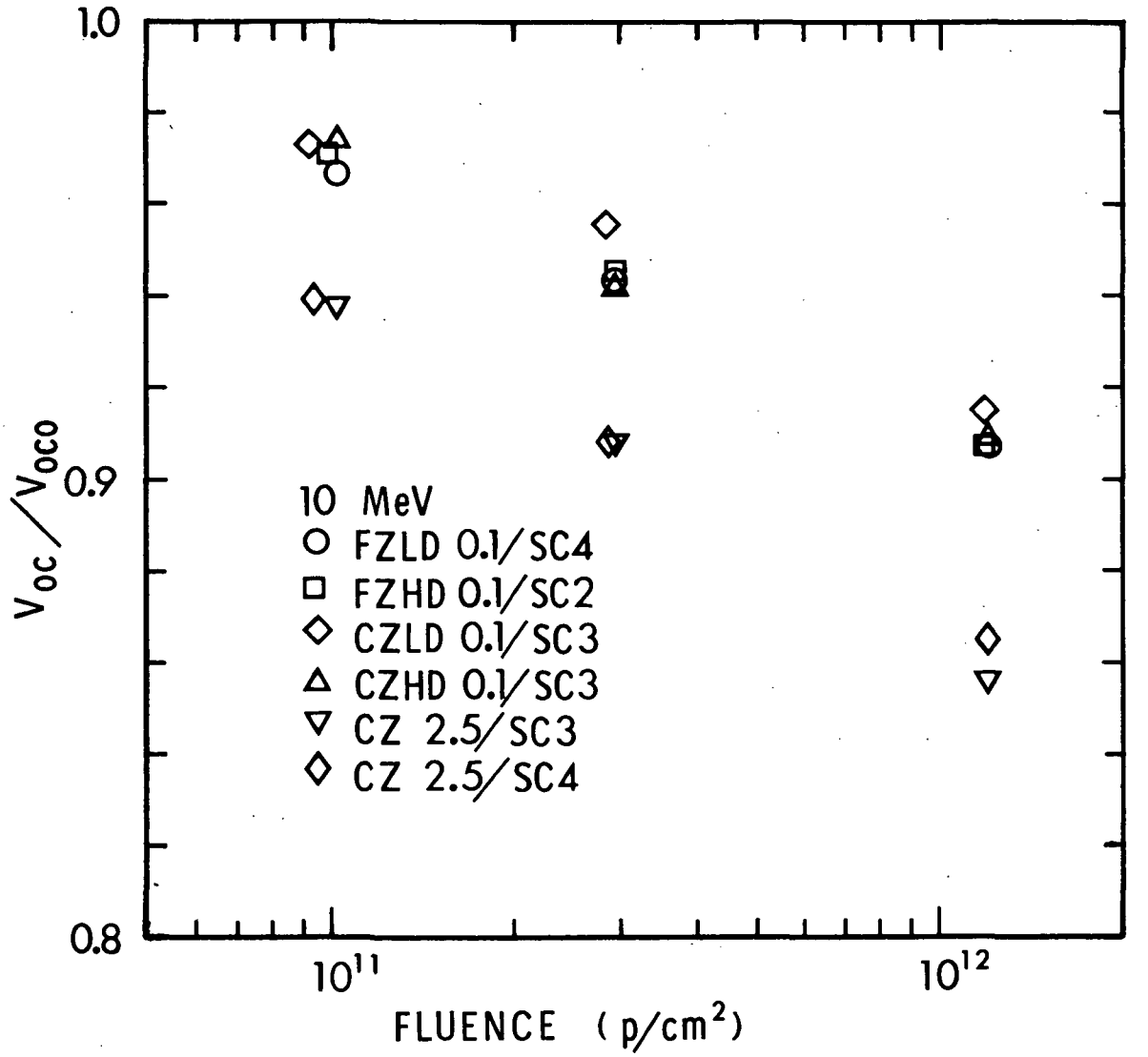

Figure 29. The quantity V_{oc}/V_{oco} vs. fluence for 10-MeV proton-irradiated silicon solar cells.

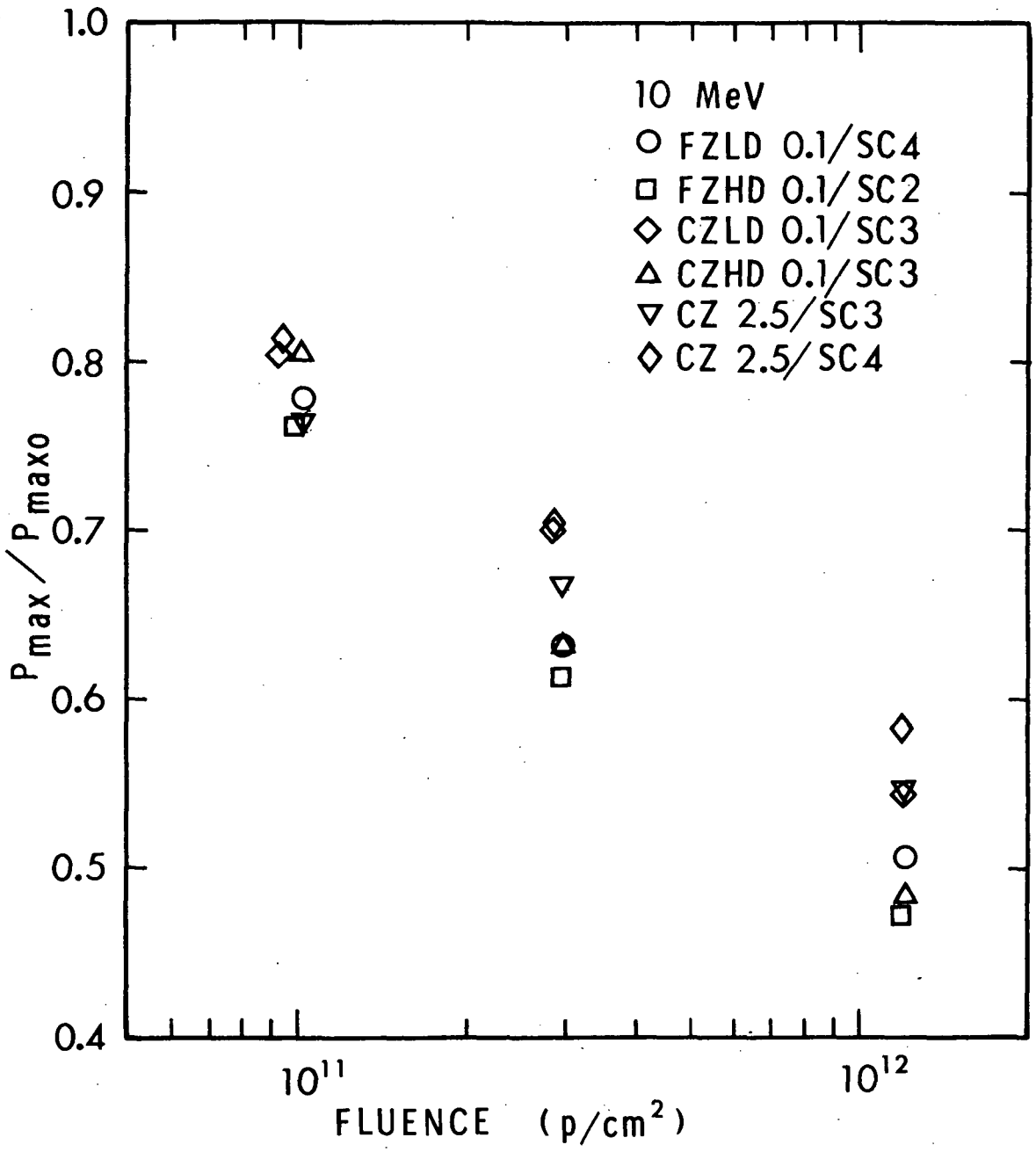

Figure 30. The quantity P_{max}/P_{maxo} vs. fluence for 10-MeV proton-irradiated silicon solar cells.

for three out of the four low-resistivity cells examined, P_{max}/P_{maxo} was somewhat less than for 2.5 ohm-cm cells which is consistent with expectations based on K_L determinations. For CZLD 0.1/SC3 this quantity was identical to that for CZ 2.5/SC3. However, in terms of absolute quantities (use Table VII in conjunction with Figure 30), the power output for CZLD 0.1/SC3 was the lowest of all six cells shown in Figure 30. (Caution must be exercised in interpreting the normalized data of Figures 23 through 30.) After 1.2×10^{12} protons/cm^2, none of the four low resistivity cells had a maximum power output as large as that for the two CZ 2.5 devices.

SECTION 5.0

DISCUSSION AND CONCLUSIONS

One finding of practical importance in the present investigation is the observation of damage coefficients that increase with decreasing resistivity (ρ) over a broad range of resistivities. The employment of low-resistivity solar cells in a space radiation environment therefore may not be advisable. However, whether low-resistivity cells may or may not be advantageously utilized in space applications will depend on both the amount of radiation-induced degradation anticipated and the pre-irradiation properties of such devices compared to those for higher-resistivity units. The obtaining of a basic mechanistic understanding of the resistivity dependence of K_L is an intriguing question that has been addressed by others.[29,36] We have also attempted to understand such behavior, and our preliminary analysis is now given.

For all three electron energies examined, empirical fits to the data yield the following approximate relation:

$$K_L \propto \rho^{-2/3} . \tag{16}$$

Hole density p_o was determined for p-type material over the resistivity range from 0.1 to 10 ohm-cm. Additionally, damage coefficient is proportional to $(L^{-2} - L_0^{-2})$, which can be interpreted as the reciprocal of radiation-induced carrier lifetime τ. Thus, $K_L \propto 1/\tau$. Equation 16 was then employed to obtain a plot of τ vs p_o, which is shown as the solid curve in Figure 31. This curve is thus representative of the experimental data obtained here for three electron energies.

We next attempted to fit the solid curve using the Hall-Shockley-Read (HSR) model. The HSR lifetime expression for a single recombination level in p-type material at low injection levels is

$$\tau = \frac{p_o + p_1}{c_n N p_o} + \frac{n_o + n_1}{c_p N p_o} , \tag{17}$$

where all terms have their usual meaning. As p_o increases, lifetime decreases due to the increased recombination rate. For ease of analysis and for purposes of illustration, a recombination level in the lower half of the bandgap was assumed. For any reasonable capture-probality-ratio assumed, Equation 17 then simplifies to

$$\tau = \frac{1}{c_n N} \left(1 + \frac{p_1}{p_o}\right) . \tag{18}$$

We attempted to fit Equation 18 to the solid curve in Figure 31 by treating the multiplicative term $1/c_n N$ as an adjustable scale factor. A reasonable fit was

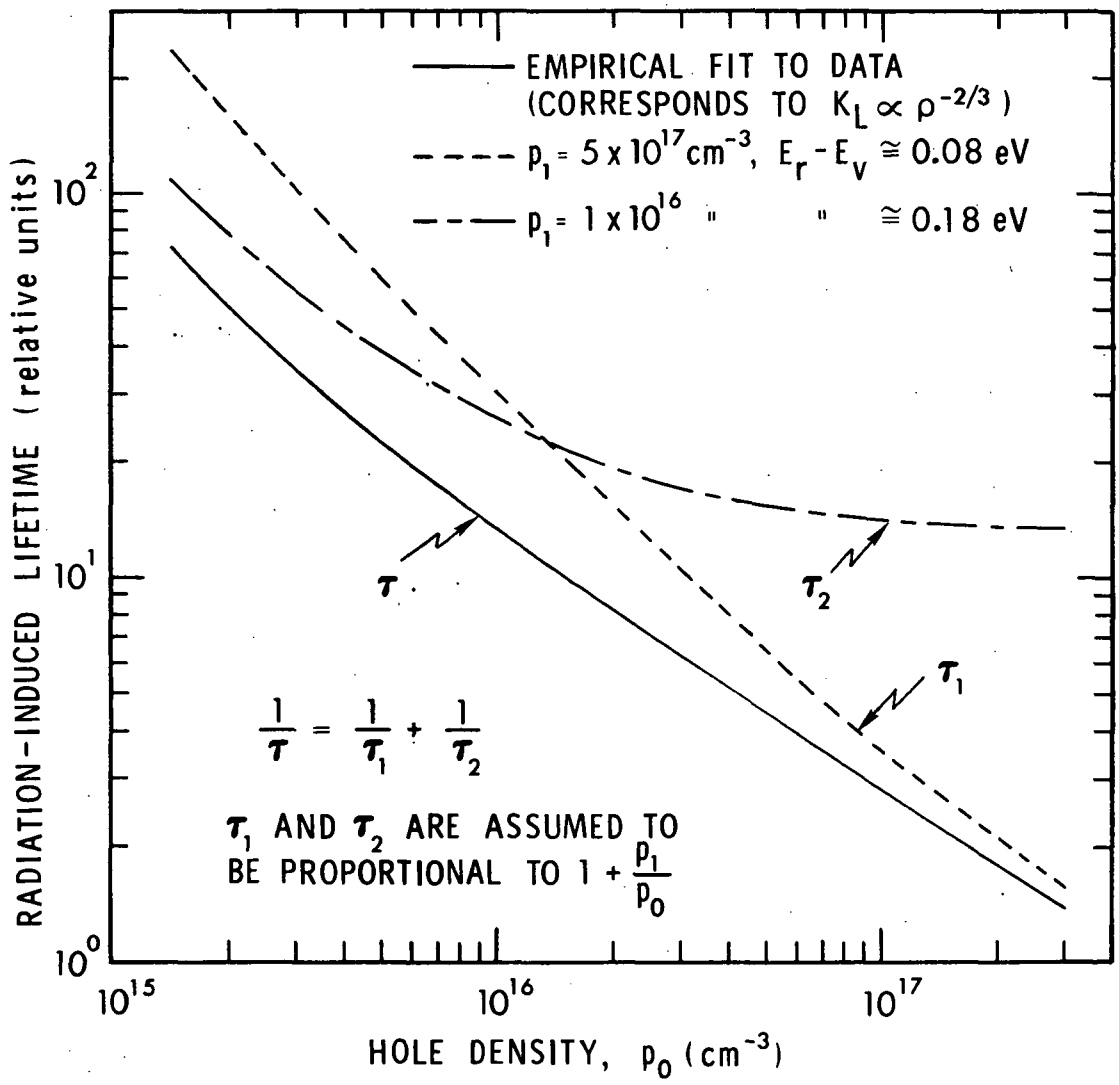

Figure 31. Radiation-induced lifetime vs. hole density. It is demonstrated that recombination through two Hall-Shockley-Read levels can be employed to qualitatively explain the observed dependence of damage coefficient on resistivity for electron-irradiated boron-doped silicon. The recombination levels given here are not unique to the experimental data and are presented for purposes of illustration only.

obtained for a level at $E_r - E_v \cong 0.12$ eV. However, an exact fit can be obtained by using a two-level HSR model, as shown in the figure. By assuming that each level can be expressed in the form of Equation 18 and by adding the contributions of each level reciprocally to obtain τ, the solid curve representing the experimental data can be fit exactly. As shown in Figure 31, the level more effective for higher resistivities is at $E_r - E_v \cong 0.18$ eV, whereas the level more effective at lower resistivities is at $E_r - E_v \cong 0.08$ eV. The ratio of the multiplicative scale factors for these two levels is ~ 22, with $c_n N$ for the 0.18 eV level being larger.

No physical significance should be attached to the above recombination parameters. Levels in the upper half of the bandgap could be effective and/or three or more levels may be effective rather than only two. (It should be noted that for the two-level model employed here, a satisfactory fit to the data requires a shallow level close to either the valence band or the conduction band.) Our purpose here was only to illustrate that a two-level HSR model describes the present data quite well. In order to obtain meaningful parameters from such a model, the temperature and injection-level dependences of radiation-induced lifetime are required.[37,38] Wilsey[36] has examined the temperature dependence of K_L for electron-irradiated p-type silicon, and it is clear that a one-level model cannot account for his data. This statement can also be made for findings of Faith.[30] In terms of gaining increased understanding of the dependence of K_L on resistivity, it would be useful to measure the temperature and injection-level dependences of damage coefficient for samples of several resistivities and then attempt to fit the data with two (or more) HSR levels.

Several of the major observations made and conclusions reached in this investigation are the following:

1. Diffusion-length damage coefficients increase with decreasing resistivity for boron-doped silicon. For low-resistivity solar cells, this decrease in radiation tolerance must be weighed against potential advantages when considering such devices for utilization in a space radiation environment.

2. For 0.5-, 1.0-, and 2.5-MeV electron bombardment, empirical fits to experimental data can be approximately expressed as $K_L \propto \rho^{-2/3}$ for $0.1 \lesssim \rho \lesssim 20$ ohm-cm. For 10-MeV proton bombardment, an empirical fit of the form $K_L \propto \rho^{-0.44}$ was found to describe the data reasonably well.

3. The dependence of damage coefficient on resistivity can be qualitatively accounted for quite well using a two-level Hall-Shockley-Read model.

4. Damage coefficients for solar cells were observed to be larger than their bulk-material counterparts.

5. Bulk samples and solar cells prepared from float-zone material were generally observed to be more radiation tolerant than their Czochralski counterparts at all resistivities examined.

6. No dependence of damage coefficient on dislocation density was apparent for 0.1 ohm-cm bulk samples and solar cells.

Regarding item 4, during the final stages of preparing this report a comparison was made of measured pre-irradiation diffusion lengths for bulk samples and solar cells fabricated from the same ingot. Bulk values were found to be a factor of 1.7 ± 0.3 larger than their device counterparts. This value is an average obtained by comparing 110 bulk samples and 33 solar cells fabricated from 7 ingots. Referring to Equation (1), it is seen that if pre- and post-irradiation values of diffusion length for a given bulk sample were a factor of 1.7 larger than the corresponding solar-cell values, then the solar cell K_L value would be a factor of 2.9 larger than the bulk damage coefficient (assuming equal fluences). This latter factor is comparable to solar-cell-to-bulk-material damage-coefficient ratios experimentally observed in this study, which suggests that a systematic error is responsible for the device-bulk differences noted.

Several items that should be considered when attempting to quantitatively account for the observed discrepancy are: a) surface photovoltage diffusion-length measurements were found to be in reasonable agreement with SSPC measurements on two bulk samples with relatively long diffusion lengths (refer to Section 4.4); b) the present 1.0-MeV solar-cell damage coefficients are in reasonable agreement with those obtained by other workers (refer to Figure 11); c) the fluence dependence of K_L for solar cells noted here and also by other workers is in a direction to bring device and bulk damage coefficients into agreement at high fluences; (this statement assumes that bulk K_L values are not fluence dependent); d) accurate determination of the generation rate in a penetrating-radiation diffusion-length measurement for solar cells is not straightforward. We presently suspect that previous workers and ourselves have not properly accounted for all of the important factors in penetrating radiation solar-cell measurements. Some of the difficulties associated with determining the generation rate for a gamma-irradiation diffusion-length measurement have been previously considered.[6,39] It seems clear that additional work will be required to obtain a satisfactory explanation for observed device-bulk differences.

APPENDIX

STATISTICAL ANALYSIS OF DATA*

Electron Damage Coefficients

The present study has examined radiation effects on four types of 0.1 ohm-cm boron-doped silicon ingots, including the four possible combinations of high and low oxygen content and high and low dislocation density. For electron-irradiated specimens, Figures 9, 11, and 13 indicate that there is no significant dependence of damage coefficient on dislocation density. However, a dependence of K_L on growth method (i.e., oxygen content) is evident. In this section, an attempt is made to quantitatively examine the statistical significance of the dependence of electron damage coefficient on oxygen content (OC), dislocation density (DD), and electron energy (EE). Additionally, the dependence of pre-irradiation diffusion length on oxygen content and dislocation density is examined.

Statistical analyses were performed by utilizing analysis of variance procedures outlined by Hicks.[40] For each 0.1 ohm-cm ingot type at a given electron energy, values of K_L for three individual samples were employed. Table XIII lists damage coefficients used in the present analysis. This table is arranged in a matrix corresponding to the four possible material combinations. (We associate a low oxygen concentration with float-zone material and a high oxygen concentration with Czochralski material.) Three variables, or factors, are of interest here: oxygen content, dislocation density, and electron energy. The first two factors were examined experimentally at two levels and the last at three levels. This situation is termed a 2 x 2 x 3 factorial experiment with three replications per cell.

The damage coefficients in Table XIII are summarized in a format usually associated with factorial designs. Because of the wide range of values observed (almost two orders of magnitude) and observation of the fact that the standard deviation of the three numbers in each box is proportional to the absolute value of the numbers, the logarithms of the damage coefficients were calculated. These are also listed in Table XIII. A second reason for this approach is that the analysis of variance statistical procedure requires that the error variance of each observation be equal. This is much more true of the logarithms than of the actual K_L values.

---

*Analysis presented in this Section was performed by S. M. Sidik and C. R. Baraona of NASA-Lewis Research Center.

	FZLD	FZHD	CZLD	CZHD
0.5 MeV	4.44 (0.65)	4.75 (0.68)	14.0 (1.15)	11.9 (1.08)
	4.13 (0.62)	4.20 (0.62)	14.0 (1.15)	11.2 (1.05)
	4.00 (0.60)	4.20 (0.62)	13.3 (1.12)	10.2 (1.01)
1.0 MeV	42.8 (1.63)	45.6 (1.66)	72.0 (1.86)	85.0 (1.93)
	42.8 (1.63)	38.2 (1.58)	72.0 (1.86)	85.0 (1.93)
	42.8 (1.63)	38.2 (1.58)	67.0 (1.83)	67.0 (1.83)
2.5 MeV	194 (2.29)	196 (2.29)	220 (2.34)	237 (2.37)
	173 (2.24)	188 (2.27)	261 (2.42)	228 (2.36)
	176 (2.46)	200 (2.30)	241 (2.38)	249 (2.40)

TABLE XIII

Damage coefficients obtained at three electron energies for samples from four 0.1 ohm-cm B-doped Si ingots. All damage coefficients listed are in units of electrons^{-1} and should be multiplied by 10^{-11}. Numbers shown in parentheses are the logarithms of the listed damage coefficient values.

Table XIV presents results of the analysis of variance for the data (logarithms) of Table XIII. Listed are the sources of variability in the experiment, the degrees of freedom, the observed mean squares, the expected mean squares, the calculated F ratio test statistic, the standard table value of the F statistic (95% confidence level), and the resulting significance of each source of variance in the experiment.

Table XIV is divided into three parts by horizontal lines. This emphasizes the structure of the expected mean squares, because these structures determine which F tests should be used. For instance, the expected mean squares for EE, OC x EE, DD x EE, and OC x DD x EE are all of the form σ_ϵ^2 plus one other source of variability, where σ_ϵ^2 is the error variance. Their significance may thus be tested by dividing those mean squares by the error mean square. These F statistics indicate that EE and OC x EE are highly significant (values far outside of most tables) and that DD x EE and OC x DD x EE are marginally significant at the 95% confidence level.

The part of the table corresponding to OC, DD, and OC x DD is somewhat different. The expected mean squares are all of the form $\sigma_\epsilon^2 + 9\sigma_\delta^2$ plus one other source of variability. The symbol σ_δ^2 denotes the variance of damage coefficients resulting merely from using different ingots. These mean squares should be tested by dividing by a mean square which has an expected value of $\sigma_\epsilon^2 + 9\sigma_\delta^2$, but there is no such estimator available in the present experiment. The only alternative available is to assume there is no interaction between DD and OC. In this event, OC and DD may be tested for significance by dividing the mean squares by the mean square for the DD x OC interaction. This was done and shows that OC is highly significant and that DD is highly insignificant. In Figure 32, average values of damage coefficients in Table XIII are plotted versus electron energy, and the trend of the data graphically verifies the statistical results.

Pre-Irradiation Diffusion Length

For the same four ingots discussed above, pre-irradiation diffusion lengths for 18 samples of each were statistically examined in a 2 x 2 factorial experiment. (See Table VI for numerical values of diffusion length.) As in the damage coefficient analysis, because of the manner in which the data were obtained there is no direct test for the effect of OC, DD, or their interaction. If the interaction is assumed not to exist, then DD and OC may be tested for significance by computing the ratio of their sums of squares and the interaction sum of squares. This was done and it was found that neither DD nor OC have a significant effect. This result may be due either to the fact that OC and DD do not, in fact, have any significant effect, or to the possibility that there is indeed an interaction between the

Sources of Variability	Degrees of Freedom	Observed Mean Squares	Expected Mean Squares	Calculated F	$F_{1,1,.95}$ or $F_{2,24,.95}$ (from table)	Significance
Oxygen (A) Content (OC)	1	0.6670	$\sigma_\epsilon^2 + 9\sigma_\delta^2 + 18\sigma_A^2$	444.67	161	High
Dislocation (B) Density (DD)	1	0.0001	$\sigma_\epsilon^2 + 9\sigma_\delta^2 + 18\sigma_B^2$	<1.0	161	None
OC x DD (AB)	1	0.0015	$\sigma_\epsilon^2 + 9\sigma_\delta^2 + 9\sigma_{AB}^2$	—	—	?
Electron (C) Energy (EE)	2	6.5238	$\sigma_\epsilon^2 + 12\sigma_C^2$	6900.0	3.4	High
OC x EE (AC)	2	0.0955	$\sigma_\epsilon^2 + 6\sigma_{AC}^2$	101.4	3.4	High
DD x EE (BC)	2	0.002559	$\sigma_\epsilon^2 + 6\sigma_{BC}^2$	2.72	3.4	Marginal
OC x DD x EE (ABC)	2	0.006497	$\sigma_\epsilon^2 + 3\sigma_{ABC}^2$	6.90	3.4	Marginal
Error	24	0.000942	σ_ϵ^2	—	—	—

TABLE XIV

Results of 2 x 2 x 3 factorial analysis of variance for the logarithms of electron damage coefficients listed in Table XIII.

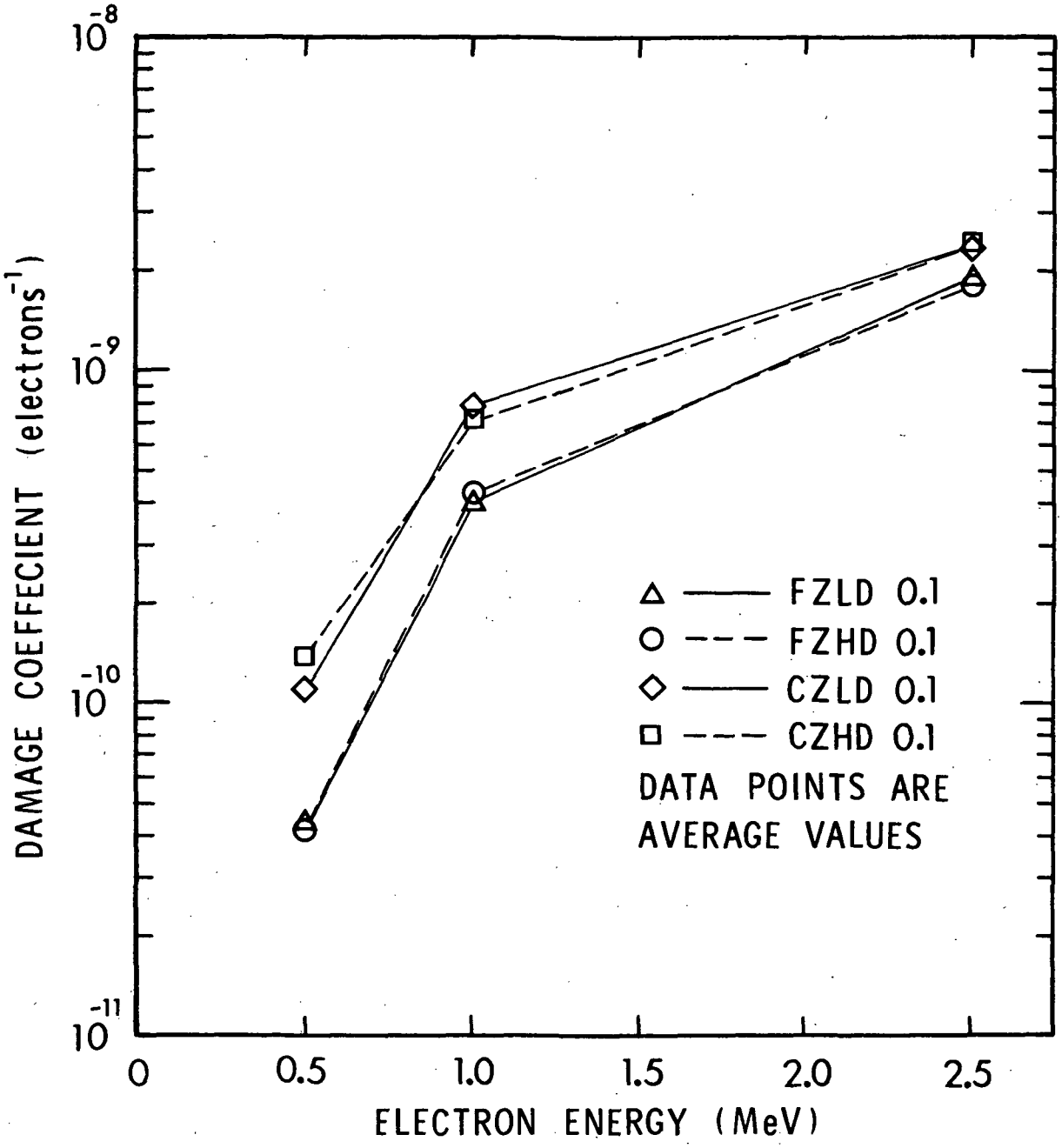

Figure 32. Average damage coefficient vs electron energy for four 0.1 ohm-cm B-doped Si ingots. Average values are based on the data listed in Table XIII.

two factors. If the latter were the case, then these tests would not be as sensitive as they should be. Therefore, no definite conclusion can be made concerning these factors.

One conclusion can be drawn, however. The ratios of the mean squares due to OC, DD, and OC x DD were calculated and all were found to be highly significant. This indicates that there are significant differences among the four ingots with regard to pre-irradiation diffusion length (which is obvious from the data in Table VI). This occurs because the error mean square estimates the variability of diffusion length among samples within an ingot while the mean squares due to OC, DD, and OC x DD estimate the variability among different ingots. It is not possible to state the cause of the difference on the basis of the present experiments.

Pre-irradiation data in Table VI suggest, on the surface, that oxygen content has a strong effect on diffusion length. However, past experience indicates that this is not necessarily the case. Lifetime (or diffusion length) is determined by the number and type of recombination centers present. In order to test properly for the dependence of pre-irradiation lifetime on oxygen content and dislocation density, all other properties for the ingots examined would have to be the same. Two factors that can affect lifetime include the impurities present in a given ingot (other than dopant concentration) and heat treatment history. For the present four-ingot comparison, one would have to characterize each in considerable detail and determine what properties are different other than dislocation density and oxygen content. Additionally, in an ideal experiment one would have to study a large number of ingots. In the absence of a detailed ingot characterization and because of the limited number of ingots employed, one cannot make a definite conclusion regarding the effect of oxygen or dislocation density on pre-irradiation diffusion length based on the present study.

REFERENCES

1. H. W. Brandhorst, Jr., in "Conference Record of the Ninth IEEE Photovoltaic Specialists Conference," (held in Silver Spring, Md., May 2-4, 1972) Catalog No. 72 CHO 613-0-ED, p. 37.
2. Annual Book of ASTM Standards, Part 8, F-28-66, pp. 515-521 (1970).
3. O. L. Curtis, Jr., and R. C. Wickenhiser, Proc. IEEE 53, 1224 (1965).
4. R. Gremmelmaier, Proc. IRE 46, 1045 (1958).
5. W. Rosenzweig, Bell Sys. Tech. J. 41, 1573 (1962).
6. J. H. Reynolds and A. Meulenberg, Jr., J. Appl. Phys. 45, 2582 (1974).
7. A. M. Goodman, J. Appl. Phys. 32, 2550 (1961).
8. S. C. Choo and A. C. Sanderson, Solid-State Electronics 13, 609 (1970).
9. W. E. Phillips, Solid-State Electronics 15, 1097 (1972).
10. W. R. Thurber and W. M. Bullis, AFCRL-72-0076, Jan. 31, 1972.
11. J. R. Carter, Jr., and H. Y. Tada, "Solar Cell Radiation Handbook," JPL Contract No. 953362, 28 June 1973.
12. F. Larin, Radiation Effects in Semiconductor Devices (Wiley and Sons, Inc., New York, 1968).
13. A. Many, Y. Goldstein, and N. B. Grover, Semiconductor Surfaces (North-Holland Publishing Co., Amsterdam, 1965), p. 259.
14. J. C. Irvin, Bell System Tech. J. 41, 387 (1962).
15. J. S. Blakemore, Semiconductor Statistics (Pergamon Press, Oxford, 1962).
16. S. M. Sze and J. C. Irvin, Solid-State Electronics 11, 599 (1968).
17. K. B. Wolfstirn, J. Phys. Chem. Solids 16, 279 (1960).
18. M. Neuberger and S. J. Welles, "Silicon", EPIC Report DS-162, Oct. 1969 (Air Force Materials Laboratory Contract No. F33615-68-C-1225).
19. A. J. R. de Kock, Appl. Phys. Lett. 16, 100 (1970).
20. A. J. R. de Kock, J. Electrochem. Soc. 118, 1851 (1971).
21. T. F. Ciszek, in Semiconductor Silicon, H. R. Huff and R. R. Burgess, Eds. (The Electrochemical Society, Princeton, 1973) pp. 150-160.

22. O. L. Curtis, Jr., Phys. Rev. 172, 773 (1968).

23. O. L. Curtis, Jr., and J. R. Srour, J. Appl. Phys. 45, 792 (1974).

24. J. A. Baker, Final Report on NASA-Lewis Contract NAS3-17356, Nov. 1973.

25. J. A. Baker, private communication.

26. R. L. Statler, Proc. 1968 Intersociety Energy Conversion Engineering Conference, Boulder, Colo., p. 122.

27. D. J. Curtin and A. Meulenberg, in "Conference Record of the Eighth IEEE Photovoltaic Specialists Conference," (held in Seattle, Wash., Aug. 4-6, 1970) Catalog No. 70C 32 ED, p. 193.

28. A. Meulenberg, Jr., and F. C. Treble, in "Conference Record of the Tenth IEEE Photovoltaic Specialists Conference," (held in Palo Alto, Calif., Nov. 13-15, 1973) Catalog No. 73CH0801-ED, p. 359.

29. R. G. Downing, J. R. Carter, Jr., and J. M. Denney, in "Proceedings of the Fourth Photovoltaic Specialists Conference," Vol. I, A-5-1, 1964.

30. T. J. Faith, IEEE Trans. Nucl. Sci. 20, 238 (Dec. 1973).

31. B. E. Anspaugh and J. R. Carter, in "Conference Record of the Tenth IEEE Photovoltaic Specialists Conference," (held in Palo Alto, Calif., Nov. 13-15, 1973) Catalog No. 73CH0801-ED, p. 359.

32. J. M. Denney and R. G. Downing, TRW Systems Report 8653-6026-KU-000, July 1963.

33. W. Rosenzweig, F. M. Smits, and W. L. Brown, J. Appl. Phys. 35, 2707 (1964).

34. T. Nakano and Y. Inuishi, J. Phys. Soc. Jap. 19, 851 (1964).

35. T. Nakano, K. Nakasima, and Y. Inuishi, J. Phys. Soc. Jap. 20, 2140 (1965).

36. N. D. Wilsey, in "Conference Record of the Ninth IEEE Photovoltaic Specialists Conference," (held in Silver Spring, Md., May 2-4, 1972) Catalog No. 72 CHO 613-0-ED, p. 338.

37. J. R. Srour and O. L. Curtis, Jr., J. Appl. Phys. 43, 1779 (1972).

38. O. L. Curtis, Jr., J. R. Srour, and R. B. Rauch, J. Appl. Phys. 43, 4638 (1972).

39. A. R. Frederickson and E. A. Burke, IEEE Trans. Nucl. Sci. 18, 162 (Dec. 1971).

40. C. R. Hicks, Fundamental Concepts in the Design of Experiments, (Holt, Rinehart, and Winston, New York, 1964).

DISTRIBUTION LIST

NASA

NASA, Scientific and Technical
Information Facility
P. O. Box 8757
Baltimore-Washington International
Airport
Baltimore, Maryland 21240
(40 copies & 1 reproducible)

Mr. Ernst M. Cohn, Code RPP
National Aeronautics and Space
Administration
Washington, D. C. 20546

Mr. Simon Manson, Code NT
National Aeronautics and Space
Administration
Washington, D. C. 20546

Mr. Norman J. Mayer, Code RWS
National Aeronautics and Space
Administration
Washington, D. C. 20546

Mr. William R. Limberis, Code KC
National Aeronautics and Space
Administration
Washington, D. C. 20546

Mr. R. D. Ginter, Code NE
National Aeronautics and Space
Administration
Washington, D. C. 20546

Office of Technology Utilization
Code KT
National Aeronautics and Space
Administration
Washington, D. C. 20546

AMES

Dr. Robert J. Debs
Code PDS N-244-14
Ames Research Center
National Aeronautics and Space
Administration
Moffett Field, CA 94035

GODDARD

Mr. Edward M. Gaddy, Code 711
Goddard Space Flight Center
National Aeronautics and Space
Administration
Greenbelt, MD 20771

Mr. Charles MacKenzie, Code 711
Goddard Space Flight Center
National Aeronautics and Space
Administration
Greenbelt, MD 20771

Mr. Luther W. Slifer, Jr., Code 711
Goddard Space Flight Center
National Aeronautics and Space
Administration
Greenbelt, MD 20771

LEWIS RESEARCH CENTER

Mr. Clifford K. Swartz, MS 302-1
NASA, Lewis Research Center
21000 Brookpark Road
Cleveland, OH 44135

M. T. Musial, MS 500-113
NASA, Lewis Research Center
21000 Brookpark Road
Cleveland, OH 44135

Carl E. Goodwin, MS 500-206
NASA, Lewis Research Center
21000 Brookpark Road
Cleveland, OH 44135

NASA, Lewis Research Center
21000 Brookpark Road
Cleveland, OH 44135
Attn: Library (2 copies)

LEWIS RESEARCH CENTER (cont.)

Mr. Cosmo R. Baraona,
MS 302-1 (10 copies)
Lewis Research Center
National Aeronautics and Space
Administration
21000 Brookpark Road
Cleveland, OH 44135

Dr. Henry W. Brandhorst, Jr.
MS 302-1
Lewis Research Center
National Aeronautics and Space
Administration
21000 Brookpark Road
Cleveland, OH 44135

Mr. Larry R. Scudder, MS 302-1
Lewis Research Center
National Aeronautics and Space
Administration
21000 Brookpark Road
Cleveland, OH 44135

Dr. Louis Rosenblum, MS 302-1
Lewis Research Center
National Aeronautics and Space
Administration
21000 Brookpark Road
Cleveland, OH 44135

Mr. Victor G. Weizer, MS 302-1
Lewis Research Center
National Aeronautics and Space
Administration
21000 Brookpark Road
Cleveland, OH 44135

LANGLEY

Mr. Walter E. Ellis, MS 448
Langley Research Center
National Aeronautics and Space
Administration
Hampton, VA 23665

Mr. Gilbert A. Haynes, MS 488
Langley Research Center
National Aeronautics and Space
Administration
Hampton, VA 23665

Mr. Jack F. Zanks, MS 488
Langley Research Center
National Aeronautics and Space
Administration
Hampton, VA 23665

JOHNSON

Mr. James L. Cioni, Code EP5
Johnson Spacecraft Center
National Aeronautics and Space
Administration
Houston, TX 77058

MARSHALL

Mr. J. L. Miller, Code EC-12
NASA/Marshall Space Flight
Center
Huntsville, AL 35812

JPL

Dr. Bruce Anspaugh
Mail Stop 198-220
Jet Propulsion Laboratory
4800 Oak Grove Drive
Pasadena, CA 91103

Mr. Paul Berman
Mail Stop 198-220
Jet Propulsion Laboratory
4800 Oak Grove Drive
Pasadena, CA 91103

Mr. John V. Goldsmith
Mail Stop 198-220
Jet Propulsion Laboratory
4800 Oak Grove Drive
Pasadena, CA 91103

JPL (cont.)

Mr. Walter A. Hasbach
Mail Stop 198-220
Jet Propulsion Laboratory
4800 Oak Grove Drive
Pasadena, CA 91103

Mr. Lloyd D. Runkle
Mail Stop 198-220
Jet Propulsion Laboratory
4800 Oak Grove Drive
Pasadena, CA 91103

Dr. Richard Stirn
Mail Stop 198-220
Jet Propulsion Laboratory
4800 Oak Grove Drive
Pasadena, CA 91103

Mr. R. Gilbert Downing
Mail Stop 198-220
Jet Propulsion Laboratory
4800 Oak Grove Drive
Pasadena, CA 91103

AIR FORCE

AFAPL/POE-2/L. D. Massie
WPAFB, OH 45433

SAMSO SAFSP-8
P.O. Box 92960
Worldway Postal Center
Los Angeles, CA 90009

AFAPL/POW-2/J. F. Wise
WPAFB, OH 45433

ARMY

Dr. Emil Kittl
USAECOM
Attn: AMSEL-TL-PE
Fort Monmouth, NJ 07703

NAVY

Mr. E. L. Brancato, Code 4101
Naval Research Laboratory
4555 Overlook Avenue, S.W.
Washington, D.C. 20375

Mr. Richard L. Statler
Naval Research Laboratory
Code 6603F
Washington, D.C. 20375

OTHER GOVERNMENT ORGANIZATIONS

Mr. William R. Cherry
Solar Research Division
Energy Research Development Administration
1800 G Street, NW
Washington, D.C. 20545

Dr. Lloyd Herwig
Solar Research Division
Energy Research Development Administration
1800 G Street, NW
Washington, D.C. 20545

Dr. Leonard M. Magid
Solar Research Division
Energy Research Development Administration
1800 G Street, NW
Washington, D.C. 20545

PRIVATE ORGANIZATIONS

Mr. E. R. Berry
Aerospace Corporation
P.O. Box 92957
Los Angeles, CA 90009

PRIVATE ORGANIZATIONS (cont.)

Dr. Leon D. Crossman
Dow Corning Corporation
12334 Goddes Road
Hemock, MI 48626

Mr. Larry Gibson
Aerospace Corporation
Box 92957
Los Angeles, CA 90009

Mr. H. J. Killian
Aerospace Corporation
Box 92957
Los Angeles, CA 90009

Mr. J. A. Albeck
Marketing Manager
Aerospace Group
Spectrolab, Division of Textron, Inc.
12500 Gladstone Avenue
Sylmar, CA 91342

Professor Joseph J. Loferski
Division of Engineering
Brown University
Providence, RI 02912

Dr. James A. Naber
Intelcom Rad. Tech.
7650 Convoy Court
P.O. Box 80817
San Diego, CA 92138

Mr. W. J. Billerback
COMSAT Labs
P.O. Box 115
Clarksburg, MD 20734

Mr. Denis Curtin
COMSAT Labs
P.O. Box 115
Clarksburg, MD 20734

Dr. Andrew Meulenberg
COMSAT Labs
P.O. Box 115
Clarksburg, MD 20734

Mr. R. C. Lyle
Exotech Systems, Inc.
1200 Quince Orchard Boulevard
Gaithersburg, MD 20760

Dr. James McCormick
Dow Corning Corporation
12334 Geddes Road
Hemlock, MI 48626

Mr. Kenneth Hanson
General Electric Company
Valley Forge Space Technology Center
P.O. Box 8555
Philadelphia, PA 19101

Dr. G. H. Schwuttke
IBM, Dept. 267, Bldg. 300-90
East Fishkill Facility
Hopewell Junction
New York, NY 12533

Mr. Robert C. Hamilton
Institute for Defense Analyses
400 Army-Navy Drive
Arlington, VA 22202

Mr. A. D. Tonelli
Department A3-253-MS 13-3
McDonnell Douglas Astronautics Co.
Huntington Beach, CA 92647

Mr. A. A. Nussberger, D/191-200, SK09
North American Rockwell Corp.
Space Division
12214 Lakewood Boulevard
Downey, CA 90241

PRIVATE ORGANIZATIONS (cont.)

Mr. Isadore M. Sachs
Optical Coating Laboratory, Inc.
P. O. Box 1599
Santa Rosa, CA 95403

Mr. Donald C. Briggs
WDL Division MS G80
Philco-Ford Corporation
3939 Fabian Way
Palo Alto, CA 94303

Mr. Richard Grant
WDL Division MS-Z-31
Philco-Ford Corporation
3939 Fabian Way
Palo Alto, CA 94303

Power Information Center
University City Science Center
3401 Market Street, Room 2210
Philadelphia, PA 19014

Mr. Paul Rappaport
RCA Corporation
David Sarnoff Research Center
Princeton, NJ 08450

Mr. Henry Oman
The Boeing Company
Research and Engineering
Division
P. O. Box 3999
Seattle, WA 98124

Solarex Corporation
1335 Piccard Drive
Rockville, MD 20850

Dr. Gerald L. Pearson
Stanford University
Stanford Electronics Labs.
Stanford, CA 94305

Mr. Arvin H. Smith
Thermo Electron Corporation
101 First Avenue
Waltham, MA 02154

Mr. Hans Rauschenbach, M1-1406
TRW Systems
One Space Park
Redondo Beach, CA 90278

Mr. Werner Luft
TRW Systems Group-MS-M1/1208
One Space Park
Redondo Beach, CA 90278

John D. Meakin
Associate Director
Institute of Energy Conversion
University of Delaware
Newark, DL 19711

Dr. Frederick Morse
Depart. of Mechanical Engineering
University of Maryland
College Park, MD 20742

Professor Martin Wolf
University of Pennsylvania
260 Towne Building - D3
Philadelphia, PA 19174

Mr. Peter A. Iles
CENTRALAB
4501 N. Arden Drive
El Monte, CA 91734

Mr. Aaron Kirpich
Electrical Systems
General Electric Company
Space Systems
P. O. Box 8555
Philadelphia, PA 19101

PRIVATE ORGANIZATIONS (cont.)

Mr. Eugene L. Ralph
Heliotek, Division of Textron
12500 Gladstone Avenue
Sylmar, CA 91342

Mr. J. R. Davis
Westinghouse R&D
Beulah Road, Churchill Boro
Pittsburgh, PA 15235

Professor J. R. Hauser
North Carolina State University
Electrical Engineering Dept.
Box 5275
Raleigh, NC 27607

Professor C. T. Sah
University of Illinois
Urbana-Champaign Campus
Dept. of Electrical Engineering
Urbana, IL 61801

Professor S. S. Li
University of Florida
College of Engineering
Dept. of Electrical Engineering
Gainesville, FL 32611

Professor F. A. Lindholm
University of Florida
College of Engineering
Dept. of Electrical Engineering
Gainesville, FL 32611